UNIVERSITY OF NOTTINGHAM

Refining in-vivo models of pulmonary fibrosis

Anthony Habgood

Thesis submitted to the University of Nottingham for the degree of Doctor of Philosophy

Abstract

Idiopathic pulmonary fibrosis (IPF) is a progressive disease with limited treatment options. IPF is characterized by excessive collagen deposition within the lung resulting in loss of lung function and a survival rate worse than most cancers. There is an urgent need to develop and better characterise animal models of this disease to further our understanding of its pathophysiology and to assist in the development of new pharmacological treatments. Researching respiratory diseases and the development of new therapies relies on the use of robust *in vivo* models.

The objective of this thesis was to better-characterise a range of animal models of pulmonary fibrosis. The principal objective was to evaluate a range of animal models of lung fibrosis to facilitate reproducibility of *in vivo* data across a range of models to increase confidence in the results of pre-clinical assessments. To try and minimise unnecessary animal usage, this thesis also investigated a number of techniques, such as non-invasive imaging, and *ex vivo* models such as the precision cut lung slice (PCLS) model to promote the principles of replacement, reduction and refinement of *in vivo* studies.

Firstly, I established and characterised the bleomycin model of acute lung injury and pulmonary fibrosis in both mice and rats. When this was achieved I used the bleomycin model to determine the effect of secretory leukocyte protease inhibitor (*Slpi*) gene deletion, and Tranilast treatment, on the development of bleomycin-induced lung injury and pulmonary fibrosis.

Using *Slpi* null mice, I set out to determine the role of SLPI in the development of pulmonary fibrosis. *Slpi*$^{-/-}$ mice have an increased ratio of active MMP-9 to pro-MMP-9 compared to wild-type animals demonstrating enhanced metalloproteinase

activity within the lung. Wild-type mice treated with bleomycin have increased TGF-β activity, as measured by increased pSmad2 levels in nuclear extracts from macrophages taken from bronchoalveolar lavage fluid. Furthermore, wild-type mice have increased collagen type I, alpha 1, type III, alpha 1, type IV, alpha 1, mRNA expression and significantly more total lung collagen 28-days post bleomycin. However, TGF-β activity in *Slpi*$^{-/-}$ mice was not increased and collagen gene expression was not upregulated but they still had a significant increase in total lung collagen deposition 28-days post bleomycin. Overall these data suggested that a lack of *Slpi* expression does not significantly modify the development of lung fibrosis following bleomycin-induced lung injury.

In this thesis, I evaluate the efficacy of Tranilast at inhibiting fibrosis in a therapeutic bleomycin model. 36 rats were split into 6 treatment groups. Rats were dosed daily with compound from day 11 to day 21 post-bleomycin administration via the oropharyngeal or oral route. The study determined that bleomycin induced collagen deposition in all of the rats, with hydroxyproline levels as follows; saline / Tranilast oral 3.77 mg Vs bleomycin / Tranilast oral 6.73 mg $^{**}P<0.01$, saline / Tranilast *o.p.* 2.39 mg Vs bleomycin / Tranilast *o.p.* 6.97 mg $^{****}P<0.0001$ but only a trend towards an increase in the lactose op control group saline / lactose *o.p.* bleomycin / lactose *o.p.* Tranilast treatment, regardless of route of administration, had no effect on collagen deposition in rats. pSmad2 levels should be determined to establish if Tranilast was affecting TGF-β activity. It is possible that Tranilast may have greater effect if used to inhibit mast cell degranulation therefore a treatment strategy investigating this may also be of interest in future studies.

A model of radiation-induced lung fibrosis was also established that showed mice administered thoracic irradiation developed substantial pulmonary fibrosis in a dose

dependent manner. 17.5 Gy was determined as the optimum dose for future studies as it caused substantial fibrosis without high mortality and radiation associated side effects. The development of pulmonary fibrosis in irradiated animals was tracked with αvβ6 SPECT/CT imaging for the first time in this model in an effort to determine whether the duration of the model could be shortened. Specific binding of ^{111}In-DTPA-A20FMDV2 to αvβ6 integrins is increased in the lungs of 17.5 Gy irradiated animals, 8.68 %, as early as 17 weeks compared with 'sham' irradiated controls 3.76 % of initial ^{111}In dose/mm3 of lung (P = 0.0517). This increase in αvβ6 in the lung is detected in lungs that show some parenchymal damage in axial CT scans. Mice went on to establish dense areas of alveolitis and connective tissue deposition as well as pleural thickening at 26 weeks.

In this thesis, I also develop a precision cut lung slice model of pulmonary fibrosis where I induce fibrosis in a small number of mice using bleomycin then attain large numbers of slices, > 30 slice 150 µm thick, of fibrotic lung. Lung slices are cultured for 5 days and treated with various interventions. After culturing for 5 days, I was able to determine an increase in hydroxyproline in bleomycin treated mice compared with saline treated mice. Therefore, this model has the potential to be used to assess a compound's ability to inhibit collagen deposition, this has the potential to greatly reduce the number of animals required when determining an EC_{50}.

Finally, I investigated whether *Elk1*$^{-/0}$ mice could be used as a potential model of age related fibrosis and demonstrated that *Elk1*$^{-/0}$ mice have evidence of widespread, although mild, pulmonary fibrosis at 12 months of age when assessed via histology. Measurement of hydroxyproline established a significant increase in collagen

deposition in *Elk1*$^{-/0}$ mice compared with *Elk1*$^{+/0}$ controls at 12 months of age (852.3, 758.4 µg/lung set, respectively, $P = 0.0346$)

This thesis has refined and further characterised a number of commonly used models of pulmonary fibrosis which were used in this thesis to further our understanding of the role of SLPI in the development of pulmonary fibrosis and also to assess the efficacy of novel drug treatments.

Acknowledgments

This Thesis would not have been possible without the support of several individuals and organisations.

My sincere thanks go to GlaxoSmithKline for funding my project and also my employment, as a research technician, for the majority of the seven and half years I spent working at the University of Nottingham whilst studying towards my PhD on part-time basis. I would also like to thank the University of Nottingham for their support during my study and employment.

I would like to thank my supervisor, Professor Gisli Jenkins, for his guidance over the last 8 years and for the opportunities to further develop myself as a research scientist, and for providing me varied research experiences and the opportunity to present my work across the world.

I would also like to express my gratitude to all of my colleagues in Respiratory Medicine between 2010 and 2018, particularly Alison John, who spent considerable

time supporting me with all aspects of the nanoSPECT/CT imaging; her knowledge and expertise where invaluable. She has also spent numerous hours at the BSU assisting me with *in vivo* dosing. Also, Amanda Harvey, who, like Alison, has been a great source of knowledge over the course of my studies and again has helped me to perform numerous *in vivo* studies. I would also like to thank her for letting me use her *Elk1*$^{-/-}$ mice to study the fibrotic changes in the ageing lung. Jo Porte, your support during my time in Respiratory Medicine was very much appreciated.

I would like to thank Professor Stewart Martin and Dr Jonathon Littler for the assistance in calculating the irradiation dosimetry for the RILF model.

I would like to thank Nurformix ltd. for allowing me to include the work using their novel Tranilast formulation in my thesis.

Last but definitely not least, I would like to thank my family and friends for their support and patience during my PhD. I would especially like to acknowledge my wife Aimie as well as our two children, Adam and Emma, who were not born when I started my PhD journey but who have been an inspiration and motivation whilst completing it.

List of publications

Habgood, A. N., Tatler, A. L., Porte, J., Wahl, S. M., Laurent, G. J., John, A. E., Johnson, S. R. and Jenkins, G. (2016) 'Secretory leukocyte protease inhibitor gene deletion alters bleomycin-induced lung injury, but not development of pulmonary fibrosis', Lab Invest, 96(6), pp. 623-31.

John, A. E., Luckett, J. C., Tatler, A. L., Awais, R. O., Desai, A., **Habgood, A.**, Ludbrook, S., Blanchard, A. D., Perkins, A. C., Jenkins, R. G. and Marshall, J. F. (2013) 'Preclinical SPECT/CT imaging of alphavbeta6 integrins for molecular stratification of idiopathic pulmonary fibrosis', J Nucl Med, 54(12), pp. 2146-52.

Tatler, A. L., Barnes, J., **Habgood, A.**, Goodwin, A., McAnulty, R. J. and Jenkins, G. (2016) 'Caffeine inhibits TGFβ activation in epithelial cells, interrupts fibroblast responses to TGFβ, and reduces established fibrosis in ex vivo precision-cut lung slices', Thorax, 71(6), pp. 565-7.

Tatler, A. L., **Habgood, A.**, Porte, J., John, A. E., Stavrou, A., Hodge, E., Kerama-Likoko, C., Violette, S. M., Weinreb, P. H., Knox, A. J., Laurent, G., Parfrey, H., Wolters, P. J., Wallace, W., Alberti, S., Nordheim, A. and Jenkins, G. (2016) 'Reduced Ets Domain-containing Protein Elk1 Promotes Pulmonary Fibrosis via Increased Integrin αvβ6 Expression', J Biol Chem, 291(18), pp. 9540-53.

List of abbreviations

AEC I	Alveolar epithelial cells (type I)
ALI	Acute lung injury
ALK	Activin receptor-like kinase
ARDS	Acute respiratory distress syndrome
ARRIVE	Animal Research: Reporting of *In Vivo* Experiments
BALF	Bronchoalveolar lavage fluid
BCA	Bicinchoninic acid
BLM	Bleomycin
BMP	Bone-morphogenetic proteins
CAT G	Cathepsin G
Cav-1	Caveolin-1
CAT	Computed axial tomography
cDNA	Complimentary DNA
CT	Computerised tomographic
CXCR	Chemokine (C-X-C motif) receptor
DLCO	Diffusing capacity of the lung for carbon monoxide
DMEM	Dulbecco's Modified Eagle Medium
DMSO	Dimethyl sulfoxide
DNA	Deoxyribonucleic acid
Dox	Doxycycline
ECM	Extracellular matrix
EMT	Epithelial-mesenchymal transition
ENA-78	Epithelial cell-derived neutrophil activator-78
ERK	Extracellular signal-regulated kinase
ERV	Expiratory Reserve Volume
FEF	Forced Expiratory Flow
FEV	Forced Expiratory Volume

FITC	Fluorescein isothiocyanate
FVC	Forced vital capacity
FRC	Functional residual capacity
GDF	Growth and differentiation factors
GRO-α	Growth regulated oncogene-α
GRO-β	Growth regulated oncogene-β
Gy	Gray's
H&E	Haematoxylin and eosin
HPRT	Hypoxanthine-guanine phosphoribosyltransferase
HRCT	High resolution computerised tomography
IC	Inspiratory Capacity
IFN-γ	Interferon-γ
IL-1, 6, 8, and 10	Interleukin-1, 6, 8, and 10
ILD	Interstitial lung disease
i.p.	Intra-peritoneal
i.t.	Intra-tracheal
i.v.	Intra-venous
IPF	Idiopathic pulmonary fibrosis
IU	International unit
JNK	c-Jun N-terminal kinase
KC	Keratinocyte chemoattractant
LAP	Latency associated peptide
LTBP	Latent TGF-β binding protein
LLC	Large latent complex
LPAR2	LPA receptor 2
LPS	Lipopolysaccharide
MCP-1	Monocyte chemotactic protein-1
MIP-2	Macrophage inflammatory protein-2
M-MLV	Moloney murine leukemia virus reverse transcriptase

MMP	Matrix metalloproteinase
MRI	Magnetic resonance imaging
NE	Neutrophil elastase
o.p.	Oropharyngeal
PaO_2:F_IO_2	Partial pressure of arterial oxygen to the fraction of inspired oxygen
PAR1	Protease-activated receptor-1
PBS	Phosphate buffered solution
PCLS	Precision cut lung slice
PCR	Polymerase chain reaction
PFA	Paraformaldehyde
PMNs	Polymorphonuclear leukocytes
PR-3	Proteinase-3
qPCR	Quantitative RT-PCR
RAGE	Advanced glycation end products
RGD	Arginine–glycine–aspartic acid
RILF	Radiation-induced lung fibrosis
RMCE	Recombinase-mediated cassette exchange
RNA	Ribonucleic acid
RV	Residual Volume
s.c.	Subcutaneous
SDS-PAGE	Sodium dodecyl sulfate-polyacrylamide
SLPI	Secretory leukocyte protease inhibitor
SPECT	Single photon emission computed tomography
TGF-β	Transforming growth factor-β
TLC	Total Lung Capacity
TLR	Toll-like receptor (-4)
TF	Transcription factor
TNF-α	Tumour necrosis factor-α
VC	Vital Capacity

Abstract i

Acknowledgments iv

List of publications vi

List of abbreviations vii

1 Introduction 1

1.1. Acute Lung Injury 1

1.1.1. Definition 1

1.2. Epidemiology 2

1.2.1. Pathophysiology 2

1.2.2. Prognosis 3

1.2.3. Treatment 4

1.3. Idiopathic Pulmonary Fibrosis 4

1.3.1. Definition 4

1.3.2. Epidemiology 5

1.3.3. Pathophysiology 5

1.3.4. Prognosis 6

1.3.5. Treatment 6

1.4. Comparison of ALI and IPF 7

1.4.1. Shared mechanisms between ALI and IPF 7

1.4.2. Differences between ALI and IPF 8

1.5. Utilising animals to study respiratory disease 9

1.5.1. Strengths 9
1.5.2. Weaknesses 10
1.5.3. The ARRIVE (Animal Research: Reporting of *In Vivo* Experiments) guidelines 12
1.6. Animal models of ALI and IPF 12
1.6.1. Bleomycin-induced acute lung injury and fibrosis 13
1.6.2. Radiation-induced lung fibrosis 14
1.6.3. Transgenic models of pulmonary fibrosis 15
1.6.4. Age-related models of lung fibrosis 17
1.6.5. FITC-induced lung fibrosis 19
1.6.6. Asbestosis 19
1.6.7. Paraquat-induced pulmonary fibrosis 20
1.6.8. Lipopolysaccharide-induced ALI 20
1.7. How well do these models reflect the disease 21
1.7.1. ALI 21
1.7.2. IPF 22
1.8. How do these models differ from the disease 23
1.8.1. ALI 23
1.8.2. IPF 24
1.9. Strategies to improve models 26
1.9.1. Endpoints 26
1.10. Ex vivo models of pulmonary fibrosis 27

1.10.1. Precision cut lung slice (PCLS) model 27
1.11. Key biological pathways involved in lung injury and fibrosis 29
1.11.1. Transforming growth factor-β (TGF-β) 29
1.11.2. TGF-β structure 29
1.11.3. TGF-β activation 30
1.11.4. Integrin mediated TGF-β activation 30
1.11.5. TGF-β signalling 32
1.11.6. The role of TGF-β in ALI and IPF 34
1.11.7. Secretory leukocyte protease inhibitor 35
1.11.8. The role of proteases in IPF 36
1.11.9. The role of ELK1 in IPF 37
1.11.10. Tranilast as a treatment for pulmonary fibrosis 38
1.11.11. Other key biological pathways 39
1.12. Methods for measuring TGF-β activity 40
1.12.1. pSmad2 ELISA 40
1.12.2. pSmad2 immunohistochemistry 41
1.12.3. Transformed Mink Lung Cell (TMLC) assay 41
1.13. Aims and Hypothesis 42
2 Materials and Methods 43
2.1. Animals 43
2.2. Genotyping 43

2.3. Bleomycin Model 44
2.3.1. Mouse 44
2.3.2. Rat 45
2.4. Bronchoalveolar lavage 45
2.5. Histology 46
2.5.1. Haematoxylin and Eosin stain 46
2.5.2. Masson's Trichrome 47
2.6. Ashcroft scoring 47
2.7. Immunohistochemistry 48
2.8. Quantification of collagen stain in lung tissue sections 49
2.9. Analysis of lung collagen content 50
2.10. Wet:dry weight ratio 50
2.11. Neutrophil elastase activity 51
2.12. Zymography 51
2.13. Quantitative RT-PCR 52
2.14. Nuclear extraction 53
2.15. pSMAD2 assay 54
2.16. Invasive whole body plethysmography 55
2.17. Thoracic irradiation dosimetry 55
2.18. Thoracic irradiations 56
2.19. NanoSPECT/CT Imaging 57

2.20. Bicinchoninic acid (BCA) Assay 59
2.21. Multiplex cytokine analysis 59
2.22. Processing lung for *ex vivo* micro CT 60
2.23. *Ex vivo* micro CT 60
2.24. Precision Cut Lung Slice (PCLS) fibrosis model 61
3 Pilot Dose Ranging Studies of Bleomycin Induced Lung Injury and Fibrosis, in Mice and Rats 63
3.1. Introduction and Aim 63
3.2. Methods 63
3.3. Results 64
3.3.1. Bleomycin dose setting and the development of ALI in mice 64
3.3.2. Protein and mRNA expression during the development of bleomycin-induced acute lung injury 70
3.3.3. Bleomycin dose setting and the development of pulmonary fibrosis in the mouse and rat 73
3.3.4. The effect of bleomycin on rat lung function 78
3.4. Discussion 81
3.5. Conclusion 83
4 The Effect of Radiation-Induced Lung Fibrosis on αvβ6 Integrin Expression 84
4.1. Introduction 84
4.2. Aims 85

4.3. Methods 86
4.4. Results 86
4.4.1. The effect of thoracic irradiation dose on mouse wellbeing 86
4.4.2. The effect of 10 Gy thoracic irradiation on the development of sub-acute inflammatory response 90
4.4.3. The effect of thoracic irradiation on the development of pulmonary fibrosis 91
4.4.4. A comparison of the effect of 10 Gy thoracic irradiation on the development of pulmonary fibrosis in male and female mice 95
4.4.5. *Ex vivo* μCT imaging of irradiated lungs 97
4.4.6. SPECT/CT imaging of αvβ6 integrins 99
4.5. Discussion 104
4.6. Conclusion 107
5 Using the Bleomycin Model of Lung Injury and Fibrosis to Understand the Role of SLPI in the Lung 107
5.1. Introduction 107
5.2. Aim 108
5.3. Methods 108
5.4. Results 109
5.4.1. Bleomycin-induced fibrosis in *Slpi*$^{-/-}$ and *Slpi*$^{-/+}$ on a B6D2F1 background 109
5.4.2. *Slpi* gene deletion promotes a proteolytic environment in the lung 113

5.4.3. Bleomycin-induced lung fibrosis does not enhance alveolar TGF-β activation in *Slpi*$^{-/-}$ mice, although they still develop pulmonary fibrosis 117

5.4.4. *Slpi* gene deletion exacerbates bleomycin-induced weight loss but does not alter hydroxyproline deposition 121

5.4.5. *Slpi* gene deletion impairs *Col1α1*, *Col3α1*, *Col4α1* gene expression during fibrogenesis but promotes an early transient increase in *Col6α1* gene expression..... 123

5.5. Discussion 126

5.6. Conclusion 131

6 Comparison of the Efficacy of a Tranilast:salt to Inhibit Fibrosis Following Both Oropharyngeal and Oral Administration to a Rat Using a Bleomycin Model 132

6.1. Introduction 132

6.2. Aims 134

6.3. Methods 134

6.4. Administration of Test Items 134

6.4.1. Analysis of lung collagen content 136

6.4.2. Masson's Trichrome 137

6.5. Results 137

6.5.1. The effect of Tranilast therapeutic treatment on body weight. 137

6.5.2. The effect of Tranilast treatment on lung weight in bleomycin treated animals 138

6.5.3. The effect of Tranilast treatment on right lung hydroxyproline concentration (µg/ml)..... 139

6.5.4. The effect of Tranilast treatment on right lung hydroxyproline concentration (µg/mg) 140
6.5.5. The effect of Tranilast treatment on right lung hydroxyproline concentration (mg/right lung) 142
6.5.6. Histological analysis on the effect of Tranilast treatment on bleomycin-induced pulmonary fibrosis 143
6.6. Discussion 144
6.7. Conclusion 146
7 Developing a PCLS Model to Help Assess the Efficacy of Tranilast in Inhibiting Fibrosis 147
7.1. Introduction 147
7.2. Aims 148
7.3. Methods 148
7.3.1. Hydroxyproline assay (tissue slices) 149
7.3.2. pSmad2 ELISA 150
7.4. Results 150
7.4.1. Determining if precision cut lung slices can be used to test the efficacy of Tranilast in inhibiting both TGF-β activation and collagen deposition. 150
7.5. Discussion 152
7.6. Conclusion 153
8 Elk1 Gene Deletion Leads to Spontaneous Early Fibrotic Changes in the Ageing Lung 154

8.1. Introduction 154
8.2. Aims 155
8.3. Methods 155
8.4. Results 156
8.4.1. Loss of *Elk1* results in age related pulmonary fibrosis. 156
8.4.2. α-smooth muscle actin expression in mice lacking *Elk1* 160
8.5. Discussion 162
8.6. Conclusion 164
9 Conclusions and future directions 164
9.1. Conclusions 164
9.2. Future directions 168
9.3. Concluding remarks 169
10 References 170

List of Figures

Figure 1.1 TGF-β signalling pathway. Injurious stimuli cause activation of the integrin αvβ6, one possible mechanism is through contraction of the cytoskeleton causing a conformational change of αvβ6. 33
Figure 2.1 Custom-made irradiation jig. 57
Figure 3.1 The effect of various bleomycin doses on the development of acute lung injury assessed by body mass. 66
Figure 3.2 The effect of various bleomycin doses on the development of acute lung injury assessed by H&E staining of lung tissue sections. 67

Figure 3.3 The effect of various bleomycin doses on BALF differential cell counts, 4 days post bleomycin administration. 68
Figure 3.4 The effect of various bleomycin doses on wet lung weight 4 days post bleomycin administration. 69
Figure 3.5 Cytokine protein expression in the lung during the development of acute lung injury. 72
Figure 3.6 The effect of bleomycin on *Itgb6* mRNA expression 0 to 10 days post administration. 72
Figure 3.7 The effect of various bleomycin doses on the development of pulmonary fibrosis in mice assessed by body mass. 74
Figure 3.8 The effect of various bleomycin doses on the development of pulmonary fibrosis in mice assessed by Masson's trichrome staining of lung tissue sections. ... 75
Figure 3.9 The effect of various bleomycin doses on the development of pulmonary fibrosis in rats assessed by body mass. 76
Figure 3.10 The effect of various bleomycin doses on the development of pulmonary fibrosis in rats assessed by Masson's trichrome staining of lung tissue sections. 77
Figure 3.11 The effect of bleomycin-induced acute lung injury on lung function – Pressure volume measurements. 79
Figure 3.12 The effect of bleomycin-induced acute lung injury on lung function – Flow volume measurements. 80
Figure 4.1 Image showing fur discolouration around the chest due to radiation exposure. 88
Figure 4.2 The effect of thoracic irradiation on body mass. 89
Figure 4.3 The effect of thoracic irradiation dose on survival. 90

Figure 4.4 The effect of 10 Gy thoracic irradiation on subacute sub-acute inflammatory response and the development of pulmonary fibrosis. 91
Figure 4.5 The effect of thoracic irradiation on the development of pulmonary fibrosis. 93
Figure 4.6 Thoracic irradiation increased immunostaining of αvβ6 integrin in a dose dependent manner. 94
Figure 4.7 The effect of thoracic irradiation on body mass in male and female mice. 96
Figure 4.8 The effect of thoracic irradiation on the development of pulmonary fibrosis in male and female mice. 97
Figure 4.9 *Ex vivo* μCT lung images following thoracic irradiation. 98
Figure 4.10 The effect of thoracic irradiation exposure on αvβ6 integrin lung expression. 100
Figure 4.11 The effect of thoracic irradiation exposure on αvβ6 integrin lung expression. 102
Figure 4.12 Binding of the ^{111}In-DTPA-A20FMDV2 peptide in the lungs of irradiated mice. 103
Figure 5.1 The effect of Slpi deletion on weight loss in *Slpi*$^{-/-}$ mice compared with *Slpi*$^{-/+}$ controls. 110
Figure 5.2 The effect of *Slpi* deletion on bleomycin induced collagen deposition in *Slpi*$^{-/-}$ mice compared with *Slpi*$^{-/+}$ controls. 111
Figure 5.3 Masson's trichrome staining 28 days post bleomycin treatment of *Slpi*$^{-/-}$ and *Slpi*$^{-/+}$ control mice. 112
Figure 5.4 Lung homogenate *Slpi* expression. 112

Figure 5.5 *Slpi*$^{-/-}$ mice do not express the *Slpi* wild type allele. Wild-type (WT) mice express the 490bp allele. 114

Figure 5.6 Neutrophil elastase activity in lung tissue 28 days post bleomycin treatment. 115

Figure 5.7 Ratio of pro and active forms of MMP-2 in BAL supernatant from wild-type and *Slpi*$^{-/-}$ mice. 115

Figure 5.8 Ratio of pro and active forms of MMP-9 in BAL supernatant from wild-type and *Slpi*$^{-/-}$ mice. 116

Figure 5.9 Mmp-9 mRNA expression in lung homogenates 28 days post-bleomycin (BLM). 116

Figure 5.10 The effect of *Slpi* deletion on alveolar macrophage TGF-β activation and pulmonary fibrosis. 118

Figure 5.11 Global tissue TGF-β activation assessed by pSmad2 immunohistochemistry. 119

Figure 5.12 Masson's trichrome staining 28 days post-bleomycin treatment. 120

Figure 5.13 Quantitative assessment of trichrome staining. 121

Figure 5.14 Body weight during the acute lung injury phase of bleomycin-induced fibrosis. 122

Figure 5.15 Lung hydroxyproline concentration during the early fibrotic and the late fibrotic stages of bleomycin induced pulmonary fibrosis in *Slpi*$^{-/-}$ and wild-type mice. 123

Figure 5.16 The effect of *Slpi* deletion on subtype specific collagen synthesis and deposition. 124

Figure 5.17 Collagen subtype specific immunohistochemistry of bleomycin treated *Slpi*$^{-/-}$ and wild-type mice. animals. 125

Figure 5.18 Collagen I and VI deposition quantification in lung tissue sections..... 126
Figure 6.1 The effect of Tranilast therapeutic treatment on mean body mass. 138
Figure 6.2 Right lung weights from animals treated with Tranilast administered by oral gavage or *o.p.* instillation. 139
Figure 6.3 Hydroxyproline concentration (µg/ml) of the lung tissue samples tested taken from animals treated with Tranilast administered by oral gavage or *o.p.* instillation. 140
Figure 6.4 Hydroxyproline concentration per mg of lung tissue assayed (µg/mg).. 141
Figure 6.5 Lung hydroxyproline levels in animals treated with Tranilast administered by oral gavage or *o.p.* instillation. 142
Figure 6.6 Masson's trichrome staining 21 days post-bleomycin treatment..... 143
Figure 6.7 Histologic scoring of Masson's Trichrome stained tissue. 144
Figure 7.1 Concentration response of Tranilast on TGF-β activation..... 151
Figure 7.2 Concentration response of Tranilast on hydroxyproline concentration.. 152
Figure 8.1 The effect of loss of *Elk1* on mean body mass. 157
Figure 8.2 The effect of loss of *Elk1* on wet lung weight. 158
Figure 8.3 Loss of *Elk1* results in age related collagen deposition. 158
Figure 8.4 Loss of *Elk1* results in age related fibrosis. 159
Figure 8.5 The effect of loss of *Elk1* on alveolar wall thickness. 159
Figure 8.6 The effect of loss of *Elk1* on *ACTA* expression at 12 weeks of age. 161
Figure 8.7 The effect of loss of *Elk1* on αSMA deposition in the lung at 12 months. 161

List of Tables

Table 1: Advantages and disadvantages of the various models of acute lung injury 23

Table 2: Advantages and disadvantages of the various models of pulmonary fibrosis 25

Table 3: Ashcroft scoring system - adapted from (Ashcroft et al., 1988) 48

Table 4: qPCR primer sequences. 52

Table 5: Treatment groups for the bleomycin-induced pulmonary fibrosis Tranilast treated rats. 136

1 Introduction

1.1. Acute Lung Injury

1.1.1.Definition

Acute lung injury (ALI) is defined as a syndrome of acute onset of inflammation and increased permeability of the alveolar-capillary membrane leading to diffuse pulmonary infiltrates, resulting in diffuse alveoli damage with potentially fatal effects on lung function (Bernard et al., 1994). The European American Consensus Committee on acute respiratory distress syndrome (ARDS) established the following diagnostic criteria for ALI. Diagnosis is confirmed by acute onset of one or more of the following: arterial blood gas measurement of partial pressure of arterial oxygen to the fraction of inspired oxygen (PaO_2:F_IO_2) ≤300 mm Hg, bilateral infiltrates seen on frontal chest radiograph consistent with pulmonary oedema and finally pulmonary artery wedge pressure of ≤18 mm Hg with no clinical evidence of left atrial hypertension to rule out hydrostatic pulmonary oedema (Bernard et al., 1994). Where PaO_2:FiO_2 deteriorates to ≤200 mm Hg, patients are considered to be suffering from ARDS, a severe subset of ALI. More recently the "Berlin Definition" of ALI/ARDS has been published. This definition now does away with the term ALI and uses three categories of ARDS; mild, moderate and severe. Patients fall into one of the three categories based on their PaO_2:F_IO_2 measurements: mild 200<, Moderate 100< and severe <100, allowing better prognosis and treatment selection (Ferguson et al., 2012).

1.2. Epidemiology

ALI is a serious and common condition with an estimated 190,000 cases and 74,500 related deaths per year in the USA alone (Rubenfeld et al., 2005).The incidence of acute respiratory distress syndrome (ARDS) is reported to be quite variable, however, a single report demonstrates the percentage of patients entering a UK Intensive Care Unit with ARDS to be 12.5 % (Summers et al., 2016). (Summers et al., 2016), also show the average onset age of ARDS to be 63 years old and 56.8 % of patients were male. This same report suggests that incidence may be stable in the UK where as there are reports of a decline of the incidence of ARDS the US population (Zambon and Vincent, 2008). The most prominent cause of ALI is sepsis; other common causes include trauma, aspiration, multiple blood transfusions and certain types of drug toxicity (Tsushima et al., 2009).

1.2.1.Pathophysiology

Regardless of the cause, the underlying pathophysiology of ALI remains relatively uniform. An initial insult to the lung results in damage to the alveoli. Histological assessment identifies damage and necrosis predominately to type I alveolar epithelial cells (AEC I) (McElroy and Kasper, 2004). This is further confirmed by high concentrations of the receptor for advanced glycation end products (RAGE), an AEC I cell death marker, present in the bronchoalveolar lavage fluid (BALF) of ALI patients (Mauri et al., 2010). Resident alveolar cells including AEC II and alveolar macrophages detect inflammatory mediators released from damaged or necrotic AEC I (Opitz et al., 2010). Activated alveolar macrophages release various mediators of neutrophil activation and transmigration into the alveolar space including;

interleukin-1, 6, 8 and 10, (IL-1, 6, 8 and 10), epithelial cell-derived neutrophil activator-78 (ENA-78) and tumour necrosis factor-α (TNF-α) (Bhargava and Wendt, 2012, Dushianthan et al., 2011). An excessive accumulation of activated neutrophilic polymorphonuclear leukocytes (neutrophils, PMNs) within the alveoli ensues. Consequential over production and activity of neutrophil derived cytokines, proteases and oxidants results in damage to the alveolar-capillary unit (Dushianthan et al., 2011). There is evidence of both epithelial and endothelial injury, the loss of the former can result in denuding of the alveolar epithelium. Thick hyaline membranes can form in the alveoli (Matthay and Zemans, 2011). Destruction of alveolar/capillary membranes leads to reduction in the gaseous exchange interface, development of pulmonary oedema and ultimately compromised lung function and death of the patient (Parekh et al., 2011).

1.2.2. Prognosis

The greatest risk factor for developing ALI is sepsis, accounting for as many as 79 % of cases (Rubenfeld et al., 2005). Both mortality and incidence increase dramatically with age. Mortality rates in hospitalised patients are disconcertingly high, 38.5 % for ALI and 41.1 % for those with ARDS (Rubenfeld et al., 2005). Long term outcomes for ALI survivors often include some form of pulmonary dysfunction, measurements of pulmonary function in ARDS survivors, at least 6 months after, show obstructive defects in 0 to 33 %, and restriction occurred in 0 to 50 % of patients (Neff et al., 2003). Often there are signs of continued injury and fibrosis in non-survivors of ALI as shown in post-mortem samples (Meduri et al., 1995) . Other defects may include a number of severe neurological complications including neuromuscular,

neurocognitive and neuropsychological dysfunctions as discussed by (Rubenfeld and Herridge, 2007).

1.2.3. Treatment

The underlying cause of ALI should be diagnosed and treated to prevent further damage (i.e. sepsis, pneumonia). However, no specific therapies for ALI exist to date, although meta-analysis of various small scale trials suggest that low dose corticosteroid therapies are effective at reducing mortality risk and improve morbidity outcomes in ALI patients (Tang et al., 2009). Prevention of fluid accumulation within the airways is also crucial (Bernard et al., 1994). Low tidal volume mechanical ventilation is utilised for treating ALI patients as traditional higher tidal volume ventilation causes distension "stretch" of the damaged alveoli further provoking the inflammatory response and damage to the alveoli (Brower et al., 2000).

1.3. Idiopathic Pulmonary Fibrosis

1.3.1. Definition

Idiopathic pulmonary fibrosis (IPF) is a chronic, progressive fibroproliferative disorder, occurring primarily in older adults, that leads to architectural remodelling of the lung with detrimental and eventually fatal effects on pulmonary function (Wells, 2013). IPF symptoms include a dry cough and dyspnoea on exertion (Wells, 2013).

1.3.2. Epidemiology

The incidence of IPF is 7.4 in 100,000 persons/year (Navaratnam 2011). IPF is the most common form of interstitial lung disease (ILD) accounting for 50% to 60% of all cases (Wang, 2009). The incidence of this devastating disease continues to rise with in excess of 5000 new cases being reported each year in the UK alone (Navaratnam et al., 2011). The incidence is higher in the elderly, with a median diagnosis age of 70 (Jenkins et al., 2015). It is suggested that males are more susceptible to developing the disease (4:1), however, there is no significant difference in median survival based on gender (King et al., 2001, Jenkins et al., 2015).

IPF is diagnosed by the identification of the following three findings using computerised tomographic (CT) scanning: subpleural honeycombing, traction bronchiectasis and thickened interlobular septae. Diagnosis of IPF can only be made if no evidence of an underlying connective tissue disease or environmental insult exists (Noble and Homer, 2005, Wells, 2013).

1.3.3. Pathophysiology

The aetiology and the underlying pathophysiology of IPF is currently hypothesised that there is a recurrent or prolonged alveolar injury in potentially genetically susceptible individuals, however, this hypothesis is still evolving (Selman et al., 2001). The classical histology of IPF is of type II pneumocyte hyperplasia, and increased proliferation of mesenchymal cells, resulting in the disruption of the alveolar-capillary interface (Goodwin and Jenkins, 2009). There is infiltration of

fibrogenic cells into the interstitial space leading to dysregulated matrix synthesis. Collagen producing myofibroblast are central to the excessive matrix deposition in IPF but alveolar macrophages are found in close proximity to these cells and can secrete pro-fibrotic mediators, chemokines and matrix metalloproteases all of which promote myofibroblast collagen production (Byrne et al., 2016). Excessive accumulation of extracellular matrix (ECM) greatly reduces lung compliance and gaseous exchange with fatal effects.

Gene polymorphisms in the transforming growth factor-β1 (TGF-β1), tumour necrosis factor (TNF)-α and surfactant protein C are increased risk factors for developing IPF, seen in almost 4 % of patients (Xaubet et al., 2003, Whyte et al., 2000, Lawson et al., 2004, Lawson and Loyd, 2006).

1.3.4. Prognosis

Even with two licenced treatments, the prognosis of IPF remains very poor with a reported median survival of 2.8 – 4.2 years from diagnosis (Maher et al., 2007). Median survival also decreases with age. Patients aged >50 years old have a median survival of 116 months but this drops to 63, 27 and 15 months for age groups 50-60, 60-70 and >70 respectively (King et al., 2001). The progressive nature of this disease results in a steady decline in lung function leading to death.

1.3.5. Treatment

Currently, there are no drug based therapies that have shown to increase long term survival. Drug based treatments include Pirfenidone and Nintedanib; these have

proven to slow declines in both forced vital capacity (FVC) and diffusing capacity of the lung for carbon monoxide (DLCO) measurements at 1 year in IPF patients compared with those not taking the medication (King et al., 2014, Richeldi et al., 2014). However, neither treatments are reported to change respiratory symptoms and quality of life

1.4. Comparison of ALI and IPF

Although ALI and IPF are unique entities, they have a number of shared mechanistic and pathological features. Similarities tend to be broader features that, under closer examination, are subtly different. Both the differences and similarities are discussed below.

1.4.1. Shared mechanisms between ALI and IPF

It is thought that the alveolar epithelium plays a critical role in the initiation and modulation of both diseases via the release of various signalling molecules (Vanderbilt et al., 2003, Selman and Pardo, 2006). Neutrophilia is also observed in both disease states. Neutrophilia in ALI has a clear pathogenic role, however, within the fibrotic lungs of IPF patients, it is unknown whether it has any role in the initiation of the disease but it might contribute to the chronic inflammatory milieu that leads to the persistent fibrotic development within the lung (Obayashi et al., 1997) and acute exacerbations (Ryerson et al., 2015). Transforming growth factor-β (TGF-β) is also thought to play an important role in both disease states. TGF-β's ability to cause an increase in the permeability of the epithelium makes it a crucial

molecule in the development of oedema (Pittet et al., 2001). Moreover, there are shared mechanisms in the activation of TGF-β as preventing integrin αvβ6 activation of TGF-β ameliorates both IPF and ALI induced oedema (Munger et al., 1999, Pittet et al., 2001). TGF-β may also play a role in proliferation of fibroblast and matrix deposition in order to seal off and contain injury which, if un-regulated, can lead to the development of fibrosis (Sheppard, 2006).

1.4.2. Differences between ALI and IPF

A number of major differences exist between these two distinct disease states. As discussed previously, ALI is driven by an inflammatory response in which there is matrix deposition and destruction whereas IPF is thought to be driven independently of inflammation and results in abnormal matrix deposition. The underlying cause of ALI is often identifiable whereas in IPF the cause remains unclear. The time course in which these diseases develop is also very different. ALI, as the name suggests, is of acute onset. This disease progresses rapidly and is mediated through an exaggerated neutrophil influx into the lungs leading to destruction of the gaseous exchange interface and alveolar oedema; both of which greatly compromise lung function (Pierrakos et al., 2012). Acute lung injury can fully resolve within 14 days (Dushianthan et al., 2011). IPF on the other hand is a chronic disease with unknown aetiology. There is progressive collagen deposition within the lung greatly reducing lung compliance (Noble and Homer, 2005). IPF is a non-resolving progressive disease.

1.5. Utilising animals to study respiratory disease

Animal models play a key role in investigating respiratory diseases and their treatments. There are numerous models that closely replicate key aspects of, or broadly replicate, the pathophysiology of various respiratory diseases. Animal models provide important tools for increasing our understanding of disease pathophysiology and can also be used for screening potential new treatments. The use of each animal model has its own strengths and weaknesses and, for these models to be used effectively, meaningful readouts must be obtained at appropriate experimental time points. Discussed below are both the strengths and weaknesses of using *in vivo* models when comparing them with *in vitro* alternatives.

1.5.1. Strengths

In vivo experimentation remains indispensable for drug development. The most advantageous factor of using an animal model is that an animal offers a metabolically active system to study the disease of interest. In animal models, it is possible to replicate a disease, or part of a disease, and observe the interactions between various cell types that are signalling through multiple metabolic pathways. This complex biology is not possible to fully replicate, even with the most advanced cell culture techniques.

In vivo models offer more analytical potential than their *in vitro* counterparts. There are many physiological measurements that can only be made *in vivo*, such as changes in lung function. This measurement is often used to track disease progression in patients with IPF therefore it is useful to be able to measure it *in vivo*. Other

clinically relevant methods developed for assessing disease progression in IPF patients that can only be performed on *in vivo* models include various imaging techniques including; CT (Rodt et al., 2010), single photon emission computed tomography (SPECT) (John et al., 2013), magnetic resonance imaging (MRI) (Caravan et al., 2013) and x-ray dark-field imaging (Yaroshenko et al., 2015).

Although IPF is not thought to result from a primary immune process, one major advantage of using *in vivo* models is the ability to study the effects of the disease with a working immune system. However, circulating monocyte-derived macrophages are found in the lungs of IPF patients suggesting that the innate immune system may have some involvement in IPF (Byrne et al., 2016).

For these reasons, *in vivo* models are hugely important and difficult to replace. They maintain the three-dimensional structure of the lung with multiple cell types that have been implicated with disease progression including fibroblast, epithelial cells and macrophages. *In vivo* models also offer the benefit of the animals still breathing, which not only allows these parameters to be measured but their effects on disease progression to be determined.

1.5.2. Weaknesses

For all the benefits that animal models bring to scientific research perhaps their greatest weakness is over or misinterpretation of their findings. One particular review demonstrates how 246 publications describe compounds with antifibrotic effects in the bleomycin-induced pulmonary fibrosis model between 1980 and 2006 (Moeller et al., 2008). At the time of publication 14 of these had been tested in clinical trials, all with little or no effect. Of the 246 compounds tested 211 were given preventively,

during the first 7 days of the model, therefore these drugs may interfere with the inflammatory response and not the fibrotic response, leading to the potential for misinterpretation of their findings. There is no single animal model that can fully replicate all features of ALI and IPF. Instead, each model attempts to either closely replicate as much of the disease as possible or replicate a particular aspect of the disease. Therefore, it is vital to understand how the models compare and differ from the disease state to allow accurate interpretation of results. Firstly, both physiological and biological differences between species must be considered when running *in vivo* models. Murine lungs may not be wholly appropriate as surrogates for the human lung due to large structural and cellular differences. In humans, there is dichotomous branching of the airways to allow airflow to the alveoli. However, in rodents, there are three branching subroutines including domain branching, planar and orthogonal bifurcation (Kling, 2011). There are also structural differences on a cellular scale; cells that function as renewing progenitors cells in rodents are made up of non-ciliated secretory cells, whereas in humans the renewing progenitors cells are the basal cells (Rackley and Stripp, 2012). It is partly due to these reasons that when testing new treatments, it is good practise to run more than one different type of model to test the theory. This helps to avoid the possibility that the treatment is working through a mechanism that was important in the disease model but not the disease state its self.

Cost can also be a burden associated with running *in vivo* models. Housing animals for long periods of time, such as in ageing studies or when breeding transgenic animals, is very expensive. The cost of breeding transgenic animals can rapidly increase these costs, particularly when using complicated breeding strategies that require large numbers of animals.

A major issue using *in vivo* models remain the ethical concerns relating to harming animals, and therefore animal models are only used if no practicable alternative exists.

1.5.3. The ARRIVE (Animal Research: Reporting of *In Vivo* Experiments) guidelines

The ARRIVE (Animal Research: Reporting of *In Vivo* Experiments) guidelines have been implemented in, 2010, and encourage researchers to have uniform design, conduct, analysis and reporting of their data. It is thought that adhering to these guidelines will promote high quality, comprehensive and accurate reporting which will aid in reducing the number of animals used in scientific research (Kilkenny et al., 2010).

1.6. Animal models of ALI and IPF

To understand disease mechanisms and assess potential new treatments for both ALI and IPF, animal models that closely mimic the pathophysiology of these diseases are required. *In vivo* models are essential for studying new therapies regardless of the disease of interest. These models are presently the only tools available for safely assessing the effect of treatments in living systems. There are a number of currently used models and the most common of which are reviewed below.

1.6.1. Bleomycin-induced acute lung injury and fibrosis

Bleomycin-induced pulmonary fibrosis is the most commonly used and best characterised model of IPF. Bleomycin (BLM) is used as an anti-neoplastic drug. Bleomycin hydrolase, the enzyme responsible for deactivation of bleomycin, is maintained in low levels in the lungs allowing the drug to accumulate in this tissue causing lung toxicity and subsequent development of fibrosis (Moeller et al., 2008).

This model involves administering bleomycin via a number of routes; intra-venous, intra-peritoneal, subcutaneous, oropharyngeal and intra-tracheal (*i.v.*, *i.p.*, *s.c.*, *o.p.* and *i.t.* respectively) to produce a delayed fibrotic response in various laboratory animals. *i.t* administration of bleomycin causes single stranded DNA breaks in epithelial cells evident at 4 hours and almost fully resolving 1 day post instillation (Chua et al., 2007). Failure to repair damaged epithelial cells results in cellular apoptosis/necrosis leading to the release of cellular content that in turn stimulates various inflammatory pathways. Alveolitis and oedema peak 3 – 9 days post bleomycin treatment before subsiding as a fibrotic response ensues (Chaudhary et al., 2006). Fibrosis can be identified biochemically and histologically as early as 14 days post *i.t.* administration with the maximum response falling between day 21 and 28 (Moore and Hogaboam, 2008). The bleomycin model is useful for studying both ALI and fibrosis, however, the model is not without its drawbacks. Early studies suggest that the fibrotic response is self-limiting beyond 28 days (Lawson et al., 2005). Both histological and biochemical assessment of collagen within the lungs shows that after peaking at 28 days the fibrosis begins to resolve which is not the case in IPF patients. This is a frequently debated feature of the bleomycin-induced lung fibrosis model as there is strong evidence demonstrating that collagen deposition in bleomycin treated mice does not resolve and increased lung collagen can be determined 3 months after

bleomycin instillation (Scotton et al., 2013). The pathological response of bleomycin-induced acute lung injury and pulmonary fibrosis is well characterised but, influenced by route of administration and concentration of the bleomycin, as well as host factors such as species, strain, age and gender of the animals used, highlighting the importance of characterisation of the model before use (Harrison and Lazo, 1987).

Since the introduction of the single dose bleomycin model, there has been great effort to try to optimise the model including producing a multiple dose model that typically involves administering a lowered dose of bleomycin every second week, when ALI has subsided, for 8 weeks. The advantages of this have been documented to be epithelial cell hyperplasia, temporal heterogeneity and, as previously mentioned, none self-resolving fibrosis (Degryse and Lawson, 2011). Despite this, the single dose model is still the most commonly used of the two as the multiple dose model still fails to fully replicate IPF, it takes much longer to perform the studies and the animals are at greater risk of harm due to multiple dosing.

1.6.2. Radiation-induced lung fibrosis

The development of pulmonary fibrosis after exposure to high doses of ionising radiation is well documented both clinically and experimentally (Coggle et al., 1986, Haston and Travis, 1997). Targeted radiation exposure to the thorax can therefore be utilised to elicit a pulmonary fibrotic response. Usually, the thorax is irradiated with a single fraction dose of between 10 – 20 Gray's (Gy). Irradiated mice develop pneumonitis as early as 10 - 12 weeks which is characterised by the accumulation of inflammatory cells within the alveoli leading to the loss of alveolar cells (Li et al.,

2009). Loss of lung parenchyma and a progressive accumulation of myofibroblast leads to alveolar collapse and the development of subpleural fibrosis (Li et al., 2009). The fibrosis is progressive and peaks 24 weeks post irradiation (Rube et al., 2000). The fact that fibrosis does not peak until 24 weeks makes this a very long-term model, however, imaging techniques such as CT and MRI scanning offer the potential to monitor disease progression non-invasively.

C57BL/6 mice are most commonly used in this model as certain strains of mouse such as C3H/HeJ and CBA/J appear to be resistant to radiation-induced fibrosis (Haston and Travis, 1997). Female mice are more sensitive than males and have a greater fibrotic score in response to irradiation (Haston and Travis, 1997).

1.6.3. Transgenic models of pulmonary fibrosis

The introduction of technologies that allow for genes to be inserted into laboratory animals and over expressed in specific tissues has allowed various new transgene models of pulmonary fibrosis to be generated. There are two main techniques that have been utilised in transgene pulmonary fibrosis models.

The first of these techniques is the use of adenoviral vectors that are delivered directly to the lung. Adenoviral vectors have been used to transiently overexpress genes in the lungs of rats. Both TGF-β1 and IL-1β gene expression peaked 7 days post insertion and returned to baseline in both studies by day 21. These transient increases in TGF-β1 and IL-1β cause lung collagen deposition in both models (Sime et al., 1997, Kolb et al., 2001).

To study the effects of permanent increases in gene expression, gene constructs can be inserted into pronuclei through microinjection of constructs into fertilised eggs. This technique has been used to overexpress both TNF-α, TGF-β and a list of other genes that make for less useful models of fibrosis (Miyazaki et al., 1995, Lee et al., 2004, Moore and Hogaboam, 2008). TNF-α over expressing mice are a useful model of pulmonary fibrosis with fibrosis being observed as early as 1-2 months but becoming more developed at 5 months suggesting a progressive disease state. Although TNF-α over expression is restricted to the type II alveolar epithelial cells containing the surfactant protein C (SP-C) promoter, there are some animals that die before birth and in the first couple of weeks of life; it is thought that these animals are the highest expressers (Miyazaki et al., 1995).

Triple transgenic models have been developed that not only allow for specific genes and specific tissue to be targeted but also allow the expression of genes to be regulated to some degree. CC10-tTS-rtTA-TGFβ_1 transgenic (tgTGF-β_1) mice have a complex inducible overexpression transgenic system. This triple transgenic system allows nuclear localisation to the lung as the CC10 promoter will only express the gene in that tissue. The second construct, tet-O-CMV-hTGF-β_1-SV40, means that biologically active TGF-β is produced. The final construct, CC10-tTS-hGH, has the CC10 promoter driving the expression of the tetracycline-controlled transcriptional silencer (tTS). Doxycycline (dox) is given to the animals in their food or water to switch on the tet-O–regulated TGF-β1 transgene (Lee et al., 2004). Fibrosis is seen as early as 7 days in these mice and is predominately in the subepithelial and adventitial regions of the airway at this time point. At 30 days, there is fibrosis in the alveolar parenchyma and honeycombing that causes an increase in chord length. Dox is not administered until the mice are fully developed, which could be one advantage

or could be given to aged animals to determine if this made any difference to the response. However, if the mice stop eating or drinking the dox due to ill health, this may cause expression of TGF-β to return to normal. Dox can also affect alveolar development and airway epithelial cell differentiation in certain backgrounds (Rawlins and Perl, 2012). Dox has been proven to ameliorate bleomycin-induced pulmonary fibrosis; this is thought to be through its effects on inflammatory processes as dox treatment post bleomycin-induced ALI day 10 does not affect lung hydroxyproline deposition (Fujita et al., 2006). It is therefore proposed that dox-induced transgenic models may serve better for discovery research rather than preclinical testing (Jenkins et al., 2017).

There are also transgenic mice that spontaneously develop fibrosis over time; these are discussed in age-related models of lung fibrosis, chapter 1.6.4.

1.6.4. Age-related models of lung fibrosis

Considering IPF is a disease of the ageing population, there are only a small number of models available where animals have an age dependent increase in fibrosis which more closely resembles the disease pathogenesis. It has been reported that older mice are more susceptible to bleomycin-induced pulmonary fibrosis (Sueblinvong et al., 2012). Using aged animals would increase the clinical relevance of the model. However, giving the extra time and money it takes to house mice for up to 24 months before using them, it has been deemed not practical to use aged mice in bleomycin studies for pharmacological testing, unless for a particular age-related target (Jenkins et al., 2017).

Genetically modified mice are frequently used in aged-related models of pulmonary fibrosis. Transgenic technology also allows for genes to be inserted that will not be expressed (knocked out). This has enabled the development of transgenic mice that spontaneously develop fibrosis over time. The transgenic deletion of genes for the receptor of the advanced glycation end products ($RAGE^{-/-}$ mice) or relaxin ($relaxin^{-/-}$ mice) have shown both increased lung hydroxyproline and collagen deposition, via histological sections, at 9 to 19 months of age (Englert et al., 2008, Samuel et al., 2003). Both gene and protein expression of RAGE are significantly reduced in lungs of late stage IPF patients (Englert et al., 2008). It has been proposed that loss of RAGE effects epithelial cell adherence to the extracellular matrix and therefore effects cellular spreading and potentially re-epithelialization (Demling et al., 2006). Relaxin is an inhibitor of collagen turnover as discussed by (Samuel, 2005) through various mechanisms including fibroblast activation and matrix metalloproteinase (MMP) induced degradation of collagenases. A novel peptide for the relaxin RXFP1/LGR7 receptor also ameliorates bleomycin-induced fibrosis (Pini et al., 2010). $Caveolin\text{-}1^{-/-}$ (cav-1) mice may also be useful as an age-related model of fibrosis as they spontaneously develop histologic findings consistent with pulmonary fibrosis at 12 months (Park et al., 2003). TGF-β1 has been shown to induce both the extracellular signal-regulated kinase (ERK) and the c-Jun N-terminal kinase (JNK) signalling pathways to produce collagen type I and fibronectin respectively and cav-1 can inhibit this (Wang et al., 2006).

1.6.5. FITC-induced lung fibrosis

Typically, BALB/c mice receive intratracheal administration of fluorescein isothiocyanate (FITC) (0.007 mg per g body weight in PBS). Instillation results in an inflammatory response with both neutrophil and monocytes infiltrating the lung interstitium within the first week (Moore and Hogaboam, 2008). There has also been protein leak into the BALF, detected at day 7 suggesting this model might be of use as an ALI model. Lung fibrosis is established between 14 and 21 days but is persistent out to 6 months and correlates closely with areas of FITC deposition, which can be visualised using immunofluorescent histology; this is a very useful tool as it provides a visual marker of where fibrosis should develop (Moore and Hogaboam, 2008).

1.6.6. Asbestosis

Murine models of asbestosis have been used for some time to investigate pulmonary fibrosis as the human disease shares a number of histopathological features with IPF, mainly the fibrosis being interstitial and has a basalsubpleural distribution (Roggli et al., 2010). The model involves administering asbestos fibres either intratracheally or through inhalation. Intratracheal administration results in an onset of fibrosis as early as 7 days and fully developed by 14 days. However, intratracheal administration of fibres can lead to less well distributed and patchy fibrosis mainly in central areas of the lung. Inhalation delivery of asbestos fibres requires special aerosolization equipment that can safely expose animals. The distribution of fibres throughout the lung is more homogenous, however, fibrosis is slower to develop, taking over one month. Regardless of the route of administration the mechanisms of action that lead

to this pathology are through the asbestos fibres causing oxidative stress and alveolar epithelial cell injury (Aljandali et al., 2001). M2 polarisation of macrophages and activation of T lymphocytes also results in the release of pro-fibrotic cytokines resulting in myofibroblast differentiation and ECM production as reviewed by (Tashiro et al., 2017)

1.6.7. Paraquat-induced pulmonary fibrosis

Paraquat, or N , N ′ -dimethyl-4, 4 ′ bipyridinium dichloride, is a widely used herbicide that causes the development of fatal pulmonary fibrosis in human and in laboratory animals. Paraquat is usually administered to rats or mice as either an *i.p.* or *s.c.* dose ranging from 10 – 15 mg/kg body weight (Seifirad et al., 2012, Rasooli et al., 2018, Shao et al., 2015). When paraquat is administered via the *i.p.* route there are normally two phases of paraquat poisoning which can lead to mortality. The first, acute phase poisoning, lasts between 24 and 48 hours and results from multiple organ damage caused by oxidative stress and lipid peroxidation (Fukushima et al., 2002). The second, later, phase of poising that leads to mortality, 2 weeks after administration, is due to progressive fibrosis especially in lungs.

1.6.8. Lipopolysaccharide-induced ALI

Lipopolysaccharide (LPS) is expressed on the outer membrane of gram negative bacteria and is a potent stimulator of the innate immune system (Park et al., 2009). Recognition of the LPS molecule is regulated through Toll-like receptor 4 (TLR-4) provoking the release of pro-inflammatory chemokines and cytokines such as TNF-α, interferon-γ (IFN-γ) and keratinocyte chemoattractant (KC) leading to an influx on

neutrophils into the lungs (Togbe et al., 2007). Exaggerated inflammation can lead to the damage of the alveolar epithelium mediated, at least in part, through increased neutrophil elastase (NE) activity (Smedly et al., 1986). This model is not routinely used to study the development of fibrosis as LPS is not known to elicit a fibrotic response (Moore and Hogaboam, 2008).

1.7. How well do these models reflect the disease

1.7.1. ALI

The models of ALI reviewed above each involve administering a substance to elicit some form of pulmonary insult that results in damage to the alveolar epithelium and matrix destruction and often relies on neutrophil influx. Histological assessment of lung tissue obtained from models of ALI demonstrate that they replicate the infiltration of leukocytes into the interstitial space and necrosis of AEC I seen in ALI (Matute-Bello et al., 2008). Damage to the epithelium allows leakage of fluid rich in plasma protein into the alveoli further exacerbating ALI (Matthay and Zimmerman, 2005). The characteristic increase of macrophages and neutrophils in BALF of ALI patients is also mimicked. Moreover, analysis of cytokines profiles in BALF shows further similarities with monocyte chemotactic protein-1(MCP-1), growth regulated oncogene-α (GRO-α) and GRO-β all being increased (Bhatia et al., 2012, Cavarra et al., 2004). The mechanisms by which lung injury is induced in these models is driven by non-specific immune responses which fits with the major causes of ALI (Christensen et al., 1999, Povirk and Houlgrave, 1988). LPS induced ALI in particular has clinical relevance as it has close links to sepsis induced ALI (Park et al., 2009).

1.7.2.IPF

Certain pathological features of IPF are well replicated in each of the models of lung fibrosis. In each model, fibrosis can be measured biochemically by an increase of collagen in the lung (Moore and Hogaboam, 2008). Histological analysis identifies a number of shared pathological features. Firstly, fibrotic lesions seen in animal models are located in the interstitial space resembling that of IPF patients (Moore and Hogaboam, 2008). The central role of the pleiotropic cytokine TGF-β in IPF is well documented. TGF-β is the most potent stimulator of ECM synthesis (Scotton and Chambers, 2007). TGF-β activity includes activation of fibroblast, increasing epithelial-mesenchymal transition (EMT) and fibroblast-myofibroblast differentiation all of which result in production of ECM (Wang, 2009). TGF-β is also capable of promoting apoptosis in epithelial and endothelial cells which is a key feature of IPF. An increase of TGF-β concentration within the lungs of IPF patients has been correlated with increased disease progression and is highest in patients within the later stages of the disease (Bartram and Speer, 2004). These features are also replicated in both the RILF and FITC models of this disease. TGF-β is increased during the fibrotic stages of both models and inhibition of TGF-β signalling can ameliorate the fibrotic response (Munger et al., 1999, Puthawala et al., 2008, Degryse et al., 2011).

1.8. How do these models differ from the disease

1.8.1. ALI

A major difference between animal models and ALI is that mice do not express IL-8. IL-8 plays an essential role in the influx of neutrophils into the lungs in humans however, in the absence of this molecule, mice mediate neutrophilia via KC and macrophage inflammatory protein 2 (MIP-2) (Modi and Yoshimura, 1999). Although still stimulating neutrophilia, this response is regulated through the mouse chemokine (C-X-C motif) receptor 2 (CXCR2) homologue, whereas the human IL-8 signals predominately through CXCR1 (Fan et al., 2007).

There are species differences in innate immune responses mainly due to differences in pattern recognition receptors, particularly TLRs, that play a crucial role in LPS recognition (Hajjar et al., 2002).

LPS model of ALI replicates the inflammatory response provoked by invading pathogens though the main underlying cause of sepsis induced ALI is through the release of exotoxins. As exotoxins are responsible for the severe epithelial and endothelial damage seen in sepsis, the LPS model only elicits an inflammatory response resulting in milder alveolar capillary membrane damage (Matute-Bello et al., 2008).

Table 1: Advantages and disadvantages of the various models of acute lung injury

Model	Advantages	Disadvantages

BLM	Well characterised response. Inflammatory response similar to that seen in ALI.	Lack of physiological relevance.
LPS	Clinically relevant aspects. Good model of neutrophil recruitment.	Damage to the epithelium and endothelium is minimal compared with ALI/ARDS.

1.8.2.IPF

Replicating this complex, chronic and progressive disease using animal models is challenging. IPF is a disease of unknown aetiology whereas the cause of fibrosis in all models of pulmonary fibrosis is some form of injurious agent. Therefore, as with models of ALI, the models of IPF mimic some of the key aspects of IPF without fully replicating the disease.

The bleomycin model does not truly represent the development of IPF. Bleomycin elicits an acute inflammatory response which is crucial to the development of fibrosis in this model as corticosteroid treatment prevents bleomycin-induced fibrosis (Dik et al., 2003). This is not however the case in IPF as corticosteroids have little or no reported effect (Chaudhary et al., 2006, Mapel et al., 1996). Furthermore, the rapid onset of fibrosis does not correspond to the slow progressive onset of fibrosis seen in IPF patients (Chua et al., 2005). Subpleural honeycombing is a well-documented feature of IPF and as previously stated is used for diagnosis. This feature is not present in bleomycin-induced pulmonary fibrosis. Furthermore, these models utilise young mice whereas IPF is a disease that effects older people, with age being a key risk factor.

Table 2: Advantages and disadvantages of the various models of pulmonary fibrosis.

Model	Advantages	Disadvantages
BLM	Short time frame (28 days).	Inflammation driven. Varied response. Fibrosis has been reported to be reversible.
RILF	Clinically relevant.	Time frame (4-6 months). High mortality. Expensive.
Transgenic models	Allows specific fibrosis-related genes to be studied.	Difficult and costly to generate transgenic animals. Transgenes are often overexpressed above physiological levels.
Age-related models	Spontaneous fibrosis development. Persistent fibrosis.	Prolonged time to develop fibrosis. Difficult and costly to generate transgenic animals.
FITC	Short time frame 14–21 days Visualise areas of lung injury using fluorescence imaging.	Not clinically relevant. Large response variation between batches of FITC.

	Persistent fibrosis out to 6 months.	
Asbestosis	Fibroblastic foci. Ability to visualize fibre deposition. Persistent fibrosis.	*i.t.* instillation may result in patchy fibrosis. Inhalation delivery difficult - due to safety.
Paraquat	Short term model. Uniform pulmonary fibrosis.	Systemic multiorgan damage.

1.9. Strategies to improve models

1.9.1. Endpoints

1.9.1.1. Inflammation

The inflammatory response is key to the development of ALI. Inflammatory responses are very complex processes involving numerous signalling pathways. As mentioned previously, no single model completely replicates the exact inflammatory response seen in ALI therefore it is important to fully understand what aspects of the disease state these models do replicate. This requires profiling the inflammatory response observed in each model. Characterisation of cellular and cytokine time courses within the lung will provide information that will allow accurate and informative data to be obtained from these models through the assessment of the most relevant outputs at the most appropriate time points.

1.9.1.2. Fibrosis

Traditional fibrotic endpoints have included hydroxyproline measurement and scoring of extent of histological damage. However, neither of these methods are used clinically and involve terminal procedures to obtain the tissue for analysis. Therefore, new ways of non-invasively investigating disease progression are required to assess the development of fibrosis longitudinally and which better reflect the measures that are obtained in the treatment of patients. High resolution computerised tomography (HRCT) scanning is a sensitive technique that is used clinically for anatomical imaging of the lung. This technology is now sensitive enough to determine architectural and density changes within the lungs of the small animals used in *in vivo* experiments. To achieve these highly sensitive images, scans are synchronised to a single respiratory phase, in a technique called respiratory gating, to reduce movement artefact brought about through breathing (Cavanaugh et al., 2004). More recently the use of SPECT imaging, a technique employed for measuring cellular signalling/functioning, has been utilised *in vivo*. The latest application of these imaging methods involves the combination of the two techniques allowing cellular functioning to be assessed in fibrotic regions identified via CT imaging. Although HRCT is clinically translatable it provides no functional data.

1.10. *Ex vivo* models of pulmonary fibrosis

1.10.1. Precision cut lung slice (PCLS) model

One recently developed strategy for studying pulmonary fibrosis *ex vivo* with the potential for reducing the use of animals includes the use of precision cut lung slices (PCLS) to model IPF. The PCLS model was originally developed as a tool for

investigating distal airway contractions in asthmatic lung tissue as lung slices maintain their structure and can be easily visualised (Dandurand et al., 1993, Bergner and Sanderson, 2002). As the technology has advanced over time, thinner tissue slices have now become attainable. The early studies conducted by (Dandurand et al., 1993), where the species used was rats, utilised slices 500 – 1000 µm thick whereas (Bergner and Sanderson, 2002) went on to use a vibrating microtome that allowed them to cut sections 75 µm thick from mouse lung. One major advantage of cutting thinner section is that more slices are obtained from one animal thus less mice would be used in an experiment.

The PCLS model of fibrosis uses lungs from mice that have been treated with bleomycin, and fibrosis allowed to develop for 28 days. The lungs are then sliced, between 150 to 300 µm thick, to be cultured *in vitro*. The development of fibrosis can be assessed via various methods in these sections. This technology allows for a large number of treatments and endpoints to be assessed on just the one lung as over 40 tissue slices are obtainable from one animal.

PCLS can be taken from human tissue as well, whether this is from biopsy or post mortem donor, allowing human tissue to be cultured and providing a direct insight into diseased tissue.

1.11. Key biological pathways involved in lung injury and fibrosis

1.11.1. Transforming growth factor-β (TGF-β)

The role of TGF-β on the development of pulmonary fibrosis has been described previously in this chapter. However, due to the importance of TGF-β in the development of ALI and IPF and the various techniques utilised for measuring TGF-β activity in this thesis, TGF-β and its signalling will be reviewed in greater detail. TGF-β exists in three different isoforms: TGF-β1, TGF-β2 and TGF-β3 in mammals. These TGF-β isoforms form part of a larger TGF-β super family including the bone-morphogenetic proteins (BMP), activins, inhibins and growth and differentiation factors (GDF) families. This family of cytokines have structural similarities and can all be characterized by a distinctive cysteine knot (Daopin et al., 1992). Evolutionary studies suggest that the BMPs/GDFs diverged firstly into activins and inhibins and later into the TGF-βs (Hinck, 2012).

1.11.2. TGF-β structure

All three isoforms of TGF-β share between 64 % and 82 % sequence homology, however, each isoforms gene is expressed on a different chromosome: in humans TGF-β1 is found at 19q13, TGF-β2 - 1q41and TGF-β3 -14q24 and for mice chromosomes 7, 1 and 2 respectively (Massague, 1990). TGF-β is synthesized as a large latent protein, with a mass of 75kDa, that, to exert a biological effect, requires activation. Its bioavailability is regulated through the noncovalent association with the TGF-β pro-peptide homodimer, also referred to as the latency associated peptide (LAP). The LAP then forms a disulphide link with a latent TGF-β binding protein

(LTBP) to form a large latent complex (LLC) (Miyazono et al., 1991). There are 4 structurally similar LTBP isoforms each with varying affinity (Saharinen and Keski-Oja, 2000). A key function of the LTBP is to allow tethering of latent TGF-β to the ECM where it can be stored for quick and localised activation when required.

1.11.3. TGF-β activation

TGF-β is activated via a number of physical and biological processes. Physiological processes include extreme changes in heat and pH (acidification) and oxidation (Pociask et al., 2004, Brown et al., 1990). Biological activation includes proteolytic cleavage of the disulfide linkages formed between the LAP and LTBP (Annes et al., 2003). These include MMP-2 and -9. Other mechanisms of activation include Thombospondin-1 binding to the LAP complex causing conformational changes that allow for the active TGF-β domain to access the TGF-β receptor (Murphy-Ullrich and Poczatek, 2000). Another well documented molecule that binds to the LAP and causes conformational changes to activate the TGF-β molecule is integrin αvβ6.

1.11.4. Integrin mediated TGF-β activation

Integrins are transmembrane proteins that are primarily involved in cell-cell adhesion and binding of extracellular proteins. Integrins are αβ heterodimers and to date there are 24 distinct associations made up from 8 β subunits and 18 α subunits (Hynes, 2002).

It is the αvβ1, αvβ3, αvβ5, αvβ6 and αvβ8 integrins that have shown specificity to interact with TGF-β_1 and TGF-β_3 via the tripeptide, arginine–glycine–aspartic acid

(RGD) sequence (Munger et al., 1999, Mu et al., 2002). αvβ6 integrin mediated TGF-β activation is important in *in vivo* models of pulmonary fibrosis, as inhibiting αvβ6 or preventing its expression can inhibit the development of fibrosis (Munger et al., 1999, Puthawala et al., 2008, Horan et al., 2008, Yang et al., 2007). Although αvβ6 integrin expression is low in the alveolar epithelium at baseline, the αvβ6 integrin is constitutively bound to the TGF-β molecule, leading to a primed system ready to react to injurious stimuli. Myofibroblast have been shown to activate latent TGF- β bound to αvβ5 in the extracellular matrix via contractile forces (Wipff et al., 2007). *itgb6* expression is increased in IPF patients which is promoting an increase in TGF-β activation which in turn leads to up-regulation of *itgb6* expression (Xu et al., 2009, Araya et al., 2007). This suggests that TGF-β and αvβ6 act as a self-amplifying paracrine loop. Expression levels of αvβ6 are linked with disease progression and therefore make for potential targets for monitoring disease progression, which will be discussed in greater detail in chapter 4.1.

Both thrombin and LPA have been shown to promote αvβ6 mediate TGF-β activation via the G-protein coupled receptors PAR1 (protease-activated receptor-1) and LPAR2 (LPA receptor 2) respectively (Howell et al., 2002, Tager et al., 2008). The G-protein G_{aq}, induces a signalling cascade that includes the activation of RhoA and Rho kinase that results in actin polymerization and cellular traction on the cytoplasmic domain of the αvβ6 integrin. This results in activation of the large latent TGF-β complex which is tethered to the ECM through binding to the αvβ6 integrin (Xu et al., 2009, Goodwin and Jenkins, 2009).

1.11.5. TGF-β signalling

The TGF-β family of receptors are a highly versatile group of transmembrane serine/threonine kinase receptors comprising of seven type I receptors, which are known as activin receptor-like kinases (ALKs), and five type II receptors (Derynck and Zhang, 2003). For the purpose of this thesis I will discuss the mechanisms of TGF-β receptor activation relevant to pulmonary fibrosis, as there are over 40 ligands for this family of receptors each with varying signalling pathways.

As previously mentioned, TGF-β is sequestered in the ECM in its inactive form and requires activation to elicit its biological effects (Rifkin, 2005). Once activated, TGF-β signals through binding to TGF-βRII causing the receptor to transphosphorlyate a type I receptor, also known as ALK5, activating its kinase domain (Derynck and Zhang, 2003). The activated serine/threonine kinase domain phosphorylates the receptor-activated (R) Smads, Smad2 and Smad3. These Smads then form a heterotrimeric complex with Smad4 before migrating to the nucleus to exert its regulatory effects on gene expression (Heldin et al., 1997). Mice that do not express Smad2 die during embryo development, however, mice that do not express Smad3 are protected from the development of bleomycin-induced pulmonary fibrosis (Zhao et al., 2002, Nomura and Li, 1998). This suggests that TGF-β signalling through Smad3 is essential for the development of bleomycin-induced fibrosis. Measuring the protein expression or immunohistochemical detection of phosphorylated-Smad2 in lung cells or macrophages collected from bronchoalveolar lavage has become a routine measurement of TGF-β activity that is utilised in this thesis.

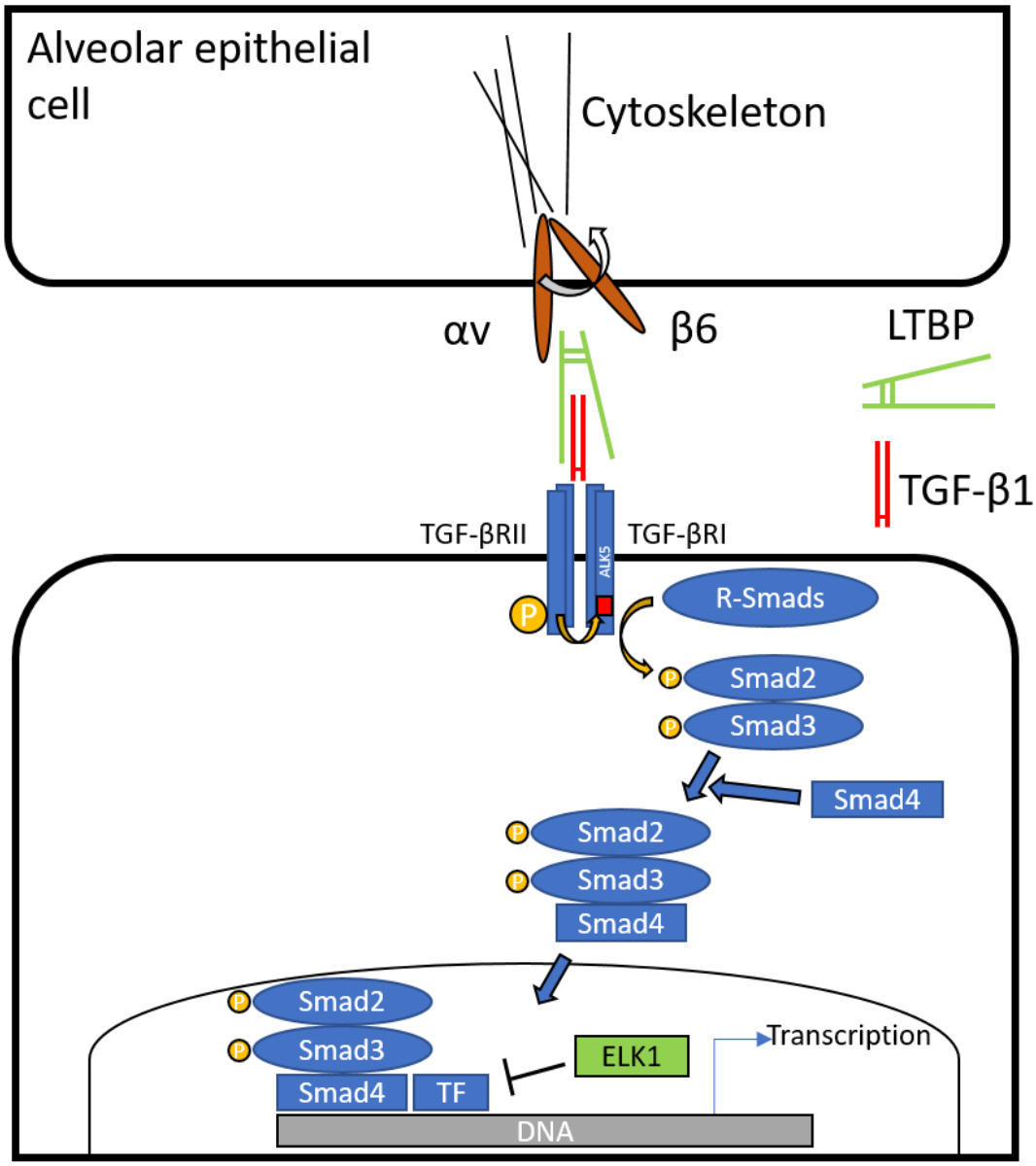


Figure 1.1 TGF-β signalling pathway. Injurious stimuli cause activation of the integrin αvβ6, one possible mechanism is through contraction of the cytoskeleton causing a conformational change of αvβ6. This leads to activation of the TGF-β molecule through structural changes to the latent TGF-β complex. Once activated TGF-β signals through binding to TGF-βRII causing the receptor to transphosphorylate a type I receptor, also known as ALK5. The activated serine/threonine kinase domain (red square) phosphorylates the receptor-activated (R) Smads, Smad2 and Smad3. These Smads then form a heterotrimeric complex

with Smad4 before migrating to the nucleus to exert its regulatory effects on gene expression through transcription factors (TF). In the case of the αvβ6 TF, ELK1 can repress it to supress TGF-β induced αvβ6 increased expression.

1.11.6. The role of TGF-β in ALI and IPF

TGF-β is pleotropic and has effects on the alveolar epithelium resulting in epithelial-to-mesenchymal transition (EMT), alveolar cell injury, lung fibroblast ECM deposition resulting in collagen deposition and inflammation (mast cells stimulated by TGF-β release various cytokines) (Wahl et al., 1987, Degryse et al., 2011). TGF-β also induces macrophages and is responsible for fibroblast recruitment (Fernandez and Eickelberg, 2012).

TGF-β plays an important role in the resolution of ALI as TGF- β1 null mice have an exaggerated bleomycin-induced inflammatory response and this is also replicated in β6 null mice, that also reduced TGF- β activation (Huang et al., 1996, Munger et al., 1999). TGF-β also causes down regulation of genes of matrix degrading proteinases that may affect wound repair and the resolution of ALI (Overall et al., 1989).

Integrin β6 null mice are protected from the development of pulmonary fibrosis demonstrating both that TGF-β is important in the development of bleomycin-induced pulmonary fibrosis as well as activation by integrin β6 being a critical step in this process (Munger et al., 1999). TGF-β promotes collagen deposition in the extracellular matrix via the upregulation of ECM genes, primarily collagen type I and III (Kenyon et al., 2003).

TGF-β stimulates epithelial-to-mesenchymal transition (EMT). Overexpression of TGF-β1 in mice caused epithelial cells to express mesenchymal markers, β-galactosidase (β-gal), at three weeks. Similar results have been shown *in vitro* using primary cells, however, when cultured on a collagen matrix cells were prone to apoptosis when treated with TGF-β1 suggesting a mechanism for limiting physiological repair after injury (Kim et al., 2006).

TGF-β can induce epithelial cell apoptosis and it has been shown that blocking apoptosis can ameliorate the fibrotic response (Lee et al., 2006). Furthermore TGF-β has been shown to stimulate the production of reactive oxygen species and NADPH oxidase 4 is highly expressed in fibroblast foci from IPF patients (Hecker et al., 2009). Reactive oxygen species are able to damage cells at the macromolecular level, including DNA.

1.11.7. Secretory leukocyte protease inhibitor

It has been suggested that SLPI can affect TGF-β activation. The concentration of active TGF-β is increased in the wounds of SLPI null mice coinciding with increased scar tissue in fully healed wounds (Ashcroft et al., 2000, Angelov et al., 2004). This increase in active TGF-β in cutaneous wounds of SLPI null mice can be reduced via treatment with exogenous SLPI suggesting that proteases may activate TGF-β and promote fibrosis (Ashcroft et al., 2000). TGF-β is activated via a number of physical and biological processes. Biological activation of TGF-β is also conducted via a number of protease, notably plasmin, tryptase, thrombin, elastase, MMP-2 and MMP-9 (Coward et al., 2010a). Latent TGF-β can be released from the ECM of epithelial cells via serine proteases (Taipale et al., 1994). In bleomycin-induced

pulmonary fibrosis TGF-β is not activated in *ne*$^{-/-}$ mice (Chua and Laurent, 2006). These findings suggest that NE has a role in both the release and activation of TGF-β, however, the mechanisms by which NE activates TGF-β remains unclear.

1.11.8. The role of proteases in IPF

Serine proteases such as NE, cathepsin G (CAT G) and proteinase-3 (PR-3) are present in the respiratory tract with basal activity being regulated by protease inhibitors. Serine proteases play a key role in innate immunity within the lung (Tkalcevic et al., 2000). Serine proteases are released in large quantities from activated neutrophils and are also present on the surface of these cells (Owen et al., 1995). Their substrates include almost all matrix proteins, particularly elastin, and, to a lesser extent, a number of other molecules that make up the basement membrane such as collagen, laminin, fibronectin and vitronectin (Chua and Laurent, 2006). IPF patients have significantly increased levels of NE in both BALF and within the lung parenchyma (Obayashi et al., 1997, Hojo et al., 1997). It is not yet fully understood whether this increase is the cause of the fibrosis or if it is a consequence of neutrophilic inflammation, however, mice null of *ne*$^{-/-}$ are resistant to bleomycin-induced pulmonary fibrosis (Chua and Laurent, 2006).

Protease activity is finely controlled by the presence of a number of protease inhibitors. SLPI is an 11.7 kDa protein containing a protease inhibitory site located at leucine 72 in the carboxy-terminal domain (Abe et al., 1991). In alveoli, SLPI is predominately secreted by epithelial cells in response to various inflammatory stimuli (Abe et al., 1991). SLPI is expressed throughout the lungs and accounts for as much as 80 – 90 % of the total inhibition of NE in the lung (Zani et al., 2011). It is

reported, in a number of disease states, a shift in the balance of protease/anti-protease activity can lead to damage of the surrounding tissue (Stockley, 1999).

Various studies have demonstrated the importance of regulating NE activity. In animal models of both lung injury and fibrosis, inhibition of NE has been reported to have a protective role (Taooka et al., 1997, Sakashita et al., 2007). In the absence of SLPI, elastolytic activity in dermal and mucosal wounds is enhanced resulting in prolonged wound repair and a substantial increase in inflammatory cell accumulation within the wound (Ashcroft et al., 2000, Angelov et al., 2004). In contrast to this, administration of truncated SLPI, in a bleomycin-induced pulmonary fibrosis model, protects against increases in elastolytic activity and the resulting decreases in body weight and survival rate, leading to amelioration of pulmonary fibrosis (Mitsuhashi et al., 1996).

1.11.9. The role of ELK1 in IPF

Ets domain-containing protein Elk1 (Elk1) is a transcription factor from the ETS family of transcriptional regulators. Elk1 is a ternary complex factor (TCF) and binding of MAP kinase to the MAP kinase domain results in phosphorylation of TCFs and enhanced transcriptional activation potential (Yang et al., 2002). However, the unphosphorylated ELK1 can repress transcription through the R domain. Elk1 binds to the ITGB6 promoter, which contain two Elk1 binding sites, and represses ITGB6 and αvβ6 expression *in vitro* (Tatler et al., 2016b). Treatment of lung epithelial cells with Elk1 siRNA reduces Elk1 protein expression and increases αvβ6 expression (Tatler et al., 2016b). Lung tissue taken from patients with pulmonary fibrosis have shown to have decreased expression of ELK1 in the epithelium and

high levels of αvβ6 in comparison to normal lung tissue that has higher levels of Elk1 and lower levels of αvβ6. In response to bleomycin, *Elk1* null ($^{-/0}$) mice have increased αvβ6 expression and lung fibrosis as assessed by both increases in hydroxyproline and masons trichrome staining (Tatler et al., 2016b).

1.11.10. Tranilast as a treatment for pulmonary fibrosis

Tranilast (N(3,4dimethoxycinnamoyl) anthranilic acid) has been used clinically to treat allergic respiratory diseases such as asthma for some time as it prevents histamine release from mast cell through the inhibition of Ca^{++} uptake in these cells (Koda et al., 1985). However, more recently its effects on TGF-β inhibition and inhibition of fibroblast proliferation have shown it to be useful as a potential antifibrotic agent. Firstly, it has been shown to inhibit TGF-β secretion in keliod scars (Yamada et al., 1994). Tranilast also has inhibitory effects on vascular smooth muscle cells which have been stimulated by TGF-β1, further suggesting that Tranilast may inhibit TGF-β (Tanaka et al., 1994). Tranilast has been previously shown to supress bleomycin-induced fibrosis in mice, when administered orally, however it was administered prophylactically and its effect may have been related to inhibition of alveolar macrophages (Mori et al., 1995). No one has as yet tested it in a therapeutic model.

1.11.11. Other key biological pathways

1.11.11.1. Platelet-derived growth factor

Platelet-derived growth factor (PDGF-A, -B, -C and -D) are tyrosine kinases and interact with two types of PDGF receptors (PDGFRs) α and β (Andrae et al., 2008). PDGFR are expressed on fibroblasts, macrophages, vascular endothelial cells and platelets (Heldin and Westermark, 1999). PDGF has been linked with bleomycin-induced pulmonary fibrosis as animals treated with bleomycin have increased gene and protein expression of PDGF-A and -C (Maeda et al., 1996, Shimizu et al., 2003). Reports show patients with IPF have increased expression of PDGF in both epithelial cells and alveolar macrophages but the mechanisms in which expression is increased is still not understood (Antoniades et al., 1990). Nintedanib, a multikinase inhibitor that inhibits PDGF, vascular endothelial growth factor (VEGF) and fibroblast growth factor (FGF), reduced the decline in lung function and number of acute exacerbations in IPF patients (Richeldi et al., 2014) VEGF and FGF are two further growth factors with links to IPF. Although the role of angiogenesis is unclear, serum levels of VEGF have been shown to be increased in IPF patients (Ando et al., 2010). VEGF receptor-2 (VGFR-2) inhibited pulmonary collagen deposition in the bleomycin-induced pulmonary fibrosis model, however, only when the tyrosine kinase inhibitor SU5416 was administered during the inflammatory stage of the model. If mice are treated only during the fibrotic stages of the model, day 15-28, there is no effect on collagen deposition (Ou et al., 2009).

1.11.11.2. Connective tissue growth factor

Connective tissue growth factor (CTGF) is a 36 to 38 kDa peptide with biological functions that include fibroblast proliferation, cellular adhesion, angiogenesis and collagen synthesis (Ihn, 2002). CTGF has been proposed to signal through the PDGFR as is competes with PDGF-B for binding to fibroblast PDGFR-B (Bradham et al., 1991). CTGF signalling in pulmonary fibroblast has also been demonstrated through the Rac1/mixed-lineage kinase 3 (MLK3)/JNK signalling cascade that in turn leads to activator protein-1 (AP-1) activation and recruitment to the collagen 1 promoter (Lin et al., 2013). Anti-CTGF antibody treatment reduces lung collagen deposition in a bleomycin-induced pulmonary fibrosis model (Wang et al., 2011).

1.12. Methods for measuring TGF-β activity

1.12.1. pSmad2 ELISA

TGF-β activity *in vivo* can be assessed via pSmad2 ELISA. TGF-β causes the phosphorylation of Smad2 upon activation of the TGF-β receptor. TGF-β is found bound to integrin on the surface of type II epithelial cells which are in direct contact with alveolar macrophages that express TGF-β receptors. Therefore, a global assessment of TGF-β alveolar activity can be obtained by measuring pSmad2 levels in macrophages obtained from BAL fluid. This is the most common and simple method for quantitively measuring TGF-β activity *in vivo*. This technique only provides you with colour changes for a positive result and it is possible to get false positive through non-selective binding. Therefore, it is sometimes appropriate to attain visual confirmation of changes in TGF-β activity to accompany this assay, such as immunohistochemical staining (1.11.2).

1.12.2. pSmad2 immunohistochemistry

A phosphorylated Smad2/3 antibody (Cell Signaling Technology) is used for immunohistochemical staining of pSmad2. Although this technique does not allow quantification of pSmad2 it provides information into the location of pSmad2 expression and thus TGF-β activity. Identification of the cells and tissues expressing pSmad2 is the key advantage of this technique.

1.12.3. Transformed Mink Lung Cell (TMLC) assay

Transformed Mink Lung epithelial Cells (TMLC)s are a reporter cell line for measuring TGF-β activity. TMLCs have a transfected construct containing a truncated plasminogen-activator inhibitor-1 (PAI-1) promoter fused to a firefly luciferase gene (Abe et al., 1994). These cells can be used to measure the amount of all three isoforms of TGF-β in a biological sample, usually conditioned media taken from cell culture or PCLSs. Active TGF-β in the samples bind to TGF-β receptors on the TMLC causing promotion of the PAI-1 gene also the firefly luciferase gene to be transcribed therefore TGF-β activity in the biological sample can be measured through luminescence measurement (John et al., 2017). A TGF-β standard curve can be generated to calculate the actual amount of TGF-β in the sample.

TMLCs can also be used in a coculture system with mouse embryonic fibroblasts (MEF)s that are stably transfected with the αvβ6 integrin (MEF-β6). The coculture determines the effects of a treatment specifically on αvβ6-mediated TGF-β activation. TMLCs are cocultured as direct cell-cell contact is required (Porte and Jenkins, 2014).

1.13. Aims and Hypothesis

The initial two aims of this thesis are to establish and further characterise the bleomycin-induced and radiation-induced pulmonary fibrosis models. Once these models are fully established 'in house' they can be used to test aims 3 - 5:

1) Characterise and evaluate the bleomycin model of lung fibrosis in both mice and rats.
2) Characterise and evaluate the radiation model of lung fibrosis.
3) Use novel SPECT/CT imaging to determine if αvβ6 can be used as a prognostic biomarker in the radiation-induced pulmonary fibrosis model.
4) Use the bleomycin model of fibrosis to assess the role of SLPI, Elk1 and the TGF-β inhibitor, Tranilast, in the development of pulmonary fibrosis.
5) Evaluate precision cut lung slices to assess the potential for anti-fibrotic molecules.

2 Materials and Methods

2.1. Animals

Slpi null mice *Slpi*$^{-/-}$ and heterozygous *Slpi*$^{-/+}$ mice on a B6D2F1 background were kindly donated by Sharon Wahl (Ashcroft et al., 2000). C57Bl/6 mice were obtained from Charles River UK (Margate, Kent, U.K.). *Slpi*$^{-/-}$ were crossed with C57Bl/6 mice to generate *Slpi*$^{-/+}$. Mice were subsequently backcrossed to C57Bl/6 for at least 5 generations to generate *Slpi*$^{-/-}$ mice on a C57Bl/6 background.

Elk1$^{-/0}$ mice were a gift from Alfred Nordheim (Tubingen, Germany). *Elk1*$^{-/0}$ mice were generated by Flp recombinase-mediated cassette exchange (RMCE) (Cesari et al., 2004). *Elk1* is only found on the x chromosome with /^{0} signifying the y chromosome.

Mice were held within the Biomedical Services Unit, University of Nottingham for at least 7 days after delivery. Animals had free access to food (Tekland Global 18% protein rodent diet; Bicester, Oxen, U.K.) and water.

2.2. Genotyping

Mice were genotyped from DNA isolated from ear notch biopsies by polymerase chain reaction (PCR) analysis. The presence of the *Slpi* allele was detected by primers: sense (5′- CAAGGCCTTCTGTGTGTAACTTC -3′) and antisense (5′- CTGCTACAGAGTAGGTGGCAGAC -3′), resulting in a 490-bp PCR product and the Neo cassette allele by primers sense (5′- CGCTTCCTCGTGCTTTACGGTATC -3′) and antisense (5′- GATGCCAGGCATTTGCACTGCCG -3′), gives a 344-bp product.

The presence of the wild-type Elk1 locus was detected by primers: sense (5′-GTGGGTAGGCGGGTGGGTGGGAAGTAAG -3′) and antisense (5′-TGGGGAAGCAAAACAAGTAGTGGAGACGAG -3′), resulting in a 340-bp PCR product and the RMCE16 mutant Elk1 locus by primers sense (5′-GCCCCTCCCCCGTGCCTTCCTT -3′) and antisense (5′-TAGCAGCCACAACCAATCCATTTCTCCATC -3′), gives a 780-bp product.

PCR reactions were analysed via electrophoresis on ethidium bromide stained agarose gels. Samples were run for 30 minutes at 100 V. A 100 base pair DNA ladder was added to all gels for accurate band identification.

2.3. Bleomycin Model

The ARRIVE (Animal Research: Reporting of *In Vivo* Experiments) guidelines were adhered to in the planning and reporting of all *in vivo* experimentation (Kilkenny et al., 2010).

All animal care and procedures were approved by the University of Nottingham Ethical Review Committee and were performed under Home Office Project and Personal License authority within the Animal (Scientific Procedures) Act 1986.

All animals were held under pathogen-free condition, within individually ventilated cages: 4 mice per cage or 3 rats per cage, under 12:12 light/dark cycles.

2.3.1. Mouse

Mice (C57BL/6, 6 – 8 weeks old, male) were anaesthetised with isoflurane-anaesthetic (2.5 %, 2 L/min flow of oxygen) and exposed to 15, 30, 50 or 75 IU of

bleomycin sulphate (Kyowa Hakko, Slough, UK) in 50 µl sterile 0.9 % saline (Sigma), or 50 µl sterile 0.9 % saline control, via oropharyngeal administration (*o.p.*) (day 0). ALI and inflammation was assessed at day 4 and the development of pulmonary fibrosis was assessed at day 28. Mice were terminally anesthetised with Euthatal (MerialAnimalHealth, Bracknell, UK).

2.3.2. Rat

Rats (Lewis, 7 weeks old, male) were anaesthetised with isoflurane-anaesthetic (2.5 %, 2 L/min flow of oxygen) and exposed to 500 IU of bleomycin sulphate (Kyowa Hakko, Slough, UK) in 250 µl sterile 0.9 % saline (Sigma), or 250 µl sterile 0.9 % saline control, via oropharyngeal administration (*o.p.*) (day 0). ALI was assessed at day 7 and the development of pulmonary fibrosis was assessed at day 21. Rats were terminally anesthetised with Euthatal.

Dose response studies were conducted using a range of bleomycin doses (300, 400, 500, 750 and 1000 IU).

2.4. Bronchoalveolar lavage

Mice were terminally anaesthetised, the trachea was cannulated and the lungs lavaged with a total of 1 ml sterile phosphate buffered solution (PBS). Cells were pelleted and the supernatant removed and stored at -80 °C for further analysis. Cell pellets were resuspended in 200 µl sterile PBS and centrifuged (Cytospin 4, Shandon, UK) at 450 rpm (23 x g) for 6 minutes. The slides were allowed to air-dry

prior to fixation in methanol and haematoxylin and eosin (H&E) staining (RAPIDIFF, Biotechnology Sciences Ltd, UK). At least 100 cells per sample were differentiated, using conventional morphological criteria for macrophages/monocytes, lymphocytes and polymorphonuclear leukocytes (PMNs).

2.5. Histology

The trachea was cannulated and the pulmonary vasculature perfused with 10 ml of heparinized PBS (40 U/ml) via the pulmonary artery. The lungs were then insufflated with formalin under constant gravitational pressure (20 cm H_2O), and the lungs removed *en bloc* and fixed in 10 ml of formalin. Fixed tissues were embedded in paraffin wax prior to sections 5 µm thick being cut, rehydrated in graded alcohol and stained by H&E and Masson's trichrome.

2.5.1. Haematoxylin and Eosin stain

Sections were incubated in Mayer's haematoxylin for 1 minute. Excess stain was rinsed off in tap water for 1 minute. Then the sections were incubated in acid/alcohol for 1 minute (350 ml ethanol, 145ml distilled H_2O, 0.5 ml HCL). Alcohol was removed from slides by briefly rinsing the slides with tap water. Sections were incubated in eosin for 3 minutes and excess eosin removed by briefly rinsing the slides in tap water. Slides were then dehydrated in graded alcohol prior to mounting.

2.5.2. Masson's Trichrome

Sections were incubated in Bouin's solution overnight. Excess Bouin's solution was then rinsed off with tap water. Slides were incubated in Weigert's reagent (Weigert's: 50:50 mixture of Solution A: 1 % haematoxylin in 100 % ethanol Solution B: 4 ml 30 % ferric chloride, 1 ml HCL (12 N) and 95ml sterile H_2O) for 5 minutes. Slides were then rinsed under running tap water for 5 minutes before being rinsed in double distilled water for 30 seconds. Sections were stained in Biebrich scarlett acid fuchsin for 5 minutes (0.9 % Biebrich, 0.1 % Fuchsin, 1 % acetic acid) and then rinsed in double distilled water for 30 seconds. Slides were then incubated in phosophomolybdic acid/phototungstic acid / distilled water (1:1:2) for 7 minutes. Transferred immediately into analine blue (2.5 % analine blue, 2 % acetic acid in distilled water) for 5 minutes. Washed in double distilled water for 2 minutes. Incubated in 1 % acetic acid for 3 minutes. Slides were then dehydrated in graded alcohol and cleared in xylene prior to mounting.

2.6. Ashcroft scoring

50 μm^2 sections of Masson's Trichrome stained tissue was assessed using the criteria set out in table (3). 8 random fields were chosen and scored, the mean score was determined for that animal then the mean for all the animal within each treatment group was reported. If a region is displaying aspects of two descriptions on the scoring system, then it should be given the score between the two descriptions. For example, there is minimal fibrous thickening throughout the alveolar walls but there is the very occasional patch where there is moderate thickening this would be scored as a grade 2.

Table 3: Ashcroft scoring system - adapted from (Ashcroft et al., 1988)

Grade of fibrosis	Histological features
0	Normal lung
1	Some minimal fibrous thickening of alveolar or bronchiolar walls.
2	
3	Moderate thickening of walls but without damage to the underlying lung architecture.
4	
5	Definite damage to the lung structure with increased fibrosis now with small fibrous masses present.
6	
7	Severe distortion of structure and large areas of fibrosis. “honeycombing of the lung”.
8	Total fibrous obliteration of the field of view.

2.7. Immunohistochemistry

5µm thick lung tissue sections were deparaffinized in xylene and rehydrated in graded ethanol. Antigen retrieval was performed via heating sections in 10mM sodium citrate buffer (pH 6.0) in a microwave for 10 min or via proteolytic digestion with pepsin for 15 minutes at 37 º C (anti-β6 and anti-pSmad2 only). Subsequently, endogenous peroxidase activity was blocked by incubating sections in 3 % H_2O_2 in

methanol for 30 minutes. Nonspecific antibody binding was blocked using goat serum (Sigma Aldrich) for 30 minutes, prior to incubation with human anti-mouse collagen type I (2 μg/ml), III (1 μg/ml), IV (0.5 μg/ml), VI (0.5 μg/ml) (Abcam, Cambridge, UK), chimeric anti-β6 (ch2A1) (0.5 μg/ml) (Hahm et al., 2007), and a phosphorylated Smad2/3 (#3108) (13.3 μg/ml) (Cell Signaling Technology Boston, MA), primary antibody overnight at 4 °C. A negative control IgG isotype was used for all antibodies to determine non-specific staining as well as no primary antibody controls. Sections were then incubated with a biotin-conjugated secondary antibody. Biotin-conjugated secondary antibody was detected through incubation with an avidin/biotinylated enzyme complex (ABC) solution (Vector Laboratories) for 30 minutes; colour development was performed using 3,3′-diaminobenzidine tetrahydrochloride (Sigma). Sections were counterstained using Mayer's hematoxylin and visualized under a Nikon 90i light microscope.

2.8. Quantification of collagen stain in lung tissue sections

Whole cross sections of the lung lobes were taken at x10 magnification and stitched together using the NIS-Elements software (Nikon instruments) The total area of collagen I, III, IV and VI, positively stained tissue, in fibrotic lesions greater than 7,500 μm^2, was measured by manually drawing around stained, brown tissue. A single cross section from all five lung lobes, per mouse, were analysed and total area of positively stained collagen was calculated as a percentage of total lung tissue area.

2.9. Analysis of lung collagen content

Lungs were removed and immersed immediately in liquid nitrogen prior to storage at -80 °C. Frozen lung tissue was ground using a pestle and mortar. Approximately half of the ground lung, was weighed and used for the measurement of lung hydroxyproline (µg per mg of lung tissue or µg/lung set). 125 µl 50 % trichloroacetic acid (Sigma) was added to each sample and allowed to incubate on ice for 20 minutes. Samples were centrifuged at 528 x g for 10 minutes at 4 °C. Supernatant was removed and discarded. Collagen was then hydrolysed via re-suspending each pellet in 1 ml of HCL (12 N) (Fisher chemicals) and baking overnight at 110 °C. Baked samples were resuspended in 2 ml of sterile H_2O. Ensuring that the samples were fully mixed, 200 µl of each sample or standard (1000, 750, 500, 250, 125, 62.5, 31.25 and 0 µg/ml) was added to 1.5 ml tubes. Samples were oxidised in 500 µl chloramine T (Sigma) for 20 minutes at room temperature, prior to addition of 500 µl of Ehrlichs solution (Sigma) and incubation at 65 °C for 15 minutes. Samples were then incubated at room temperature for 2 hours prior to colourimetric analysis at an OD of 550 nm.

2.10. Wet:dry weight ratio

Lungs were excised and extrapulmonary connective tissue removed by dissection prior to recording lung “wet” weight. Lungs were then incubated at 60 °C for 24 hours, to remove all lung water, prior to measuring the “dry” weight. Wet:dry weight ratios were calculated.

2.11. Neutrophil elastase activity

28 days post-bleomycin treatment, lungs were excised and snap-frozen in liquid nitrogen prior to storage at -80 °C. Lung tissue was ground to a fine powder under liquid nitrogen and resuspended in 1 ml 0.1 M Tris (pH 7.4). After 3 cycles of freezing and thawing, the lung lysates were centrifuged at 10 000 x g for 30 minutes at 4 °C. Neutrophil elastase (NE) activity was measured in lung homogenate using the synthetic fluorescent, MeOSu-AAPV-AMC substrate (Santa-Cruz, Dallas, TX, USA). Lung homogenate (1.5 mg/ml protein concentration) was incubated with MeOSu-AAPV-AMC (0.1 nM final concentration) in 0.1 M Tris (pH 7) (total volume 250 µl) in a black bottom/wall 96 well plate and the amount of NE released fluorescent product was determined at 2 hours. Plates were read using excitation 355 nm and 460 nm emission wavelengths; background fluorescence of the substrate only was subtracted from each sample.

2.12. Zymography

MMP-2 and MMP-9 activity was assessed via gelatine zymography. 10 µl of lung homogenate, was diluted in Tris-Gly SDS Zymogram 1:4 (Invitrogen) and incubated at 21 °C for 10 minutes. 15 µl of sample, (or standard) was loaded onto sodium dodecyl sulfate-polyacrylamide (SDS-PAGE) gels containing 1 mg/ml gelatin (Invitrogen) and subjected to electrophoresis at constant voltage of 125 V for 100 minutes. The gels were incubated at 21 °C (room temp) for 60 minutes in 100 ml of Zymogram renaturing buffer (Invitrogen) to recover enzymatic activity. Gels were then further incubated in Zymogram developing buffer (Invitrogen) for 1 hour prior

to overnight incubation at 37 °C. Gels were then stained with coomassie blue-stain (Coomassie Blue 0.1 % (w/v) in H_2O 50 % (v/v), methanol 40 % (v/v) and acetic acid 10 % (v/v)) for 60 minutes before destaining in the same solution without the dye for 30 minutes. Areas of gelatinolytic degradation appeared as transparent bands on the blue background. Bands were then visualized by image analysis (Gel Doc system) and densitometry determined using Image J software. A wide range molecular mass marker set (Sigma) was used to identify MMP species. Band densities were standardized to the mean density of two control samples, per gel, to allow comparisons between multiple gels. All gels were run in parallel.

2.13. Quantitative RT-PCR

Frozen lungs were ground and RNA was isolated using a Trizol based extraction protocol. 2 µg of RNA was reverse transcribed into complimentary DNA (cDNA) using moloney murine leukemia virus reverse transcriptase (M-MLV) (Promega). cDNA was subjected to quantitative RT-PCR (qPCR) analysis to assess expression of the genes of interest listed in table (4) using hypoxanthine-guanine phosphoribosyltransferase (HPRT) as a housekeeping gene. The following distinct primer sets were used to amplify cDNA.

Table 4: qPCR primer sequences.

Gene	Primers
Hprt	sense: 5′-TGAAAGACTTGCTCGAGATGTCA-3′ antisense: 5′-CCAGCAGGTCAGCAAAGAACT-3′
Slpi	sense: 5′- GCTGTGAGGGTATATGTGGGAAA -3′ antisense: 5′- CGCCAATGTCAGGGATCCAG -3′
Mmp-9	forward - 5’-TGAATCAGCTGGCTTTTGTG-3’

	reverse - 5'-GTGGATAGCTCGGTGGTGTT-3’
Col Iα1	forward - 5′-GGAGGGCGAGTGCTGTGCTTT-3′ reverse, 5′-GGGACCAGGAGGACCAGGAAGT-3′
Col IIIa1	forward - 5′-AGGTACCGATTTGAACAGGCT-3′ reverse, 5′- TTTGCAGCCTGGGCTCATTT -3′
Col IVa1	forward - 5′- AAGGACAAATCGGACCCACT -3′ reverse - 5′- AAGCCCATTCCTCCAACTGA -3′
Col VIa1	forward - 5′-GATGAGGGTGAAGTGGGAGA-3’ reverse, 5′-CAGCACGAAGAGGATGTCAA-3′
Itgb6	forward - 5′-TCTGAGGATGGAGTGCTGTG-3’ reverse, 5′- GGCACCAATGGCTTTACACT-3′

Amplification was performed using an MXPro3000 (Stratagene) with SYBR Premier Ex Taq (Takara Bio). After an initial denaturation at 95 °C for 10 minutes, 40 cycles of a three-step PCR thermal profile were utilized to amplify DNA. Denaturation, annealing and extension times and temperatures were optimized for each primer set. Amplification of a single DNA product was confirmed by melting curve analysis. Data were expressed as relative expression using the $^{\Delta\Delta}$Ct equation as described previously (Marino 2011).

2.14. Nuclear extraction

Lungs were lavaged with a total of 4.5 ml (4 x 1 ml lavages, 500 µl to flush cells out cells trapped in the dead space of the cannula) of PBS/phosphatase inhibitor (active-

motif). Cells were pelleted via centrifugation at 528 x g for 10 minutes (4 °C) and the supernatant removed for protein analysis. Pellets were then re-suspended in 4 ml PBS/phosphatase inhibitor and cells were counted. Cells were then re-pelleted and the supernatant was removed and discarded. Cells were re-suspended in 250 µl of hypotonic lysis buffer and incubated on ice for 15 minutes. 12.5 µl of detergent was then added to each tube and the samples were vortexed for 10 seconds. Samples were then centrifuged for 1 minute at 14 000 x g (4 °C) the supernatant (cytoplasmic fraction) was removed and stored at -80 °C. The cell pellet was then resuspended in 25 µl of complete lysis buffer (active-motif). Samples were vortexed and placed onto a rocking platform for 20 minutes prior to a further 30 seconds of vortexing. Samples were then centrifuged for 1 minute at 14 000 x g (4 °C) and the nuclear fraction removed into a pre-chilled tube and stored at -80 °C.

2.15. pSMAD2 assay

pSMAD2 concentration in nuclear extract was determined using the PathScan® Phospho-Smad2 (Ser465/467) Sandwich ELISA Kit #7348 (Cell Signaling Technology, Inc, Boston). The supplied protocol was followed. 10 µg of nuclear extract was used from each sample. This was made up to a total volume of 100 µl using the supplied sample diluents.

2.16.Invasive whole body plethysmography

Rats undergoing invasive plethysmography received ketamine (75 mg/kg) and medetomidine (500 μg/kg) *i.p* prior to cannulation of the trachea and measurement of lung function using Buxco's Forced Manoeuvres system (Buxco research systems). Conventional plethysmographic measurements of lung function were performed with measures of Boyle's law functional residual capacity (FRC) followed by quasistatic pressure volume manoeuvres measuring Total Lung Capacity (TLC), Inspiratory Capacity (IC), Residual Volume (RV), Vital Capacity (VC) and Expiratory Reserve Volume (ERV). Finally, fast flow manoeuvres were conducted for measurements of Forced Expiratory Flow (FEF) and Forced Expiratory Volume (FEV). These animals were not allowed to recover from anaesthetic and lungs were removed for analysis of lung collagen content.

2.17. Thoracic irradiation dosimetry

The dose rate to the midline of the mouse thorax was calculated to insure accurate dosing. Both the measurement and calculation of dose rate were assisted by, J Littler (medical physics, NCH). An x ray source generated by a Gulmay RS225 Orthovoltage cabinet (Gulmay Medical Ltd, Surrey, UK) was utilised for all irradiations. Standard irradiation parameters utilised were as follows; 195 kV, 10 mA, filter used, no applicator and the turn table was set to the maximum distance (487 mm). A PTW Farmer ionising chamber (PTW, Freiburg, Germany) was used for all dose measurements. The dose rate to the midline of the thorax was calculated to be 0.91 Gy/min.

2.18. Thoracic irradiations

Mice were anaesthetised with 90 mg/kg ketamine, 0.3 mg/kg medetomidine (Domitor) (Pfizer) and placed into the custom-made irradiation acrylic animal restraint 'jig'. The anaesthetised mice were inserted into the acrylic jig (figure **2.1, i**) that sat inside a 3 mm thick lead shield (figure **2.1, ii**), a 2 cm window, highlighted with a blue arrow, exposes the thorax of the mouse for irradiation. The mice were then carefully held in position with an acrylic stopper (figure **2.1, iii**). Figure **2.1 iv**, shows both the restraint and stopper in position inside the shield. The jig was then placed into the centre of the orthovoltage cabinet and half of the desired dose was administered in a ventral - dorsal manner. The mouse was then rotated and the remainder of the dose was administered in the opposing direction. The dose was delivered in two opposing directions to ensure a homogenous dose and to reduce the risk of superficial burns to the skin surface. Irradiation dose was adjusted via irradiation time which was calculated using the dose rate of 0.91 Gy/min. Once the mouse was removed from the irradiation cabinet, anaesthesia was reversed using atipamezole (1 mg/kg) (Antisedan) (Pfizer) and the mice were allowed to recover on a warming mat (Vet Tech Solutions).

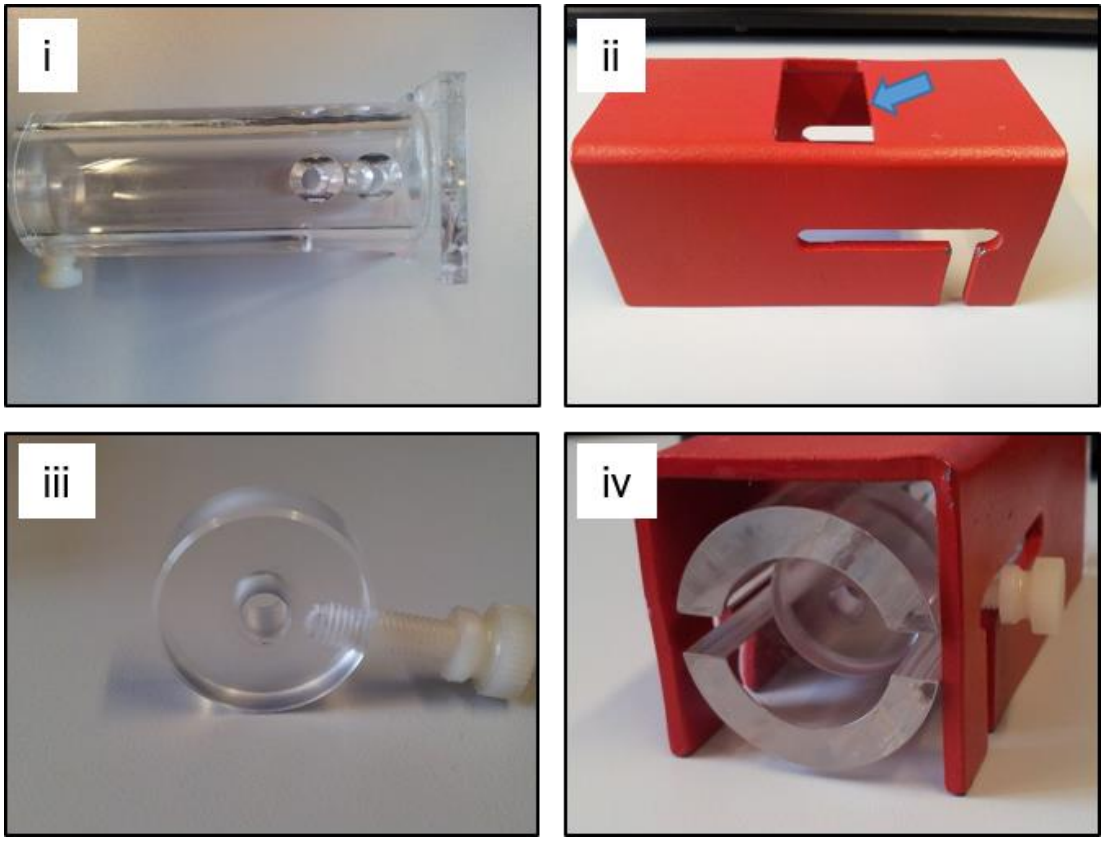


Figure 2.1 Custom-made irradiation jig. To derive thoracic irradiation only a custom-made acrylic restraint and lead shield were designed and engineered. i) An acrylic mouse restrain was produced based on standard tail vein bleed restraints. ii) 3 mm thick lead shield that encases the acrylic restraint with a 2 cm opening to allow the thorax to be irradiated (marked with a blue arrow). iii) Acrylic stopper to hold mouse in place. iv) Demonstrates the entire jig setup.

2.19. NanoSPECT/CT Imaging

DTPA-A20FMDV2 (αvβ6-specific) were synthesized with biotinyl lysine at position 2 by the Cancer Research U.K. Peptide Synthesis Laboratory using standard fluoroenylmethyloxycarbonyl (FMOC) solid-phase peptide synthesis (SPPS) protocols and conjugated with the chelating agent diethylenetriamine pentaacetate-

tetra (DTPA) at the N terminus. Radio labelling was performed as previously described (Saha et al., 2010).

Whole-body helical CT and SPECT scans were conducted as per (John et al., 2013) but briefly scans were obtained with a nanoSPECT/CT imaging system (Bioscan Inc.) fitted with 4 tungstencollimators and nine 1.4-mm-diameter pinholes. SPECT images were obtained with a time per view of 60 sec, resulting in a scan time of 30 – 45 min. CT images were obtained using a tube voltage of 45 kVp and an exposure time of 500 ms per view. Mice were injected intravenously via the tail vein with 5 mg of 111In-DTPA-A20FMDV2 in a 50 mL volume, 1 hour before SPECT/CT imaging. Mice were anesthetised using 3 % isoflurane, 2 L/min flow of oxygen and maintained at 1%–1.5%, 2 L/min flow of oxygen during imaging. The mice were placed in a prone position, tail first, in a Minerve (Siemens) air-warmed chamber, and breathing rates were monitored. after data collection, CT and SPECT images were coregistered, and image analysis performed using InVivoScope molecular imaging software (Bioscan Inc.).

Analysis was conducted at per (John et al., 2013). briefly, a region of interest was created around the lung including both normal and diseased tissue using the density range (21,000 to 1100). Peptide binding specifically within this region of interest could be determined for each mouse. Data are expressed as percentage of the initial activity of ^{111}In-labeled peptide administered by intravenous injection.

2.20. Bicinchoninic acid (BCA) Assay

Pierce BCA Protein Assay Kit. bovine serum albumin P standards were prepared as directed in the kit. The BCA working reagent was prepared by mixing 50 parts of BCA Reagent A (containing sodium carbonate, sodium bicarbonate, bicinchoninic acid and sodium tartrate in 0.1 M sodium hydroxide) with 1 part of BCA Reagent B (containing 4% cupric sulfate) (50:1, Reagent A:B). 25 µL of each standard or sample replicate was pipetted into a 96-Well Plate. 200 µL of the working reagent was then added to each well the plate was covered, mixed thoroughly on a plate shaker for 30 seconds and then incubate at 37 °C for 30 minutes. The plate was then allowed to cool to room temperature before measurement of absorbance at 562 nm on a plate reader.

2.21. Multiplex cytokine analysis

Whole mouse lungs were snap frozen and later homogenised in 1ml PBS containing protease inhibitor (Complete Mini protease inhibitor tablet, Roche). The assay was run as per the instruction manual. BCA assay was used to determine lung homogenate protein concentration and samples were loaded onto the multiplex plate at a protein concentration of 900 µg/ml. The mean fluoresce intensity was determined for each analyte on the Bio-rad plate reader and concentrations were extrapolated from the standard curve.

2.22. Processing lung for *ex vivo* micro CT

Lungs were perfused with 10 ml (40 U/ml) heparin insufflated with 4 % paraformaldehyde (PFA) in PBS and carefully removed *en bloc*, and placed in a 50 ml PVC tube containing 15 ml of 4 % PFA, on ice, at 4 ºC for 4 hours. At the end of the fixation the PFA was removed and the lungs left overnight in 15 % sucrose in PBS at 4 ºC. The 15 % sucrose/PBS solution was removed and the lungs briefly washed in 50 % ethanol, prior to incubation in 70 % ethanol for storage at 4 °C. Due to lungs fragility when completely dehydrated, lungs were fully dehydrated immediately prior to imaging.as follows. Lungs were incubated in 80 % ethanol and 90 % ethanol 2 hours each before overnight incubation in 100 % ethanol. Finally, lungs were incubated in hexamethyldisilazan (HDS) for 2 hours and air dried overnight.

After imaging lungs were fully rehydrated in 100 % ethanol overnight, then 2 hours each in 90 %, 80 % and the 70 % ethanol prior to dehydration for wax embedding for histological examination.

2.23. *Ex vivo* micro CT

µCT scanning was conducted by Dr Chris Scotton at The University of Exeter. Briefly, lungs were packaged for micro-CT scanning to prevent movement. Lungs were scanned in a SkyScan 1072 micro-CT scanner (Bruker MicroCT, Kontich, Belgium) at 40 kV·100 µA−1, without a filter, using two-frame averaging and 0.9 ° angular rotation step size; based on the typical measured 10 % modulation transfer function in the SkyScan 1072, spatial resolution was in the region of 20–30 µm.

Voxel size was set at 13.7 μm giving a scan time of ~10 min, allowing high-resolution visualisation and analysis of fibrosis, with good throughput. Reconstruction was carried out with the SkyScan NRecon software (Bruker MicroCT).

2.24. Precision Cut Lung Slice (PCLS) fibrosis model

Day 0 – male, C57BL/6, mice, 6-8 weeks old, were anaesthetised with isoflurane-anaesthetic (2.5 %, 2 L/min flow of oxygen) and exposed to 60 IU of bleomycin sulphate in 50 μl sterile 0.9 % saline, or 50 μl sterile 0.9 % saline control, via oropharyngeal administration (*o.p.*). The development of lung fibrosis was allowed to occur as usual until day 28 when mice were euthanized by anaesthetic overdose. The thoracic cavity was opened and the trachea cannulated. The lungs were inflated with 1.2 ml, 2 % low melting point agarose (in liquid state) and then 0.3 ml air injected to flush the agarose into the distal air spaces. The lungs were then rinsed with ice cold PBS before being removed *en-bloc* and placed in ice cold Dulbecco's Modified Eagle Medium (DMEM) to gel the agarose. Once gelled, the lobes are separated and one lobe was sliced at a time. Each slice was cut 150 μm thick using a vibrating microtome (1 mm amplitude. 1mm/sec speed.). Slices were cut in ice cold HANKS buffer to insure tissues remained hydrated and the agarose remained solid. Slices were incubated overnight at 37 ºC, 5 % CO_2 to melt remaining agarose. 3 slices were then added to each well containing 500 μl of pre-warmed DMEM for 1 hour to allow the slices to acclimatise before the media was aspirated and the slice were treated 500 μl Tranilast or DMEM only as a control.

Tranilast preparation: Tranilast is readily soluble in dimethyl sulfoxide (DMSO) at 2500 µM. 40.8mg of Tranilast was dissolved in 0.5ml of DMSO. Then added in a drop-wise manner to 49.5ml of DMEM (using a pipette) whilst stirring. There was some initial cloudiness but this rapidly dissolved with stirring to give a clear solution of a concentration of 2500µM. The final DMSO concertation in the DMEM was 1 %.

Compound was diluted to 20 % w/v in DMSO and then added to DMEM to maintain a volume of 1% DMSO in DMEM. Concentrations used were 2500, 500, 100, 20 and 4 µM. Media/compound was replaced daily and lung slice were processed 5 days post initial treatment.

3 Pilot Dose Ranging Studies of Bleomycin Induced Lung Injury and Fibrosis, in Mice and Rats

3.1. Introduction and Aim

The aim of work in this chapter was to establish robust models of both bleomycin induced acute lung injury (ALI) and fibrosis in both mice and rats without causing unnecessary suffering. Initially, conducting dose ranging studies in order to determine an appropriate dose of bleomycin to aid the understanding of the role of inflammation and repair in these models. Once attained I aim to define the time course of expression of key pro- and anti-inflammatory cytokines and fibrotic mediators in both ALI and pulmonary fibrosis respectively.

3.2. Methods

Bleomycin induced lung injury and fibrosis were assessed in both mouse and rats. Male C57Bl/6 mice, between 6 – 8 weeks old, were anaesthetised with isoflurane-anaesthetic (2.5%, 2 L/min flow of oxygen) and exposed to doses of bleomycin between 30 to 75 IU of bleomycin sulphate (Kyowa Hakko, Slough, UK) in 50µl sterile 0.9% saline (Sigma), or 50 µl sterile 0.9% saline as a control, via oropharyngeal administration (*o.p.*). Lungs were assessed at various time points following exposure to bleomycin up to day 28 dependent on the analysis required which included, BALF differential cell counts, wet lung weights, morphological

assessment of lung histology, cytokine profiling by multiplex immunoassay and RNA analysis by qPCR (see methods for full methodology, chapter 2.

7-week-old, male, Lewis rats were anaesthetised with isoflurane-anaesthetic (2.5%, 2 L/min flow of oxygen) and exposed to doses of bleomycin between 300 IU, 400 IU, 500 IU, 750 IU and 1000 IU of bleomycin sulphate (Kyowa Hakko) in 250µl sterile 0.9 % saline (Sigma), or 250 µl sterile 0.9 % saline as a control, via *o.p.* administration. The development of pulmonary fibrosis was assessed (n = 3 rats per group) at day 21 via Masson's trichrome staining of tissue sections. Lung function was measured 7 days post bleomycin treatment (n = 2 rats per group) as stated in method section (3.14) with BALF cells count being taken to confirm ALI at this time point.

3.3. Results

3.3.1. Bleomycin dose setting and the development of ALI in mice

I initially assessed the effect of two concentrations of bleomycin on body weight during the phase of ALI (see figure **3.1**). Mice given saline via *o.p.* administration did not show any change in body weight over 4 days, whereas mice treated with 30 IU bleomycin showed a slight reduction in weight from day 2 to day 4 compared with, saline controls, but this was not statistically significant. In contrast, mice given 75 IU bleomycin showed significant weight loss up to day 4.

To assess the effect these two doses of bleomycin had on the lung, histological sections were stained with H&E. Upon bleomycin instillation, I observed an obvious

lung inflammatory response, including mild interstitial inflammation, in mice administered with 30 IU bleomycin (see figure **3.2**), but in mice administered 75 IU bleomycin there was significant influx of inflammatory cells, macrophages and neutrophils, into the alveolar space clearly visible (see figure **3.2**).

The inflammatory cell influx into the lungs 4 days post bleomycin instillation was evaluated further through the assessment of BAL cell profiles. Cell profiles from mice administered 30 IU showed a significant neutrophil influx into the lungs with neutrophils accounting for 15.5 % of total cells compared to just 0.16 % of cells within the BALF of saline treated animals (figure **3.3**). Neutrophilia was exaggerated further in mice administered 75 IU with neutrophils making up 27.5 % of all cells counted (***P<0.001, compared with 30 IU) (figure **3.3**).

For the final readout of acute lung injury, I assessed lung wet weights, 4 days after bleomycin instillation (see figure **3.4**). Increasing the concentration of bleomycin administered also increases the wet weight of the lung 4 days after instillation. The mean wet lung weight of saline control animal was 119.4 mg, which was not significantly different from the wet lung weight of animals exposed to 30 IU bleomycin, significantly lower than the wet lung weight of (200.1 mg) following exposure to 75 IU bleomycin treatment (**P<0.005).

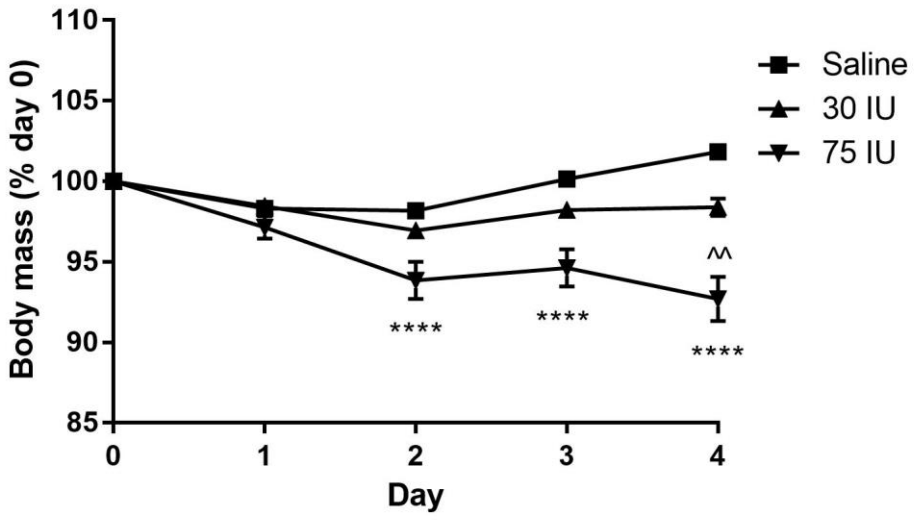


Figure 3.1 The effect of various bleomycin doses on the development of acute lung injury assessed by body mass. Mice were administered 30 IU, 75 IU bleomycin or saline (*o.p.*) at day 0 and body weight was recorded daily until study end. Data expressed as mean percentage of initial (day 0) body mass (%) ± SEM; n = 15 - 17; ^^P<0.01 30 IU vs saline control at day 4 and ****P<0.0001 75 IU vs. saline control at individual time points, two-way ANOVA performed. Mean average starting body mass; saline 22.1 g, 30 IU 22.2 g and 75 IU 21.7 g.

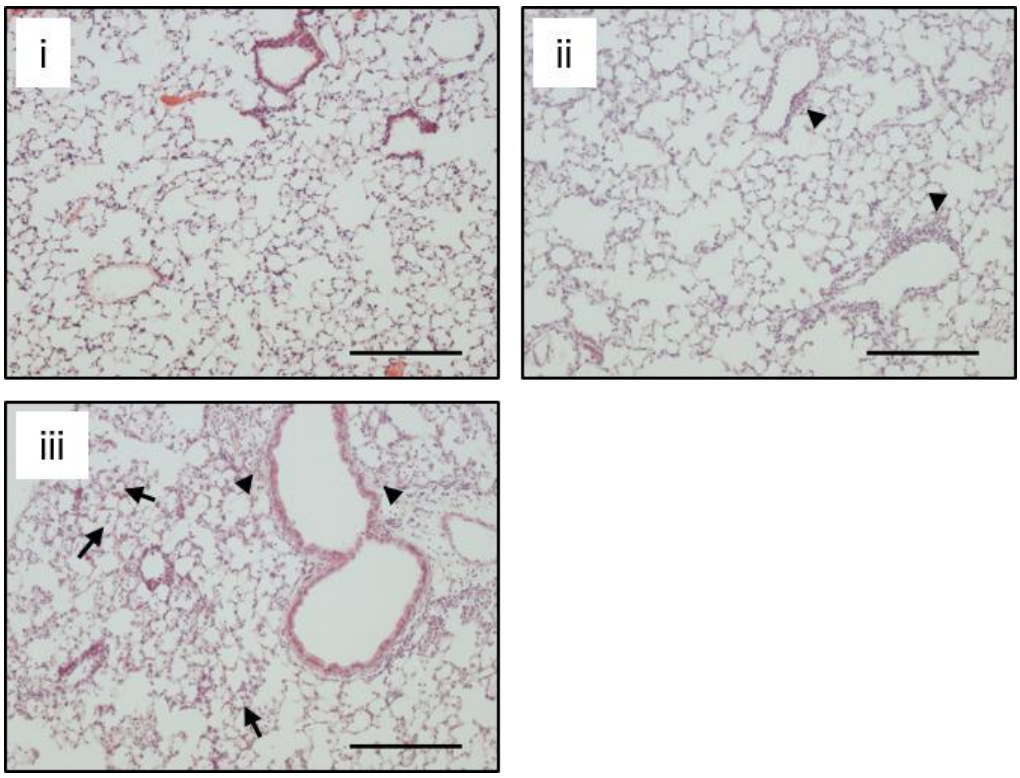


Figure 3.2 The effect of various bleomycin doses on the development of acute lung injury assessed by H&E staining of lung tissue sections. i) Saline treated control ii) 30 IU bleomycin iii) 75 IU bleomycin. There is mild interstitial inflammation, marked with arrow heads, in mice treated with 30 IU bleomycin that increases in severity in the 75 IU treated animals. A significant influx of inflammatory cells, macrophages and neutrophils, into the alveolar space is highlighted by arrows in the75 IU treated animals only. Representative images captured using x10 magnification, scale bars 100 µm.

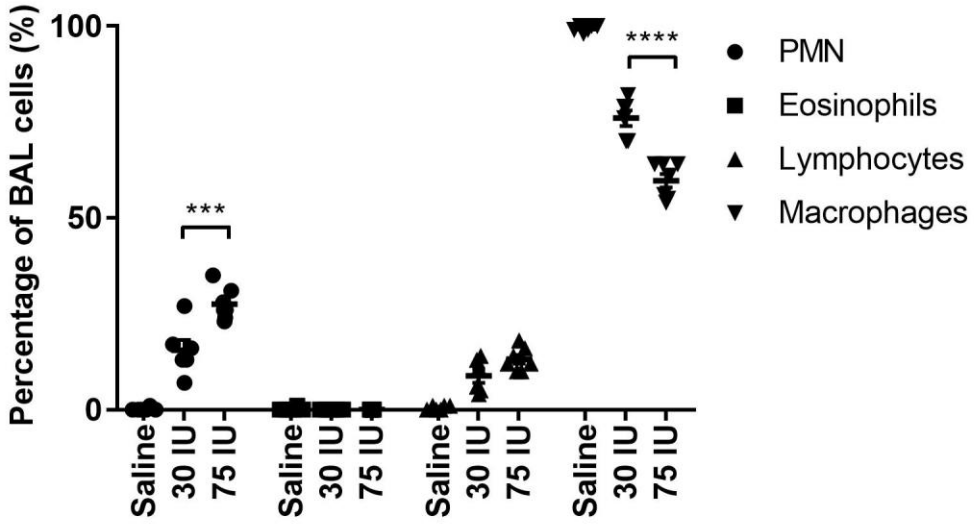


Figure 3.3 The effect of various bleomycin doses on BALF differential cell counts, 4 days post bleomycin administration. Mice were administered 30 IU, 75 IU bleomycin or saline (*o.p.*) and lungs were lavaged upon study end at day 4. Data expressed as mean percentage of cells counted (%) ± SEM; $n = 6$; ***$P<0.001$ and ****$P<0.0001$ 75 IU vs. 30 IU.

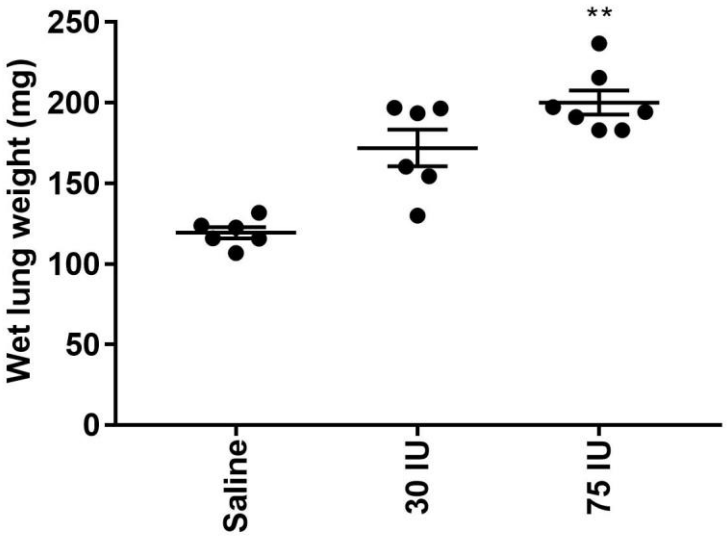


Figure 3.4 The effect of various bleomycin doses on wet lung weight 4 days post bleomycin administration. Mice were administered 30 IU, 75 IU bleomycin or saline (*o.p.*) and lungs were removed and wet lung wets were recorded at day 4. Mean wet lung weight (mg) ± SEM; n = 6 - 7; $^{**}P<0.01$ vs. saline control.

3.3.2. Protein and mRNA expression during the development of bleomycin-induced acute lung injury

Having determined that 75 IU bleomycin was required to generate sufficient ALI, I wanted to understand the role of inflammatory cytokines during the development of bleomycin-induced acute lung injury. A multiplex assay was used to determine the expression of IFN-γ, IL-1β, IL-4, IL-6, KC, IL-10, IL-13, TNF-α in lung tissue homogenate from mice at 0, 1, 2, 3, 4, 6, 8 and 10 days post 75 IU of bleomycin.

IL-1β expression increased 1 day following bleomycin instillation and returned to baseline by day 3 but this increase was not statistically different when correcting with a Dunn's multiple comparisons test (see figure. **3.5**). Both KC and IL-6 were significantly increased at day 1 with concentrations peaking 2 days following bleomycin exposure before declining to baseline 8 and 10 days post bleomycin respectively (figure **3.5**). No other cytokines measured were above the limit of detection of the assay.

As the time points under investigation crossed into the late stages of acute lung injury and the very early stages of bleomycin-induced pulmonary fibrosis, I also determined the gene expression of a key mediator of TGF-β activation and subsequent pulmonary fibrosis, ITG-β6, which has been reported to be increased as early as 14 days post bleomycin (Tatler et al., 2016b). The relative expression of *Itgb6* mRNA was significantly increased at days 8 and 10 post bleomycin 5.3 and 4.1 ($2^{-\Delta\Delta}$Ct) respectively (see figure **3.6**).

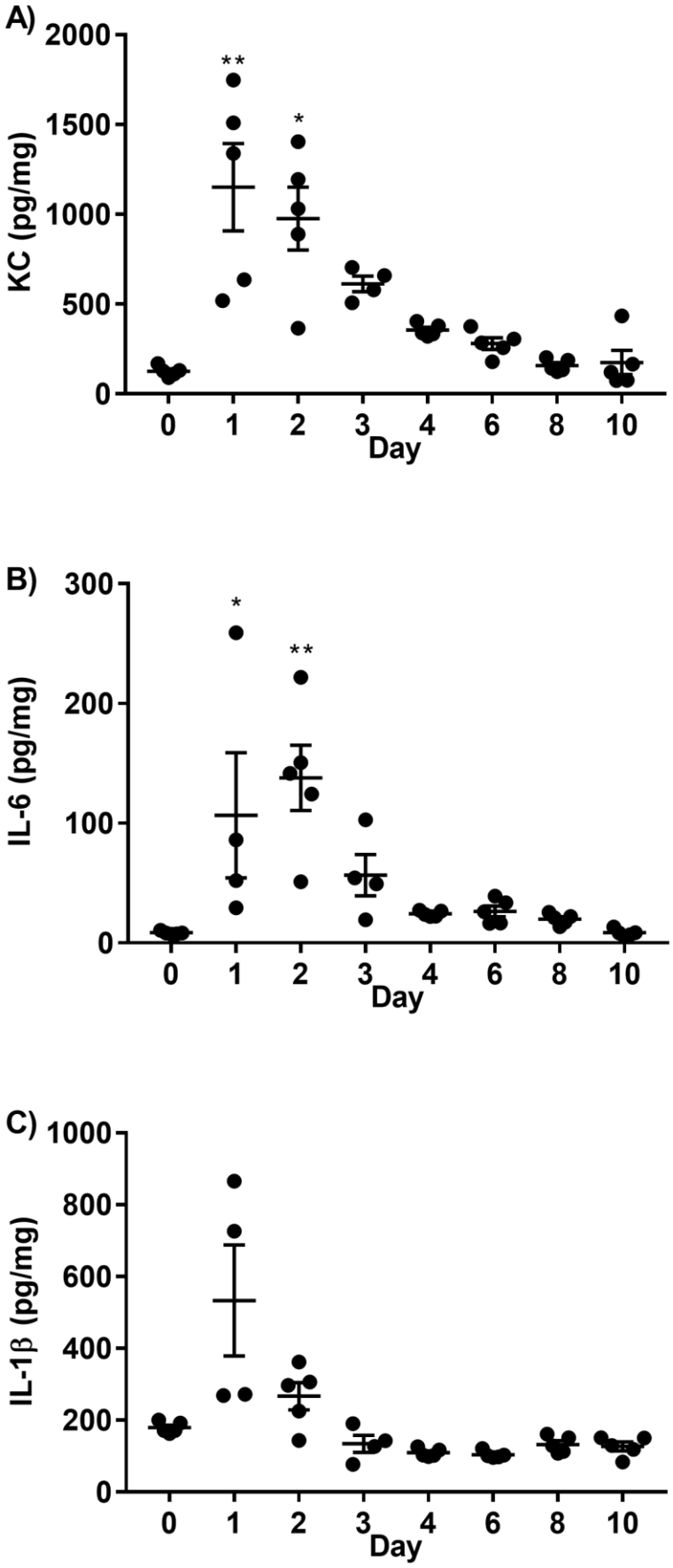

A)
KC (pg/mg)
2000
1500
1000
500
0
**
*
0 1 2 3 4 6 8 10
Day
B)
IL-6 (pg/mg)
300
200
100
0
*
**
0 1 2 3 4 6 8 10
Day
C)
IL-1β (pg/mg)
1000
800
600
400
200
0
0 1 2 3 4 6 8 10
Day

Figure 3.5 Cytokine protein expression in the lung during the development of acute lung injury. Mice were administered 75 IU bleomycin at day 0 and the concentration of various cytokines were determined in lung homogenate at 0, 1, 2, 3, 4, 6, 8 and 10 days post bleomycin instillation. Data are expressed as mean concentration pg/mg of lung protein ± SEM. A) KC, B) IL-1β and C) IL-6. n = 4 - 5; *P<0.05 and **P<0.01 vs. day 0. ANOVA.

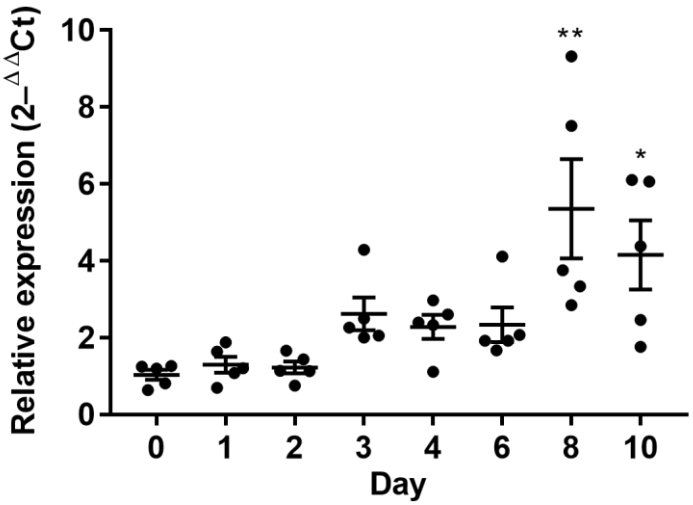


Figure 3.6 The effect of bleomycin on *Itgb6* mRNA expression 0 to 10 days post administration. Mice were administered 75 IU bleomycin at day 0 and the gene expression of *Itgb6* in lung homogenate was determined at 0, 1, 2, 3, 4, 6, 8 and 10 days post bleomycin instillation. Data are expressed as mean relative expression ($2^{-\Delta\Delta}$Ct) ± SEM. n = 5; *P<0.05 and **P<0.01 vs. day 0 control. ANOVA.

3.3.3. Bleomycin dose setting and the development of pulmonary fibrosis in the mouse and rat

Prior data had demonstrated that 30 IU bleomycin were insufficient to generate robust lung injury (see results section 3.3.1), therefore I assessed 50 IU and 75 IU bleomycin for inducing pulmonary fibrosis in mice. Mice were administered bleomycin via oropharyngeal administration (*o.p.*) at day 0 and fibrosis was assessed 28 days later.

Body weight was recorded over the 28-day period and showed that mice receiving saline (control) slowly gained weight over the study period (see figure **3.7**). Mice receiving 50 IU of bleomycin showed a similar weight gain to that of the saline control group although did weigh slightly less than the saline controls at the end of the 28-day period. Mice administered 75 IU bleomycin lost a significant amount of weight and reached a low of 83.9 % at day 4 and it was not until day 18 when the mean percentage of starting body weight reached the mean starting body weight.

To determine what effect these two doses have on the development of pulmonary fibrosis I assessed Masson's trichrome staining of histological sections. Normal lung architecture can be seen in mice treated with saline (see figure **3.8, i**). Lower power (x10 magnification) images show that 50 IU of bleomycin caused widespread but minor areas of inflammatory cell influx and also collagen deposition, as identified by blue staining (see figure **3.8, ii**). Animals treated with 75 IU bleomycin had more severe inflammatory cell influx into the interstitial space and airways. There was a large amount of collagen deposited around the areas of inflammation and alveolar destruction, marked with arrows (see figure **3.8, iii**).

Dose ranging studies were conducted in rats to determine the optimal dose to establish bleomycin-induced pulmonary fibrosis with minimal necessary distress. Rats were administered either 300, 400, 500, 750 or 1000 IU bleomycin or saline via *o.p.* administration at day 0 and fibrosis was assessed at day 21. Body weight, recorded over the 21- day period, showed a concentration dependent reduction in weight gain (see figure **3.9**). Rats treated with 750 IU and 1000 IU had signs of considerable distress with hunching, lethargy and laboured respiration 3 days posts bleomycin administration therefore for animal welfare reasons they were euthanized.

Lung tissue sections were stained with Masson's trichrome for analysis of collagen deposition in the lung. A concentration of 500 IU produced severe fibrosis with 400 IU causing reduced but substantial fibrosis whereas 300 IU appeared to have little effect (see figure **3.10**).

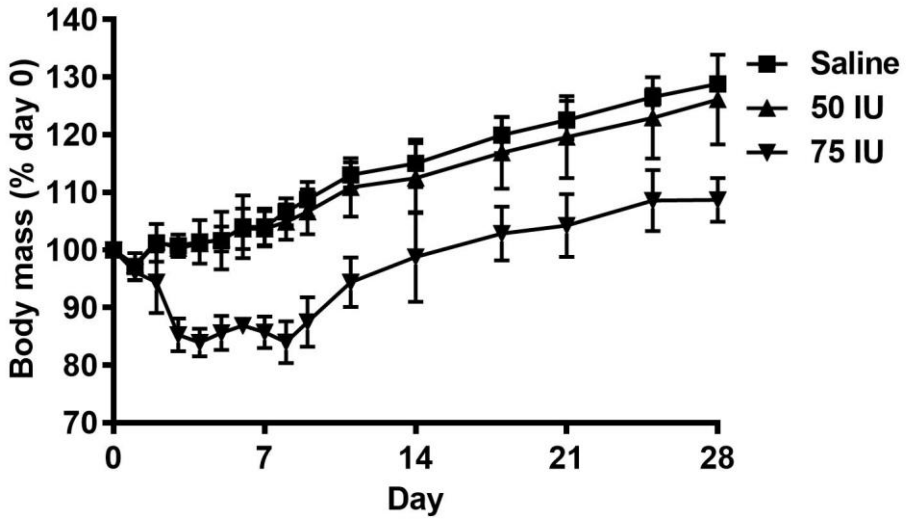


Figure 3.7 The effect of various bleomycin doses on the development of pulmonary fibrosis in mice assessed by body mass. Mice were administered saline (control), 50 IU or 75 IU bleomycin *o.p.* on day 0. Data expressed as mean percentage initial (day

0) body weight (%) ± SD; *n* = 3. Mean average starting body mass; saline 20.5 g, 50 IU 20.1 g and 75 IU 19.3 g.

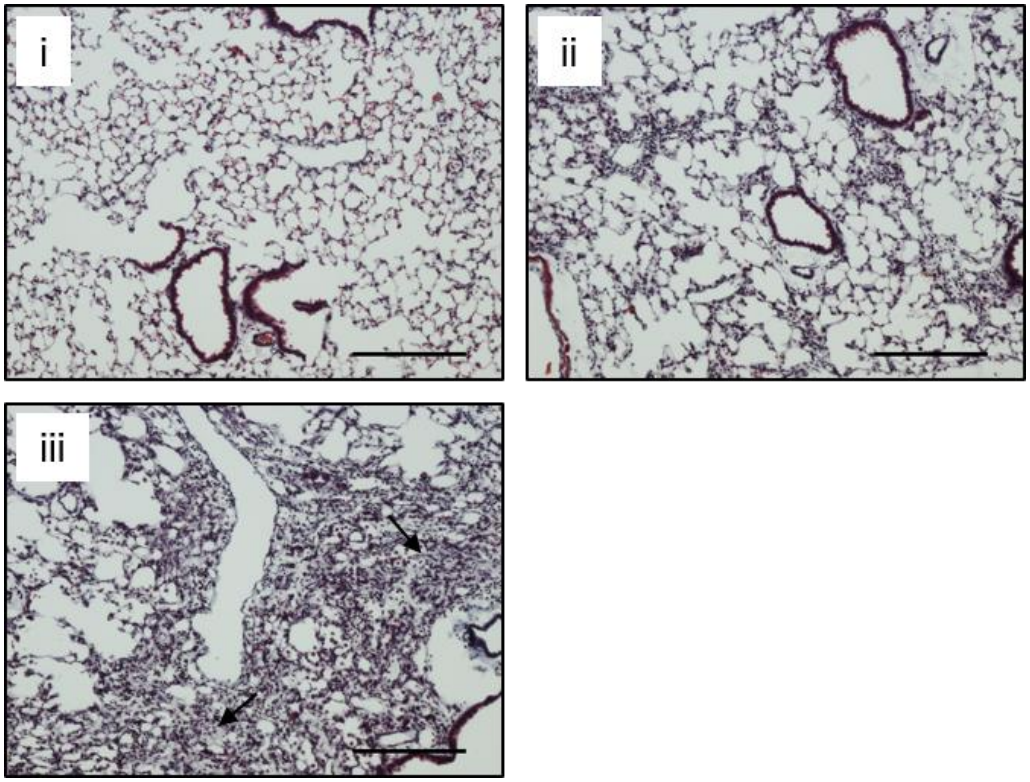


Figure 3.8 The effect of various bleomycin doses on the development of pulmonary fibrosis in mice assessed by Masson's trichrome staining of lung tissue sections. Masson's trichrome staining of lung tissue sections 28 days post dosing i) saline, (control) ii) 50 IU and iii) 75 IU bleomycin. Extracellular matrix is stained blue and representative areas of bleomycin induced collagen deposition are marked with arrows in the 75 IU treated lung section. Representative images captured using x10 magnification, scale bars 100 µm.

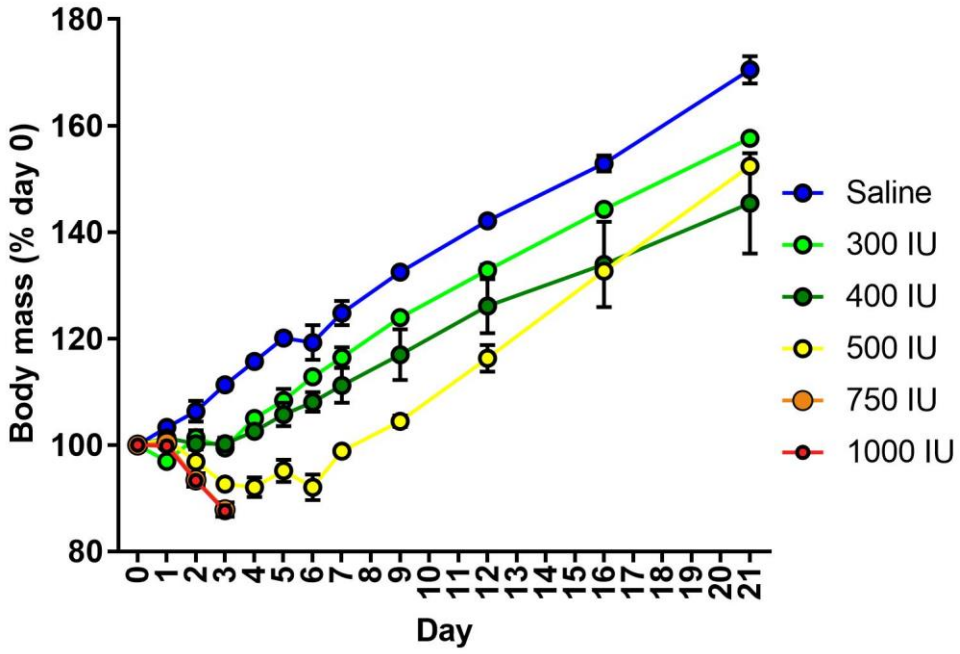


Figure 3.9 The effect of various bleomycin doses on the development of pulmonary fibrosis in rats assessed by body mass. Rats were administered saline (control), 300 IU, 400 IU, 500 IU, 750 IU or 1000 IU bleomycin *o.p.* on day 0. Data expressed as mean percentage initial (day 0) body weight (%) ± SD; $n = 3$. Mean average starting body mass; saline 184.6 g, 300 IU 179.5 g, 400 IU 191.5 g, 500 IU 177.5 g, 750 IU 173.6 g and 1000 IU 180.6 g.

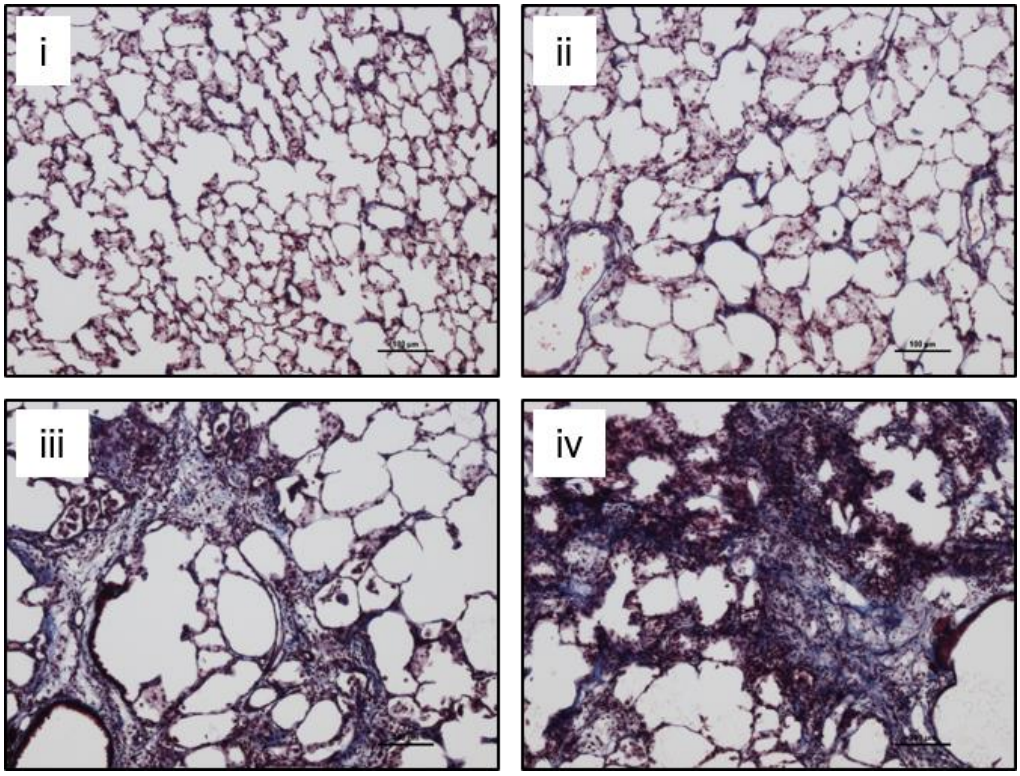


Figure 3.10 The effect of various bleomycin doses on the development of pulmonary fibrosis in rats assessed by Masson's trichrome staining of lung tissue sections.

Masson's trichrome staining of lung tissue sections 21 days post dosing. Rats were administered; i) saline (control), ii) 300 IU, iii) 400 IU and iv) 500 IU bleomycin *o.p.* on day 0. Representative images captured using x10 magnification, scale bars 100 µm.

3.3.4. The effect of bleomycin on rat lung function

Based on the results of the experiments in results section 3.3.3 rats, male 7-week-old, were administered either 500 IU bleomycin or 250 µl saline by *o.p.* administration only as a control and lung function measured using Buxco's Forced Manoeuvres system (Buxco research systems).

Measures of lung volumes demonstrated that inspiratory capacity (IC) vital capacity (VC) and total lung capacity (TLC) were reduced in bleomycin treated animals compared with saline treated animals (see figure **3.11**). However, there was no difference in expiratory reserve volume (ERV) between rats receiving bleomycin or saline (see figure **3.11**).

There was a modest reduction in forced expiratory volume in 200 milliseconds (FEV200) from 9.28 to 8.54 ml and FEV400 11.38 to 9.37 ml in bleomycin exposed rats. The forced vital capacity (FVC) was also reduced in bleomycin exposed animals (9.58 ml) compared with 11.88 ml in wild-type mice (figure **3.12**).

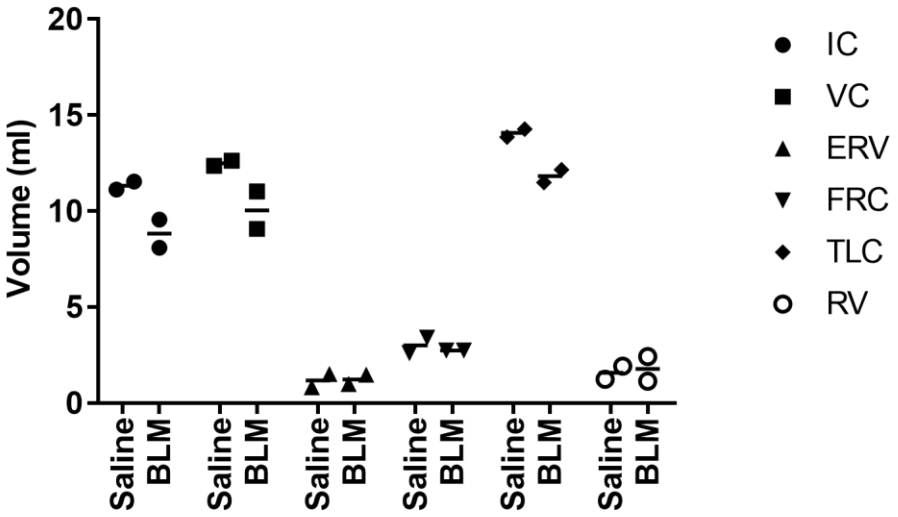


Figure 3.11 The effect of bleomycin-induced acute lung injury on lung function – Pressure volume measurements. Rats were treated with 500 IU bleomycin (BLM) or saline as a control and at day 7 pulmonary function testing was conducted. Initially measures of Boyle's law functional residual capacity (FRC) was assessed followed by quasistatic pressure volume manoeuvres measuring Total Lung Capacity (TLC), Inspiratory Capacity (IC), Residual Volume (RV), Vital Capacity (VC) and Expiratory Reserve Volume (ERV) all volumes and capacities are measured in millilitres (ml). Lines represent median volume, $n = 2$.

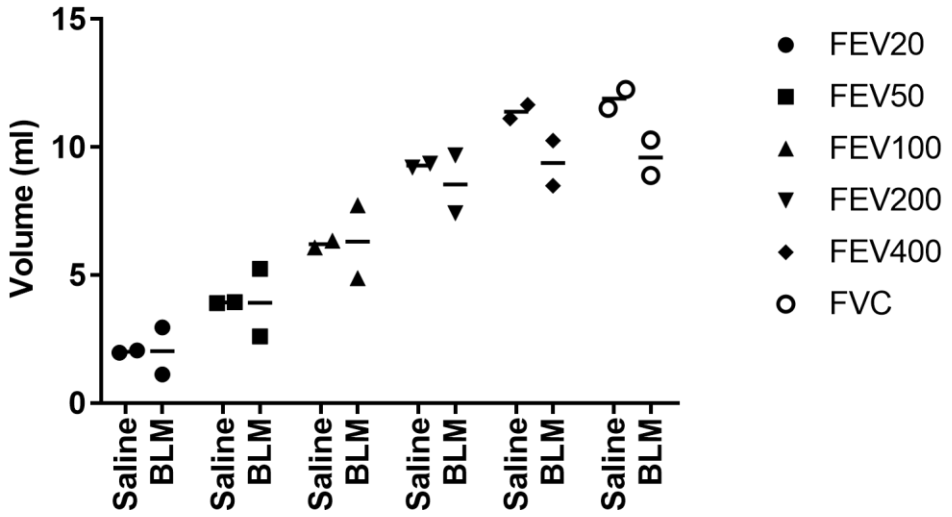


Figure 3.12 The effect of bleomycin-induced acute lung injury on lung function – Flow volume measurements. Rats were treated with 500 IU bleomycin (BLM) or saline as a control and at day 7 pulmonary function testing was conducted. Fast flow manoeuvres were conducted for measurements of Forced Expiratory Volume at 20, 50, 100, 200 and 400 milliseconds and forced vital capacity (FVC). All volumes and capacities are measured in millilitres (ml). Lines represent median volume, $n = 2$.

3.4. Discussion

To study fibrotic respiratory diseases and their treatments successfully it is important to develop robust and reproducible disease models. Initially, pilot studies investigating an appropriate dose of bleomycin to be administered for inducing both lung injury and pulmonary fibrosis in mice were conducted.

These studies suggest that a loss of body weight can give an indication as to the extent of injury and subsequent fibrosis. Little or no weight loss suggests the bleomycin dose has been insufficient to induce enough injury to study; particularly when determining differences between treatment groups. My data suggests that weight loss of less than approximately 10 % of initial body weight may result in a poor fibrotic response, in mice. Whereas in rats weight loss of 5 % or more during the first 4 - 5 days post bleomycin exposure suggests a robust fibrotic response will follow. Although 75 IU induced pronounced ALI at day 4, mice treated with 75 IU lost a significant amount of body weight (mean >15 %) and did not begin to regain weight until 9 days after bleomycin treatment. Therefore, taking the welfare of the mice into account a dose somewhere between 75 and 50 IU may be optimal for bleomycin-induced fibrosis studies.

The multiplex assay used in this study was chosen as the majority of the target analytes, IL-1β, IL-4, IL-6, KC (IL-8 homologue), IL-10, IL-13, TNF-α, are cytokines that have been reported to be important in acute lung injury in a pro- or anti-inflammatory role (Cross and Matthay, 2011). Data obtained in this study showed IL-6 to be increased at day 1 and day 2 post bleomycin instillation. IL-6

plays a crucial role in the development of both bleomycin-induced ALI and fibrosis. IL-6 deficient (IL-$6^{-/-}$) mice 2 days post bleomycin have reduced alveolar macrophage and neutrophil accumulation and this results in attenuated fibrotic response (Saito et al., 2008). IL-1β is a pro-inflammatory cytokine with expression that was slightly but not significantly increased at day 1 before declining at day 2 and back to baseline at day 3. IL-1β is known to cause ALI as intratracheal administration causes both an increase of neutrophils and alveolar leakage (Hybertson et al., 1997). However, IL-1β may also play a role in tissue repair as prolonged overexpression, out to 7 days, in rat lung has been reported to lead to chronic repair and pulmonary fibrosis (Kolb et al., 2001). The murine IL-8 homologue KC was also determined to be increased at the early time points of day 1 and 2 post bleomycin administration. IL-8 causes both neutrophil and monocyte recruitment and activation. Furthermore, increased IL-8 as well as IL-6 levels in blood plasma are associated with morbidity and mortality in acute lung injury (Parsons et al., 2005). These data suggest that measuring any of these cytokines in lung tissue at 4 - 5 days, the time point which is commonly used to investigate ALI in animal models, is not appropriate as levels may have declined to baseline already. The expression of *Itgb6* is significantly increased at 8 - 10 days post bleomycin which coincides with previously published data demonstrating increases in αvβ6 integrin in the alveolar epithelium at 14 days post bleomycin; a time point thought to represent the early stages of fibrosis (Nakagome et al., 2006).

The rat bleomycin-induced fibrosis experiments conducted testing a range of bleomycin concentrations determined that a concentration of 500 IU was most suitable for use in this model. 750 IU and 1000 IU of bleomycin caused significant caused substantial distress to the animals, which therefore needed to be humanely

euthanized using an appropriate schedule 1 procedure. 500 IU was chosen as rats develop extensive fibrotic lesions but did not suffer substantial distress. Lung function was assessed in a small number of rats, 7 days post bleomycin to better characterise the model. Both pressure volume and flow volume measurements taken from these animals approximate lung function measurements obtained in humans. Lung volumes (IC, VC and TLC) were decreased. Mouse models of bleomycin-induced pulmonary fibrosis have demonstrated reductions in lung volumes during acute lung injury, day 7, but also during the early and later fibrotic phases, day 14 and 21 respectively. The reduction in lung volume has been linked with inflammatory infiltration at day 7 and reduced static compliance of the lung due to excessive collagen deposition at day 21. Post treatment of mice with Protectin DX, remedied bleomycin induced fibrosis and improved lung respiratory function at 21 days(Li et al., 2017). The force at which air can be expelled from the lung was also reduced (FEV200 and FEV400) suggesting that lung function could be a useful tool for studying treatment effect in ALI.

3.5. Conclusion

Pilot studies have suggested that between 50 and 75 IU bleomycin administered via *o.p.* aspiration could be used for both ALI and fibrosis models in mice. 500 IU bleomycin *o.p.* is the optimal dose for pulmonary fibrosis studies using rats. The initial pilot studies and characterisation of models performed in this chapter proved vital in attaining accurate, reproducible and innovative research throughout the remainder of this thesis and beyond.

4 The Effect of Radiation-Induced Lung Fibrosis on αvβ6 Integrin Expression

4.1. Introduction

A radiation-induced lung fibrosis (RILF) model was established as it has advantages over the bleomycin-induced fibrosis model. Firstly, RILF is not dependent on inflammation and although mice develop pneumonitis at 10-12 weeks this is not linked to the development of fibrosis. With the onset of RILF being delayed, occurring 20 weeks post irradiation and peaking beyond 24-26 weeks it is an ideal model for monitoring disease progression during the development of fibrosis.

Activation of TGF-β by the αvβ6 integrin is central in the pathogenesis of idiopathic pulmonary fibrosis (IPF). It is now established that the αvβ6 is upregulated in patients with IPF, as determined by immunohistochemistry (Xu et al., 2009, Horan et al., 2008), unfortunately there are risks associated with lung biopsy therefore a none-invasive strategy to identify the αvβ6 integrin is urgently required. Disease models of pulmonary fibrosis further support a link between increased TGF-β activation by αvβ6 integrins and increased severity of fibrosis.(Munger et al., 1999, Puthawala et al., 2008). These animal models include the radiation-induced pulmonary fibrosis model where mice deficient of the integrin αvβ6 gene are protected from radiation induced TGF-β activation and subsequent pulmonary fibrosis (Puthawala et al., 2008). Puthawala et al, also demonstrate that increased expression of αvβ6 by alveolar epithelium is potentially a late event with a sharp increase seen 18-20 weeks post irradiation, via immunohistochemistry. Due to the long-term nature of the radiation-induced pulmonary fibrosis model, requiring 26 weeks to develop,

predicting disease outcome using a disease marker such as αvβ6 would be a valuable tool. As increases in αvβ6 by immunohistochemistry are not determined until 18-20 weeks, this measurement offers no advantages over other commonly used measurements of fibrosis, such as collagen.

Recent advances in technology and emerging new techniques such as single-photon emission computerised tomography (SPECT) now offer the potential to monitor disease progression non-invasively in small animals. Furthermore, measurement of αvβ6 integrins *in vivo*, non-invasively, by micro SPECT/CT scanning is an emerging technique (John et al., 2013). Due to the non-invasive nature of SPECT/CT imaging, mapping expression throughout longitudinal studies are possible. The DTPA-A20FMDV2 peptide (αvβ6 specific) has proven to be highly sensitive and its binding is quantifiable (John et al., 2013). It has also been noted that the DTPA-A20FMDV2 peptide is more sensitive than measuring αvβ6 using histology (John et al., 2013).

Utilising β6 as a prognostic biomarker to predict disease progression in the radiation-induced pulmonary fibrosis model will provide an early indication into whether a treatment is having an affect potentially weeks/months before the study ends at 26 weeks and fibrosis is assessed. Therefore, imaging would allow quantification of αvβ6 integrin levels and reduce the time of the study thus having a positive impact on animal welfare.

4.2. Aims

The aims of this chapter were to develop a robust model of radiation-induced pulmonary fibrosis that incorporated the progressive nature of fibrotic lung disease.

The secondary aim was to determine if SPECT/CT imaging can utilise αvβ6 as a prognostic biomarker in the radiation-induced pulmonary fibrosis model.

4.3. Methods

Firstly, radiation-induced lung fibrosis pilot studies were conducted; mice were irradiated with 10, 12.5, 15, 17.5 and 20 Gy thoracic irradiation using a Gulmay RS225 orthovoltage cabinet as detailed in method section (2.18). Dosing was conducted in an escalating manner from 10 Gy increasing to 20 Gy to ensure that mice would survive initial radiation induced pneumonitis and did not suffer unnecessary side effects. $n = 6 – 8$ mice were exposed per irradiation dose and lungs were taken for histological analysis at 26 weeks or as soon as animals reached severity limits. Upon completion of pilot studies further animals were irradiated and αvβ6 SPECT/CT was conducted at week 8, 12 and 17 as detailed in methods section (2.19). Removed, fixed lungs were imaged via μCT and images were visually assessed for fibrotic changes (see chapter 2.23 for full method).

4.4. Results

4.4.1. The effect of thoracic irradiation dose on mouse wellbeing

To determine a suitable dose for future studies mice received 0 (sham), 10, 12.5, 15, 17.5 or 20 Gy of thoracic irradiation. Mice were continually monitored over the 26 week study period. It was noticed that five weeks post irradiation (10 Gy) the fur covering the thorax began to discolour. Only fur within the irradiated field lost

colouration demonstrating that the radiation was administered specifically to the thorax (figure **4.1**). Body weight was also recorded as an indication of general mouse wellbeing. Mice receiving sham irradiation continued to gain weight for the 26 weeks of the study (see figure **4.2**). Mice receiving 10-15 Gy also gained weight albeit at a reduced rate up to 20 weeks, where after mice that received 10 Gy gained substantial weight whereas mice that received 12.5 or 15 Gy plateaued. Mice receiving 17.5 or 20 Gy did not gain any weight over the 6 months of the study.

Survival was plotted over the course of the 26 week experiment (see figure **4.3**), it shows that 100 % of 'sham' irradiated mice survive to the end of the study. The majority of mice receiving 10 and 12.5 Gy irradiation survived the whole 26 week experimental period with just one mouse from both irradiation dose groups having to be euthanized at 25 weeks due to ill health. There was a single mouse from the 10 Gy group that did not survive past week 4. It was unclear as to why this mouse only survived 4 weeks as all mice at higher doses survived past this time point apart from a number of mice that were irradiated with 20 Gy that were euthanized early due to substantial radiation induced cutaneous burns. Mice receiving doses of 15 Gy or greater had a rapid decline in survival at 20 weeks with just 20 % of mice receiving 15 Gy surviving until 26 weeks and all of the 17.5 Gy group had to be euthanized by week 25. It was noted in a number of mice, receiving 15 Gy or greater, suffered cutaneous radiation injury 3-5 weeks post irradiation. The frequency and severity of injury was dose dependent and generally subsided over a 1-2 week period. Incidence was dose dependent with approximately 50 % of mice treated with 20 Gy suffering cutaneous burns (data not shown). As previously mentioned, 4 mice receiving the largest irradiation dose, 20 Gy, had to be euthanized prior to week 12 due to cutaneous burns and the remaining animals were euthanized at week 20 due to ill

health. Fluid was found in the thoracic cavity of a few of the 20 Gy treated mice which survived to 20 weeks, most likely caused by pleural effusion.

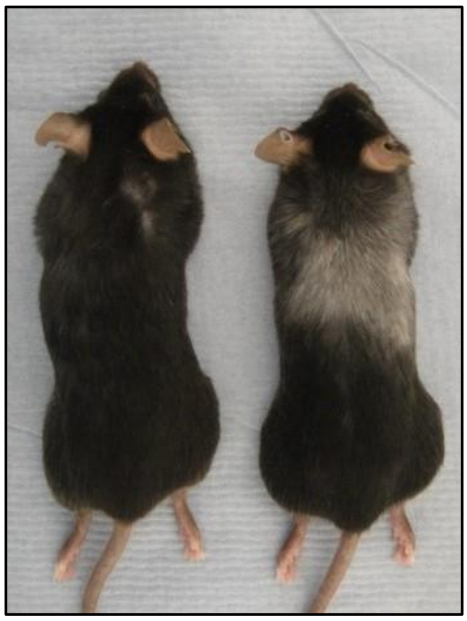


Figure 4.1 Image showing fur discolouration around the chest due to radiation exposure. Left mouse ‘sham’ irradiated right mouse received 10 Gy thoracic irradiation. Approximately five weeks post irradiation, the fur within the thoracic region of irradiated mice began to discolour and remained discoloured for the duration of the study.

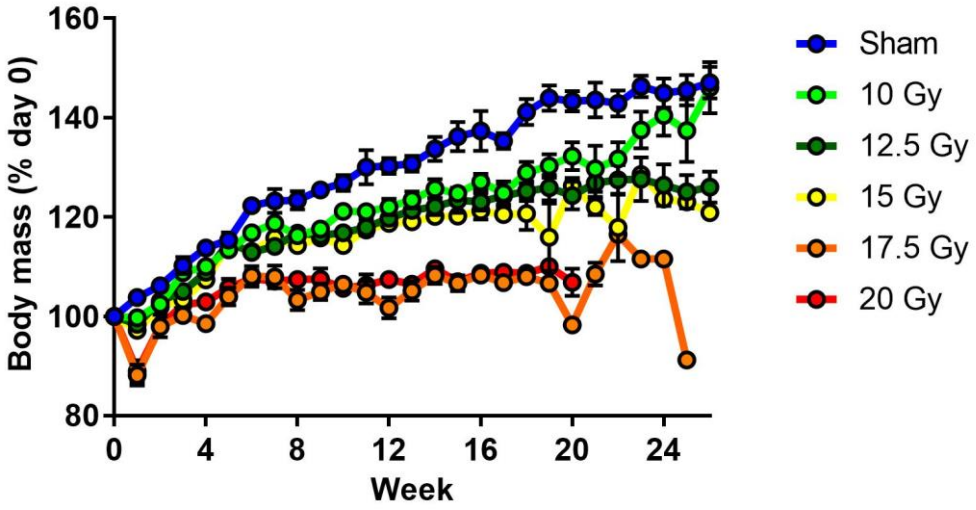


Figure 4.2 The effect of thoracic irradiation on body mass. Mice (female, C57BL/6) received thoracic irradiation 10, 12.5, 15, 17.5 or 20 Gy or were 'sham' irradiated on day 0. Body weight post irradiation. There is a dose dependent failure to gain weight during both the subacute pneumonitis phase (8-16 weeks) the fibrotic phase of the model (16 weeks onwards). Data expressed as mean percentage initial (day 0) body weight (%) ± SEM; *n* = 5 - 8. Mean average starting body mass; sham irradiated 17.7 g, 10 Gy 18.1 g, 12.5 Gy 18.1 g, 15 Gy 18.5 g, 17.5 Gy 18.4 g and 20 Gy 18.8g.

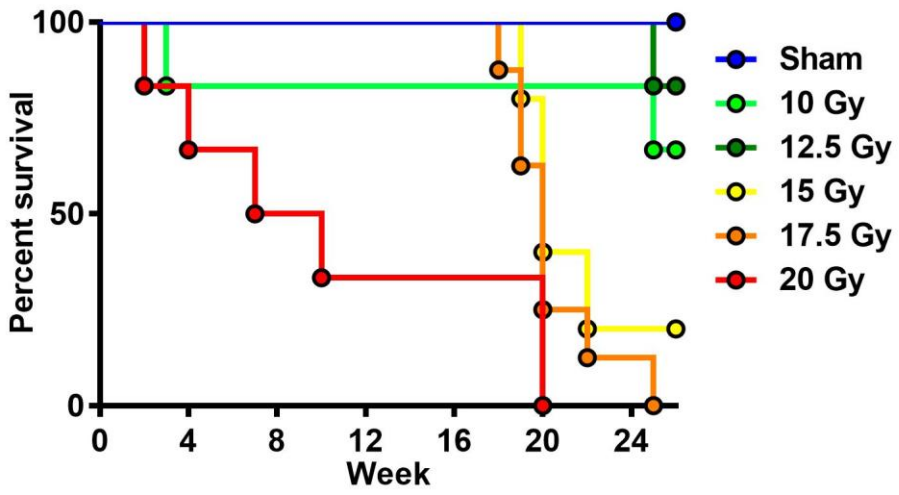


Figure 4.3 The effect of thoracic irradiation dose on survival. Mice (female, C57BL/6) received thoracic irradiation 10, 12.5, 15, 17.5 or 20 Gy or were 'sham' irradiated on day 0. Mice that became sick or had substantial cutaneous burns that did not heal within 1-2 weeks were euthanized using an appropriate schedule 1 procedure. Survival post irradiation (%); n = 5 - 8.

4.4.2. The effect of 10 Gy thoracic irradiation on the development of sub-acute inflammatory response

Histological sections were taken from male, mice, treated with 10 Gy, 10 weeks post irradiation, a time point that has previously been regarded as the start of a sub-acute inflammatory response (Li et al., 2009). H&E staining of lung tissue sections shows no sign of tissue damage or inflammatory cell influx (figure **4.4 i** and **ii**). Masson's trichrome staining revealed no obvious increase in connective tissue 10 weeks post 10 Gy thoracic irradiation (figure **4.4 iii** and **iv**).

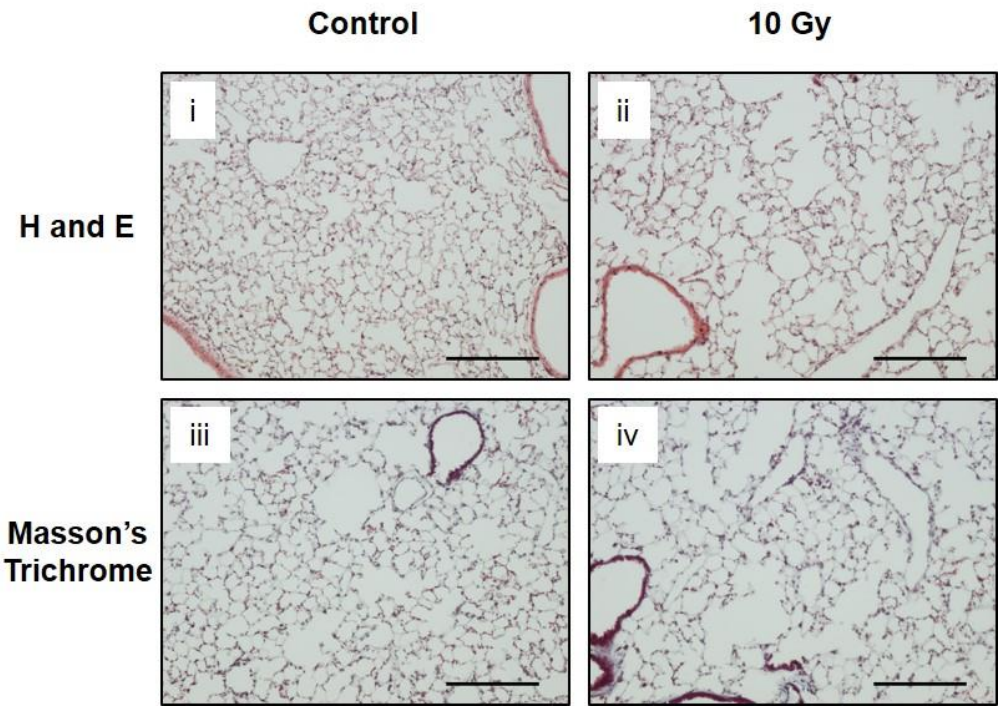


Figure 4.4 The effect of 10 Gy thoracic irradiation on subacute sub-acute inflammatory response and the development of pulmonary fibrosis. Histological staining of lung tissues sections taken from male, C57BL/6 mice, 10 weeks post irradiation. Haematoxylin and eosin (H and E) staining i) control ii) 10 Gy; Masson's trichrome staining iii) control iv) 10 Gy; 10 weeks post irradiation. Representative images captured using x10 magnification, scale bars 100 µm.

4.4.3. The effect of thoracic irradiation on the development of pulmonary fibrosis

Upon sacrifice or study end (26 weeks post irradiation), Masson's trichrome staining of lung tissue sections revealed that at the lowest irradiation dose, 10 Gy, mice had very minimal and infrequent fibrotic changes across the whole lung (see figure **4.5** (**ii**)). At doses of 12.5, 15 and 17.5 Gy (**iii - v**) there was a substantial fibrotic response with numerous architectural changes, including; large areas of tissue had

alveolar septal thickening due to a combination of type II epithelial cell hypertrophy and hyperplasia, as well alveolar septal fibrosis. There was also extensive alveolitis with comprehensive deposition of connective tissue throughout the alveoli and the peripheral airways (black arrows). Individual sections also showed evidence of pleural thickening, identified by a green arrow (see figure **4.5** (**iii**)). Mice treated with 20 Gy (**vi**) only survived to 20 weeks, had less fibrotic changes but had severe inflammatory cell influx into the airways.

Lung tissues sections from mice, 26 weeks post irradiation with 'sham', 10 Gy, 12.5 Gy, 15 Gy, 17.5 Gy were stained with an αvβ6 (clone ch2.A1) antibody. There are positively stained epithelial cells found in mice irradiated with 10 Gy's, however, as the dose of irradiation to the lung increases so did the number of positively stained cells, as identified by arrow heads in figure 2.6, with mice treated with 17.5 Gy having fibrotic lesions with large areas of positively stained cells (see figure **4.6** (**v**)).

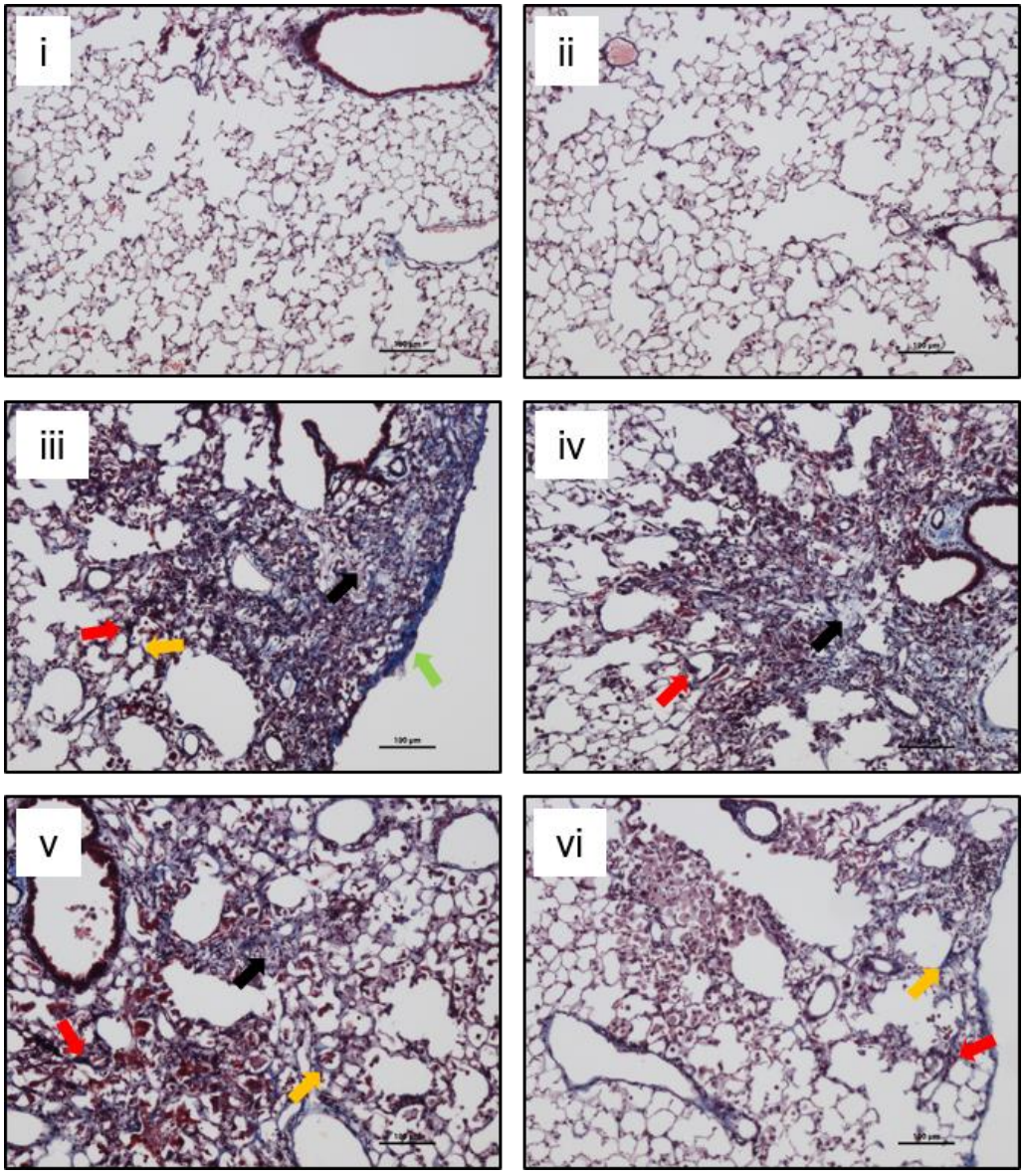


Figure 4.5 The effect of thoracic irradiation on the development of pulmonary fibrosis. Mice (female, C57BL/6) received thoracic irradiation 10, 12.5, 15, 17.5 or 20 Gy or were 'sham' irradiated on day 0. Tissue sections 5 µm thick were stained using Masson's trichrome staining to assess the development of fibrosis. i) 'sham', ii) 10 Gy, iii) 12.5 Gy, iv) 15 Gy, v) 17.5 Gy, 26 weeks post irradiation vi) 20 Gy; 20 weeks post radiation. Mice irradiated with 12.5 Gy or higher doses demonstrate substantial fibrotic changes. There was alveolar thickening caused by type II pneumocyte hypertrophy and hyperplasia, examples are highlighted with (red arrows), and septal fibrosis, examples identified by (orange arrows). Irradiation

promoted development of dense areas of alveolitis and connective tissue deposition (black arrows) as well as pleural thickening, identified by the (green arrow). Representative images captured scale bars 100 µm.

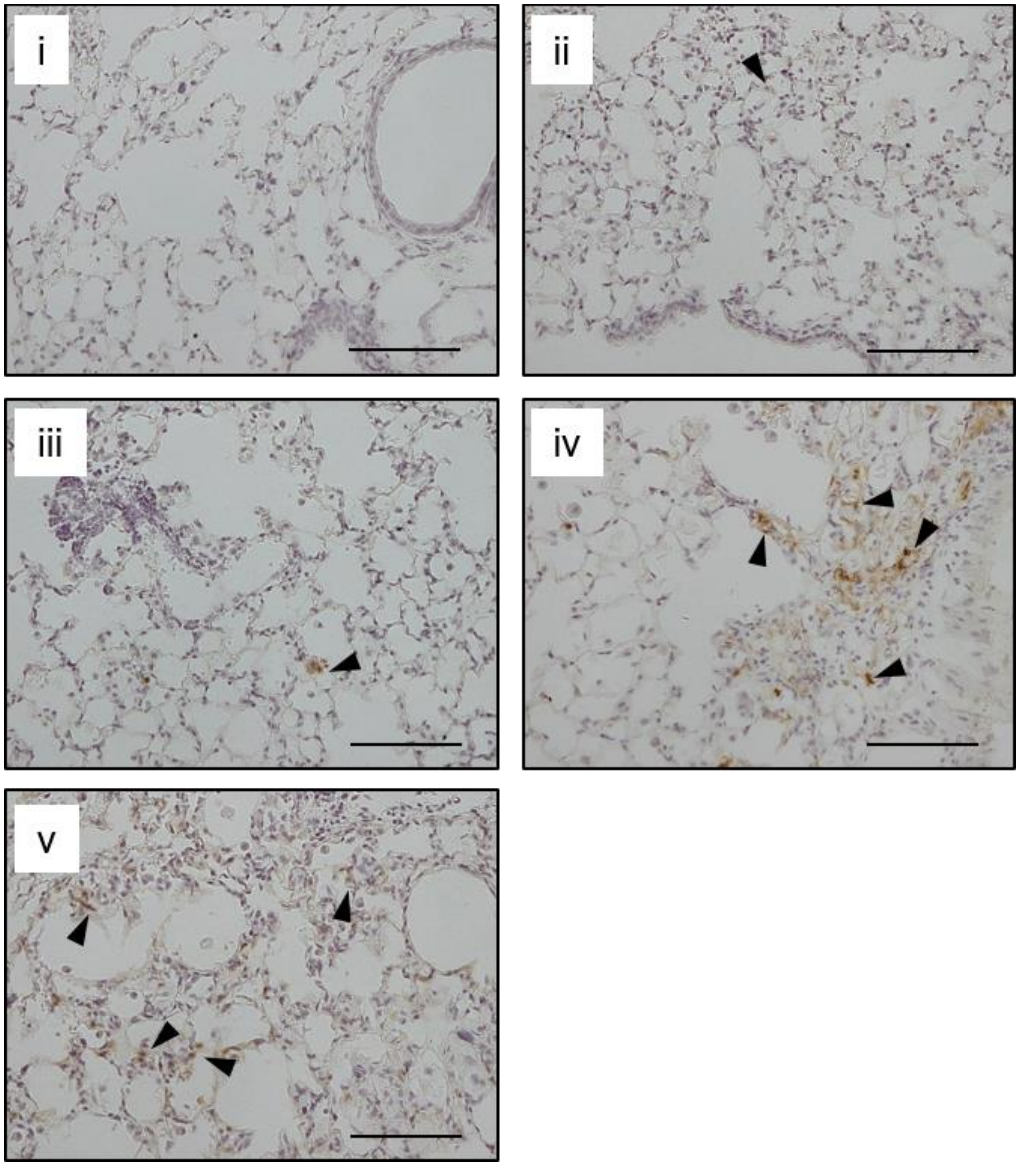


Figure 4.6 Thoracic irradiation increased immunostaining of αvβ6 integrin in a dose dependent manner. Lung tissue sections were stained with human/mouse chimeric anti-αvβ6 (ch2A1), 24-26 weeks post thoracic irradiation. i) 'sham', ii) 10 Gy, iii) 12.5 Gy, iv) 15 Gy, v) 17.5 Gy. Positively stained alveolar epithelium expressing

αvβ6 integrin are identified with black arrow heads. Arrow heads were used in the 17.5 Gy image to identify the most intensely stained epithelial cells but expression was extensive. Representative images captured using x20 magnification, scale bars 100 μm.

4.4.4. A comparison of the effect of 10 Gy thoracic irradiation on the development of pulmonary fibrosis in male and female mice

Previous reports suggest that female mice are more susceptible to irradiation-induced pulmonary fibrosis (Haston and Travis, 1997). Therefore, I compared the effect of irradiation in both male and female mice. Firstly, body weight was recorded over the 26 week study period, shows that over the first 8–12 weeks, sham irradiated male mice gain significantly more weight than their female counter parts. As discussed previously female mice, irradiated with 10 Gy, gain weight at a slower rate than sham irradiated mice up to week 20 before putting weight on rapidly to eventually become the same weight as the control group at week 26. Irradiated male mice appear to gain weight at a slightly reduced rate, compared with their 'sham' irradiated counterparts, up until week 10 (however at this time-point 3 mice are removed from the experiment for analysis of the sub-acute inflammatory response) they then gain weight at the same rate as their control counterparts (see figure **4.7**). Male mice, both 'sham' irradiated and irradiated, gain significantly more weight than female counterparts during the first 6–8 weeks post irradiation. After 8 weeks, the rate at which animals gained weight levels out between the two sexes.

Upon sacrifice or study end (26 weeks post irradiation), Masson's trichrome staining of lung tissue sections revealed there was very little or no evidence of fibrosis in either male or female mice irradiated with 10 Gy (see figure **4.8**).

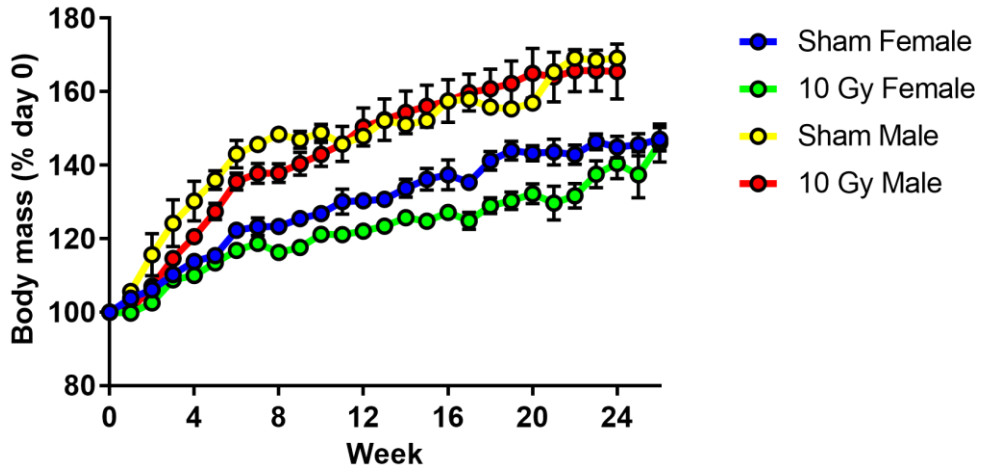


Figure 4.7 The effect of thoracic irradiation on body mass in male and female mice.

Male and female mice received thoracic irradiation 10 Gy or were 'sham' irradiated on day 0. Data expressed as mean percentage initial (day 0) body weight (%) ± SEM; female n = 6 – 8, male 10 Gy n = 6, sham n = 2 then at 10 weeks onwards n = 3 and 1, respectively. Mean average starting body mass; sham irradiated female 17.5 g, female 10 Gy 18.1 g, 'sham' irradiated male 19.8 g, male 10 Gy 18.9 g.

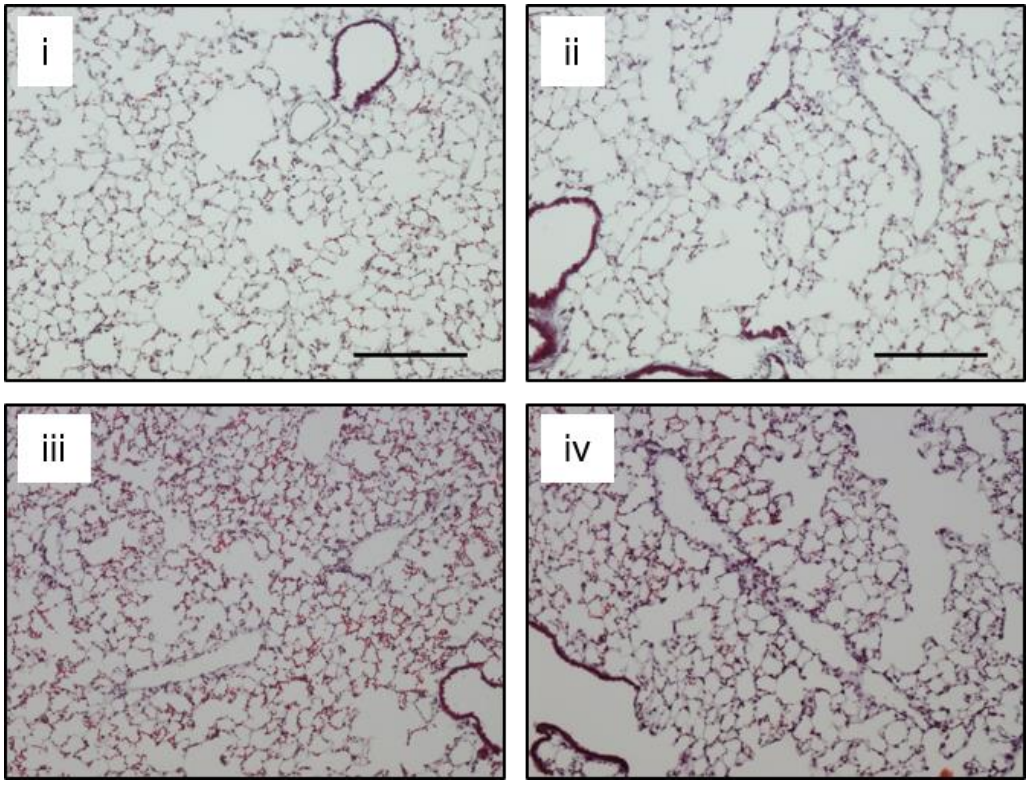


Figure 4.8 The effect of thoracic irradiation on the development of pulmonary fibrosis in male and female mice. Male and female mice received thoracic irradiation 10 Gy or were 'sham' irradiated on day 0. Tissue sections 5 µm thick were stained using Masson's trichrome staining to assess the development of fibrosis. Female i) sham and ii) 10 Gy; male iii) sham and iv) 10 Gy. Representative images captured using x10 magnification, scale bars 100 µm.

4.4.5. *Ex vivo* µCT imaging of irradiated lungs

Ex vivo µCT has previously been used as a quantitative end point for assessing pulmonary fibrosis in animal models (Scotton et al., 2013). Whole lungs were imaged and representative mid-lung transaxial µCT sections are shown in figure **4.9**. Image (**i**) shows the normal lung architecture of the 'sham' irradiated mouse. Images visually demonstrate increases in density consistent with fibrotic lesions these

increase in both number and severity as the dose of thoracic irradiation increases from 12.5, 15 and 17. 5 Gy (Figures **4.9 ii**, **iii** and **iv**, respectively). Subpleural fibrosis appears to be a dominant feature in the radiation induced pulmonary fibrosis model with severe areas of subpleural fibrosis being highlighted with white arrows in the 17.5 Gy treated animal.

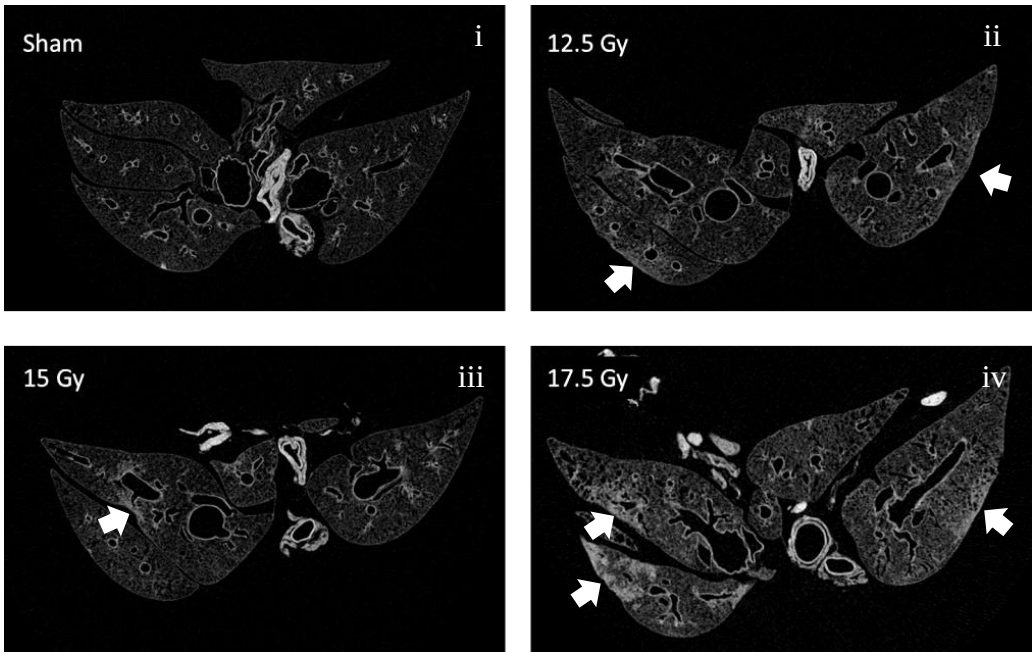


Figure 4.9 *Ex vivo* μCT lung images following thoracic irradiation. Representative mid-lung transaxial μCT sections 24-26 weeks post thoracic irradiation. i) 'sham' irradiated, ii) 12.5 Gy iii) 15 Gy and iv) 17.5 Gy. The white dense areas of the images towards the peripheral portions of the lung relate to subpleural fibrosis or inflammation which is predominantly evident (white arrows) but there are also dense white regions throughout the lungs, evident at all doses of radiation and increase in severity with increasing irradiation exposure.

4.4.6. SPECT/CT imaging of αvβ6 integrins

To determine if SPECT/CT could be used to non-invasively measure αvβ6 integrins during the development of radiation-induced pulmonary fibrosis specific binding of ^{111}In-DTPA-A20FMDV2 to αvβ6 integrins in the lung was assessed. Levels of αvβ6 were determined 8, 12 and 17 weeks post 17.5 Gy thoracic irradiation. Firstly, the percentage of ^{111}In activity in the lung was determined (figure **4.10 a**) to account for variation in the amount of ^{111}In injected (figure **4.10 b**). At 8 weeks post irradiation, the amount of ^{111}In in the lungs of both 'sham' (red lines) and irradiated (blue lines) mice was approximately the same and accounts for roughly equal amounts of the initial injected dose in all 5 mice (0.11 %, 0.88 % in mice 1.3 and 2.4 respectively, as an example) (see figure **4.10 a**). The amount of ^{111}In in the lungs rises at 12 weeks but activity remains approximately the same between sham and irradiated animals. At 17 weeks, there was a further increase in the amount of measured ^{111}In activity in the lungs of irradiated animals but not sham irradiated animals with the % of initial ^{111}In activity in the lungs in the same two example mice now being almost double in the irradiated mouse 0.48 % and 0.26 %, respectively. Total lung volume was determined at each time point and demonstrated a trend towards increased lung volume in irradiated mice 17 weeks post irradiation compared with sham irradiated animals (see figure **4.10 c**). To obtain a measurement of αvβ6 expression in the lung, the percentage of initial ^{111}In per mm^3 of lung was calculated and individual readings from mice were plotted in figure **4.10 d**. The mean average results of this data were plotted in figure **4.11** and these data show no difference in expression was determined 8 weeks post irradiation between irradiated and 'sham' irradiated animals (1.71×10^{-4} and 1.34×10^{-4} % of initial ^{111}In dose/mm^3 of lung, respectively). There was a trend towards increased expression 12 weeks post 17.5 Gy irradiation (6.40

x10^{-4} Vs 5.20 x10^{-4}, % of initial ^{111}In dose/mm^3 of lung, respectively) and became significantly increased 17 weeks post irradiation (8.68 x10^{-4} Vs 3.76 x10^{-4}, % of initial ^{111}In dose/mm^3 of lung, respectively, P = 0.0517 (figure **4.11**). Figure **4.12** shows representative cross-sectional SPECT/CT scans at 17 weeks. There is only low level ^{111}In-DTPA-A20FMDV2 peptide retention in the sham irradiated control lung (**i**) and normal lung architecture visualised in the CT scan (**iii**). The irradiated mice have retention of the radiolabelled peptide (**ii**) in areas of dense or damaged tissue determined via the CT scan (**iv**).

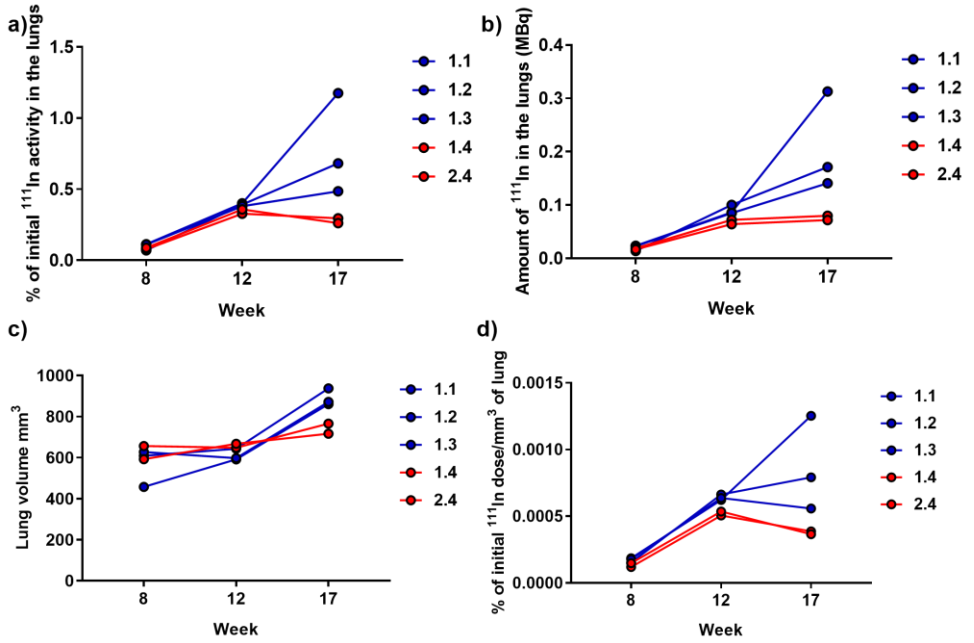


Figure 4.10 The effect of thoracic irradiation exposure on αvβ6 integrin lung expression. αvβ6 integrin expression was determined by SPECT/CT imaging of αvβ6 integrins 8, 12 and 17 weeks post 17.5 Gy thoracic irradiation. ^{111}In-DTPA-A20FMDV2 binding protein, in the lung of irradiated mice 1.1, 1.2 and 1.3 (blue) and sham irradiated mice 1.4 and 2.4 (red). (a) Amount of ^{111}In activity in the lung

(% of initial dose). (b) Total amount ^{111}In in the lung (MBq). (c) Lung volume (mm^3). The percentage of the initial ^{111}In dose per mm^3 of lung. (d) percentage of the initial ^{111}In dose per mm^3 of lung.

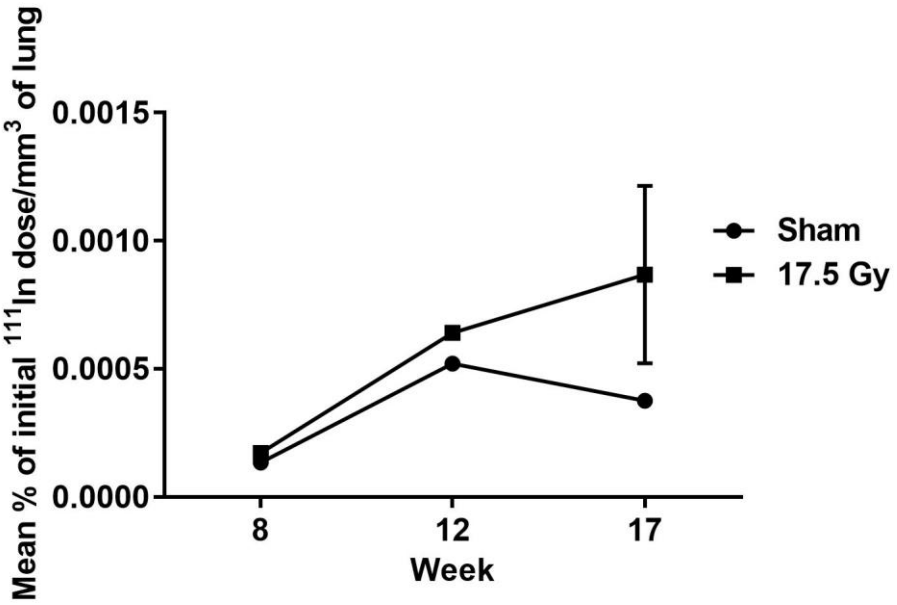


Figure 4.11 The effect of thoracic irradiation exposure on αvβ6 integrin lung expression. αvβ6 integrin expression was determined by SPECT/CT imaging of αvβ6 integrins 8, 12 and 17 weeks post 17.5 Gy thoracic irradiation. Data expressed as mean percentage of the initial ^{111}In dose per mm^3 of lung ± SD; 'sham' n = 2 and 17.5 Gy n = 3. P=0.0517 weeks, irradiated vs 'sham', two-way ANOVA.

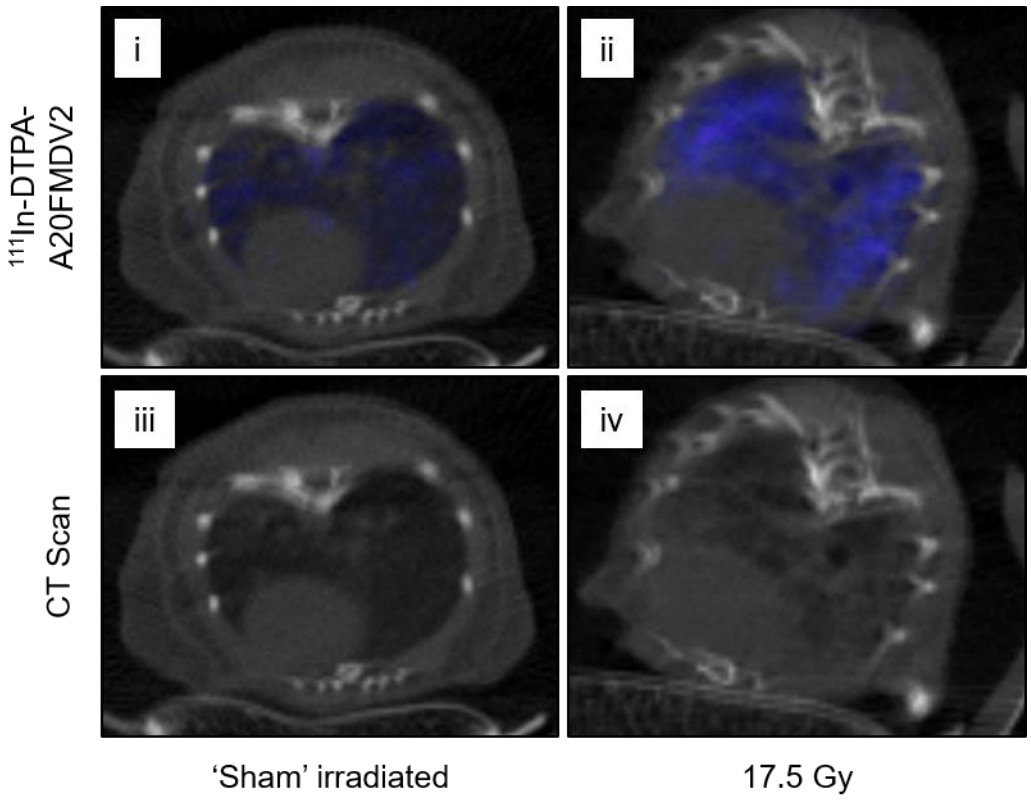


Figure 4.12 Binding of the ^{111}In-DTPA-A20FMDV2 peptide in the lungs of irradiated mice. (i) low levels of ^{111}In-DTPA-A20FMDV2 binding in the 'sham' irradiated controls at 17 weeks, with no evidence of parenchymal damage on the corresponding CT scans (iii). ^{111}In-DTPA-A20FMDV2 retention was significantly increased in the 17.5 Gy irradiated mice at 17 weeks (ii), with some evidence of early parenchymal damage in axial CT scan (iv).

4.5. Discussion

The radiation-induced pulmonary fibrosis model is utilised by various research groups, however, the irradiation source, dose rate and anaesthesia utilised vary broadly between research groups. The pathophysiological response to a specific dose of ionising radiation can be altered by changing any one of these factors; particularly the source and dose rate (Travis et al., 1985, Hurmuz et al., 2014). This has ultimately resulted in a range of doses being utilised by different research groups in order to elicit a fibrotic response. It was therefore necessary to determine the optimal dose to be used using my unique setup that utilised an x ray source generated by a Gulmay RS225 orthovoltage cabinet.

Targeting the irradiation exposure solely to the thorax is essential due to the high susceptibility of the gastrointestinal tract and the brain to ionising radiation. Approximately 5 weeks post irradiation, the fur within the thoracic region of irradiated mice began to discolour. Hair follicles are constantly renewed and their pigments are produced by melanocytes. Hair greying through ionizing radiation exposure is due to DNA damage. DNA damage causes melanocyte stem cells to prematurely differentiate into mature, pigment forming, melanocytes. However, this leads to rapid early depletion of melanocyte stem cells causing premature fur greying (Inomata et al., 2009) Fur greying in the chest area only confirms that the dose was delivered to the thorax only. This provides reassurance that the dose dependent increase in weight loss is linked to acute pneumonitis as seen in various other studies utilising this model, rather than through systemic radiation exposure (Flechsig et al., 2012).

Histological analysis of lung tissue section taken from male mice, 10 weeks post 10 Gy thoracic irradiation, showed little or no sign of inflammation or fibrosis. It has been reported that 10 weeks post irradiation there is a significant increase in lung density which correlates with the start of a sub-acute phase of pneumonitis (Li et al., 2009). The lack of pathological findings at this time point may be due to male mice being less prone to the effects of ionising radiation compared with females as previously mentioned (Haston and Travis, 1997). In my initial studies, a small number of male and female mice were irradiated with 10 Gy so that a comparison can be made between sexes in our model. However, due to no abnormal clinical signs in mice treated with 10 Gy in both male and female at 10 weeks post irradiations a decision was made to make all comparisons 26 weeks post irradiation. Fibrosis has been reported as early as 20 weeks in irradiated mice (Puthawala et al., 2008). These initial pilot studies determined that a dose of 17.5 Gy was optimal, because 17.5 Gy gave robust and reproducible fibrosis as evidenced by histology and β6 integrin expression and increasing the dose further, 20 Gy, caused substantial radiation burns to the skin, substantial and rapid weight loss after 20 weeks. The fluid found in the thoracic cavity of a few of the 20 Gy treated mice, was most likely caused by pleural effusion. Large accumulations of pleural fluid at 6 to 9 months post irradiation have been noted in C57BL/6 mice (Jackson et al., 2010) further complicating the interpretation of the model.

SPECT imaging demonstrated a small trend towards increased αvβ6 expression in mice 12 weeks post irradiation. αvβ6 expression further increased 17 weeks post irradiation. αvβ6 integrin mediated TGF-β activation has been previously documented as essential in the development of pulmonary fibrosis with increased expression also being linked with severe fibrosis and reduced survival time in IPF

patients (Saini et al., 2015). Integrin αvβ6 expression is significantly increased throughout the alveolar epithelium 18-20 weeks post irradiation as assessed by immunohistochemistry (Puthawala et al., 2008). In keeping with this, SPECT/CT imaging demonstrates an increase in β6 17 weeks post irradiation in mice treated with 17.5 Gy. Imaging also demonstrated a slight trend towards an increase in peptide binding to β6 in the lungs of mice 12 weeks post irradiation. It is therefore possible that increases in β6 expression may be detectable earlier than 17 weeks but further studies would be required to confirm this.

For SPECT/CT imaging to be useful as a tool for stratifying radiation induced lung fibrosis and their treatments then binding of the ^{111}In-labeled peptide must correlate to the other endpoints assessed. Firstly, immunohistochemical staining for αvβ6 integrin 26 weeks post irradiation confirmed increased αvβ6 expression in the alveolar epithelium within fibrotic regions (figure **4.6 v**). Furthermore, lung sections stained from the same animals that underwent SPECT/CT demonstrated fibrotic changes assessed by Masson's trichrome staining, with *ex vivo* μCT images also identifying these fibrotic lesions. SPECT/CT has proven to be a sensitive measure of β6 expression in the lung.

In the absence of being able to respiratory gate with the setup used during *in vivo* CT imaging this meant that *ex vivo* CT imaging gave the highest clarity images as the lungs are no longer moving. Although only a small number of lungs were sent away for *ex vivo* CT imaging, clear subpleural scarring and fibrotic regions are evident. These images could allow for the quantification of density changes as previously conducted by (Scotton et al., 2013). Although micro CT images have been shown to replicate findings from histological images, it is not yet thought that this technique is

suitable for the assessment of pulmonary fibrosis in preclinical assessment although, if the technique could be performed *in vivo*, it would make a very useful tool for non-invasive imaging.

4.6. Conclusion

This proof of concept study confirms that exposing the thorax to ionising radiation induced β6 expression within the lung tissue, assessed via histology, that results in substantial fibrosis. Further experiments utilising SPECT/CT imaging show that αvβ6 is increased at earlier time points, 17 weeks, and there was also a trend towards an increase at 12 weeks. These data suggest that that radiation-induced pulmonary fibrosis model in combination with SPECT/CT analysis are valuable as a long-term model with an early indication tool as to if a therapy might be beneficial.

5 Using the Bleomycin Model of Lung Injury and Fibrosis to Understand the Role of SLPI in the Lung

5.1. Introduction

The role of inflammation in the pathogenesis of IPF remains controversial (discussed in further detail in chapter 1.3.3), but neutrophils have been associated with severe, progressive fibrosis and acute exacerbations (Kakugawa et al., 2016).

Neutrophil granules contain serine proteases such as neutrophil elastase (NE), cathepsin G (CAT G) and proteinase-3 (PR-3). These elastases are released in large quantities from activated neutrophils and these proteases have various matrix degrading properties that are discussed in the main introduction (1.10.7). It remains unclear how serine proteases might promote fibrosis although they have been shown to activate TGF-β directly via proteolytic cleavage of the latency associated peptide (LAP) *in vitro* (Wang et al., 2001, Taipale et al., 1992, Lyons et al., 1990). Protease activity is tightly regulated in the lung by a number of protease inhibitors. SLPI is predominately secreted by epithelial cells (Abe et al., 1991) and in the absence of SLPI, elastolytic activity in dermal and mucosal wounds has been shown to be enhanced resulting in increased active TGF-β, prolonged wound repair and increased scarring (Ashcroft et al., 2000, Angelov et al., 2004), suggesting that proteases may activate TGF-β and promote fibrosis (Ashcroft et al., 2000).

5.2. Aim

This chapter aims to determine the role of SLPI regulated protease activation on the development of pulmonary fibrosis.

5.3. Methods

Mice, 6-8 weeks old, were exposed to 15 IU of bleomycin sulphate (Kyowa Hakko, Slough, UK) in 50 µl sterile 0.9 % saline, or 50 µl sterile 0.9 % saline control, via oropharyngeal administration (*o.p.*) (day 0). 15 IU bleomycin was used to induce fibrosis as higher doses caused a significant reduction in survival during the acute lung injury stage of the model (data not shown). *Slpi* null mice ($Slpi^{-/-}$) and heterozygous ($Slpi^{-/+}$) mice on a B6D2F1 background (Ashcroft et al., 2000) were

kindly donated by Sharon Wahl (NIH Bethesda). The development of pulmonary fibrosis was assessed at day 28 in *Slpi*$^{-/-}$ and *Slpi*$^{-/+}$ animals on a B6D2F1 background. Further studies were conducted investigating elastase activity and the development of fibrosis (28 days post 30 IU BLM) in wild-type (wt) and *Slpi*$^{-/-}$ on a C57Bl/6 background, as this background is known to be prone to bleomycin-induced fibrosis (Schrier et al., 1983). Collagen subtype specific gene expression through the acute lung injury (day 7), early (day 14) and late fibrotic phases (day 28) of the bleomycin model was assessed via qPCR. Subtype specific collagen deposition was then examined at 28 days via immunohistochemistry.

5.4. Results

5.4.1. Bleomycin-induced fibrosis in *Slpi*$^{-/-}$ and *Slpi*$^{-/+}$ on a B6D2F1 background

Initial studies sought to determine the effects of *Slpi* gene deletion on the development of bleomycin-induced pulmonary fibrosis using a *Slpi*$^{-/-}$ mouse on a B6D2F1 background, utilising *Slpi*$^{-/+}$ mice as a control, as it was not possible to generate wild type controls on the correct genetic background using the mice available for breading. *Slpi*$^{-/-}$ and *Slpi*$^{-/+}$ mice on a B6D2F1 background are more susceptible to bleomycin-induced lung injury as the standard 60 IU dose had to be reduced to 15 IU due to a large number of mice being lost to reaching Home Office severity limits, data not shown. *Slpi*$^{-/-}$ mice administered 15 IU of bleomycin *o.p.* were more susceptible to acute lung injury as determined through a greater loss in body weight during the first 6 days post bleomycin administration compared to *Slpi*$^{-/+}$ control mice (see figure **5.1**). *Slpi*$^{-/-}$ mice, 6 days post bleomycin administration,

weigh significantly less than *Slpi*$^{-/+}$ bleomycin exposed mice. However, these mice do not go on to develop more fibrosis than their control counter parts as measured by hydroxyproline assay (figure. **5.2**) and Masson's trichrome staining (figure **5.3**) at 28 days. Slpi expression in *Slpi*$^{-/+}$ mice was greatly reduced, potentially explaining the lack of phenotypical differences between -/- and -/+ animals (figure **5.4**).

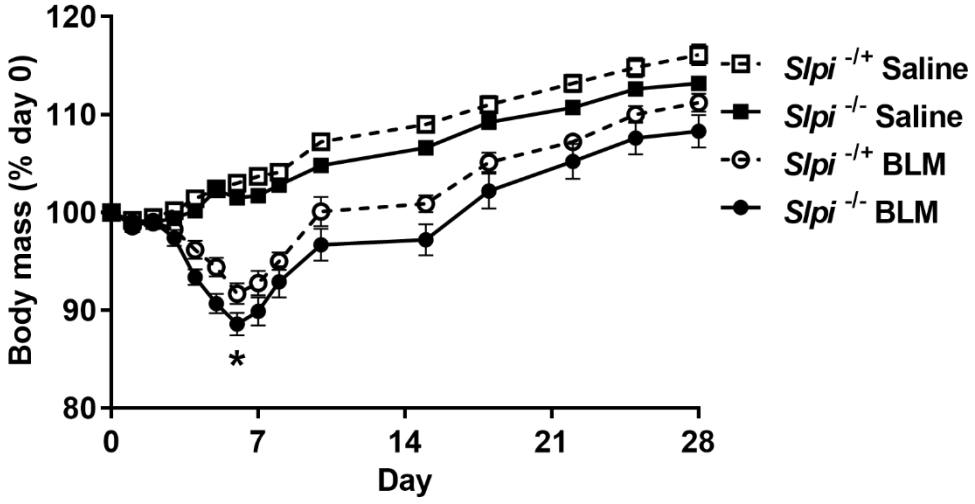


Figure 5.1 The effect of Slpi deletion on weight loss in *Slpi*$^{-/-}$ mice compared with *Slpi*$^{-/+}$ controls. This graph shows body weights for *Slpi*$^{-/-}$ and *Slpi*$^{-/+}$ mice across the 28 day study period after treatment with either 15 IU bleomycin (BLM) or saline as a control. Data expressed as mean percentage of initial (day 0) body mass (%) ± SEM; n = 18-27; Significant difference determined at day 6 *P<0.05 *Slpi*$^{-/-}$ vs. *Slpi*$^{-/+}$ post-bleomycin Two-way ANOVA. Mean average starting body mass; *Slpi*$^{-/+}$ saline 24.7 g, BLM 23.5 g and *Slpi*$^{-/-}$ saline 22.9 g and BLM 22.9 g. No statistical difference between genotype starting weight (t-test P= 0.14).

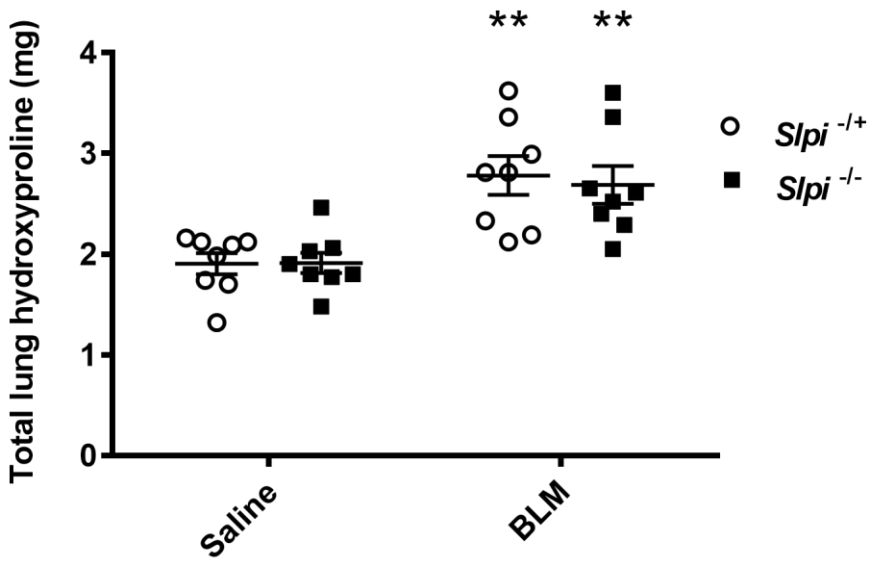


Figure 5.2 The effect of *Slpi* deletion on bleomycin induced collagen deposition in *Slpi*$^{-/-}$ mice compared with *Slpi*$^{-/+}$ controls. Lung hydroxyproline levels were assessed 28 days following 15 IU bleomycin (BLM) in *Slpi*$^{-/-}$ vs. *Slpi*$^{-/+}$ mice. Data expressed as the amount of hydroxyproline (mg) per lung set ± SEM; $n = 8$. **$P<0.01$ BLM vs saline control.

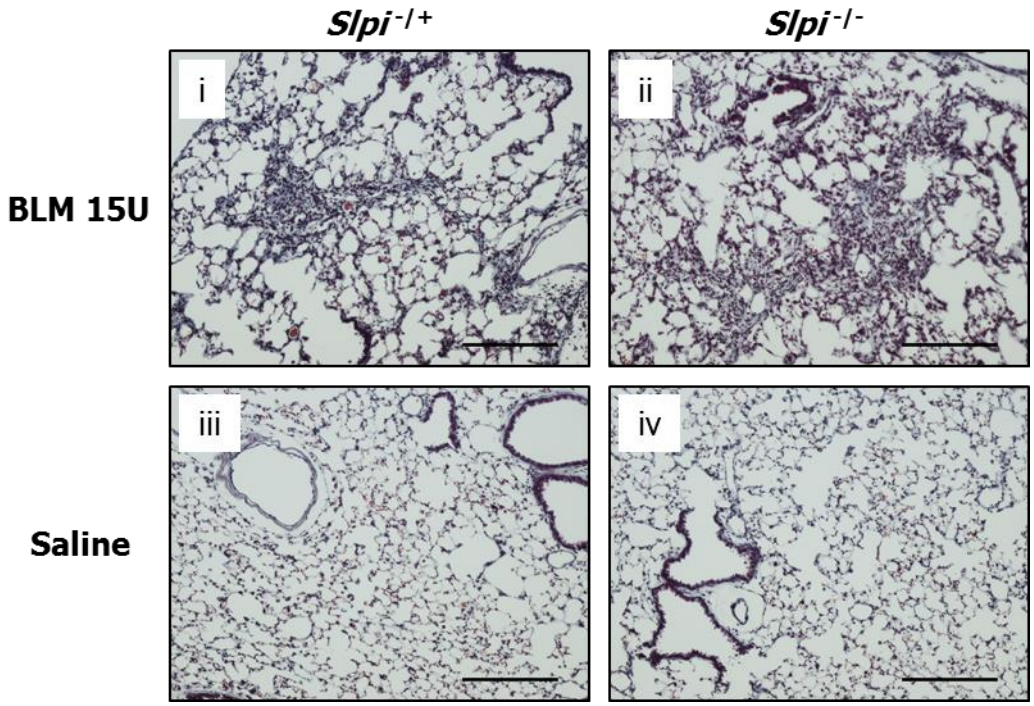


Figure 5.3 Masson's trichrome staining 28 days post bleomycin treatment of *Slpi*$^{-/-}$ and *Slpi*$^{-/+}$ control mice. Representative images of bleomycin treated i) *Slpi*$^{-/+}$, ii) *Slpi*$^{-/-}$ mice and saline treated iii) *Slpi*$^{-/+}$, iv) *Slpi*$^{-/-}$ mice, captured using x10 magnification, scale bars 100 µm $n \geq 4$.

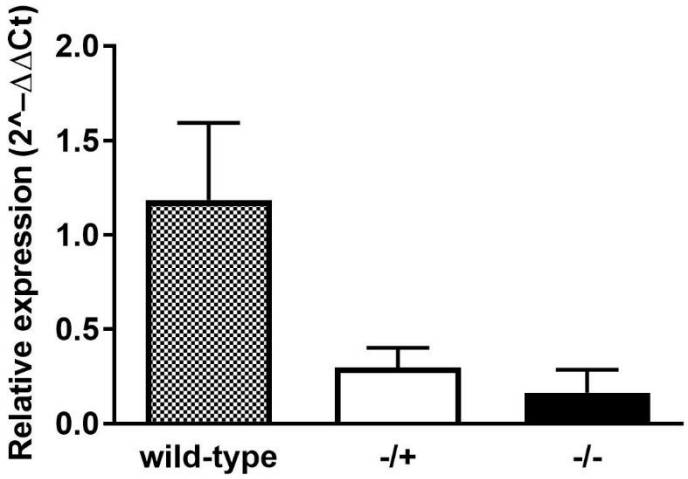


Figure 5.4 Lung homogenate *Slpi* expression. *Slpi* gene expression was assessed in lung homogenate from naive animals to determine basal expression levels. *Slpi*

relative expression was calculated using the $2^{-\Delta\Delta}C_t$ equation with HPRT used as the housekeeper gene. $n = 3$.

5.4.2. *Slpi* gene deletion promotes a proteolytic environment in the lung

To further clarify the effects of *Slpi* on the development of lung fibrosis *Slpi*$^{-/-}$ mice were crossed with C57Bl/6 mice for at least 5 generations and the development of lung fibrosis assessed in *Slpi*$^{-/-}$ mice and compared with wild-type (wt) controls. Genetic susceptibility plays an important role in fibrogenesis, with genetic background of mice being used in the model being essential. C57Bl/6 mice have been demonstrated to be the most susceptible strain variation to bleomycin-induced fibrosis (Schrier et al., 1983). *Slpi* gene deletion was confirmed in C57Bl/6 mice via PCR (figure **5.5**). To determine the effect of loss of SLPI in the lung NE activity in the lung was measured 28-days post bleomycin treatment. No difference in NE activity was seen between wild-type and knock out mice (figure **5.6**). Serine proteases are known to activate MMP-2 and MMP-9 (Pezzato et al., 2003, Ferry et al., 1997). Therefore, the ratio of pro-MMP-2 and MMP-9 and active MMP-2 and MMP-9 was determined 28-days post-bleomycin (figures **5.7** and **5.8** respectively). Mice treated with saline showed no increase in either MMP2 or MMP9. However, there was no increase in active MMP-2 (figure **5.7**) but an increase in active MMP-9 in bleomycin exposed *Slpi*$^{-/-}$ mice compared with either saline or wild-type controls ($P = 0.05$) was detected (figure **5.8**). The effects of SLPI on active MMP-9 levels were not due to increased expression of MMP-9 because no differences in *Mmp-9*

mRNA levels were found between wild-type and *Slpi*$^{-/-}$ mice exposed to saline or bleomycin 28 days post bleomycin (figure **5.9**).

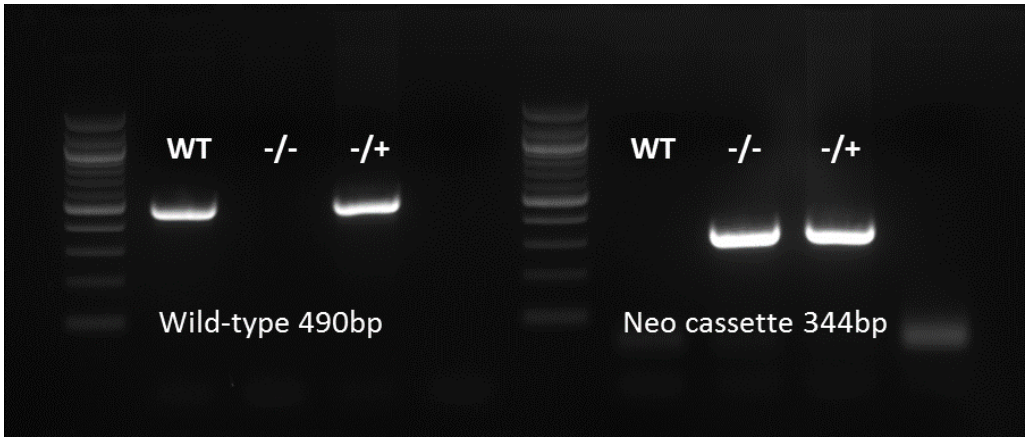


Figure 5.5 *Slpi*$^{-/-}$ mice do not express the *Slpi* wild type allele. Wild-type (WT) mice express the 490bp allele. *Slpi* null mice (-/-) do not express the WT allele but instead express the smaller (344bp) neo-cassette. The heterozygous animal (-/+) expresses both the WT allele and neo cassette.

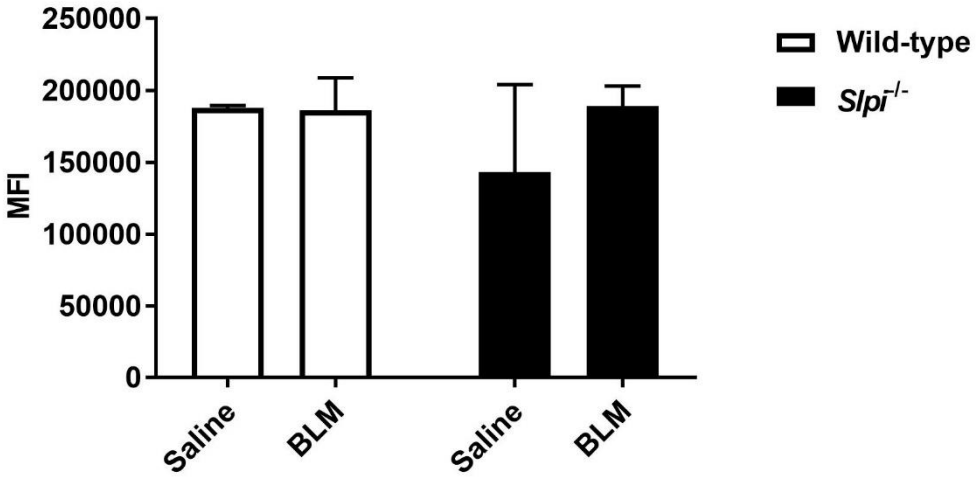


Figure 5.6 Neutrophil elastase activity in lung tissue 28 days post bleomycin treatment. There was no increase in lung NE activity regardless of genotype or injury. Data expressed as mean fluorescence intensity (MFI) ± SEM; $n \geq 2$.

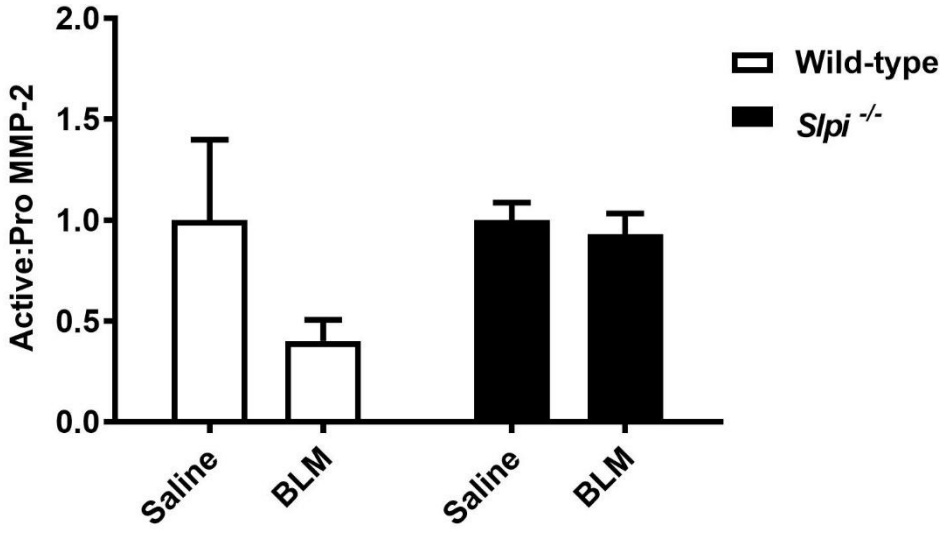


Figure 5.7 Ratio of pro and active forms of MMP-2 in BAL supernatant from wild-type and *Slpi*$^{-/-}$ mice. MMP-2 activity was assessed via gelatine zymography in BAL supernatant 28 days post bleomycin exposure. Mean Active:Pro ratio ± SEM; $n = 8$.

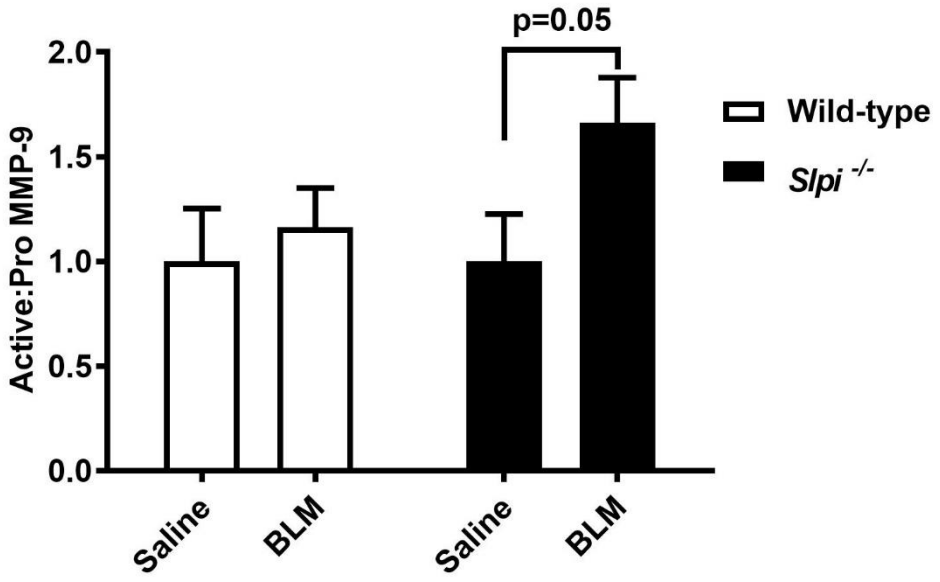


Figure 5.8 Ratio of pro and active forms of MMP-9 in BAL supernatant from wild-type and *Slpi*$^{-/-}$ mice. MMP-9 activity was assessed via gelatine zymography in BAL supernatant 28 days post bleomycin exposure. Mean Active:Pro ratio ± SEM; *n* = 8.

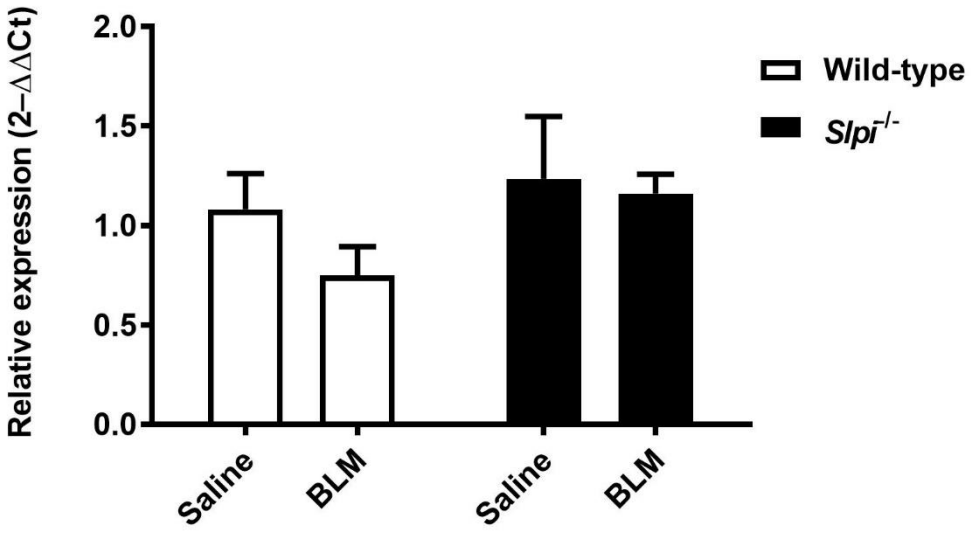


Figure 5.9 Mmp-9 mRNA expression in lung homogenates 28 days post-bleomycin (BLM). Data expressed as mean relative expression ($2^{-\Delta\Delta}C_t$) ± SEM; *n* = 8.

5.4.3. Bleomycin-induced lung fibrosis does not enhance alveolar TGF-β activation in *Slpi*$^{-/-}$ mice, although they still develop pulmonary fibrosis

To determine the effect of SLPI gene deletion on the development of pulmonary fibrosis, TGF-β activation was measured in alveolar macrophages and assessed in histological sections. pSmad2 levels from alveolar macrophages were significantly increased in wild-type mice 28 days post-bleomycin exposure compared with saline controls (P=0.003; figure **5.10**). However, in the *Slpi*$^{-/-}$ mice, there was a trend towards increased basal pSmad2 levels which was not increased by bleomycin treatment. Global tissue TGF-β activation was measured by pSmad2 immunostaining. In saline treated *Slpi*$^{-/-}$ mice, there was evidence of increased pSmad2 staining around the alveoli and large airways (figure **5.11**, **iv**). Saline treated wild-type control lung tissue sections had very few positively stained cells, further indicating increased basal levels in the *Slpi*$^{-/-}$ mice compared with wild-type controls. After bleomycin treatment, pSmad2 staining was significantly increased in both wild-type and *Slpi*$^{-/-}$ mice, primarily in areas of injury and fibroproliferation (figure **5.11**, **i** and **ii**). Lung tissue sections were stained with Masson's trichrome to examine collagen deposition. Lung sections from both wild-type, and *Slpi*$^{-/-}$ mice demonstrated areas of severe fibrosis following bleomycin exposure, predominately around the large airways, compared with saline controls (figure **5.12**). The extent of lung fibrosis was quantified using a modified Ashcroft score and revealed that there was no difference in the actual severity of fibrosis in wild-type mice compared with *Slpi*$^{-/-}$ animals (figure **5.13**).

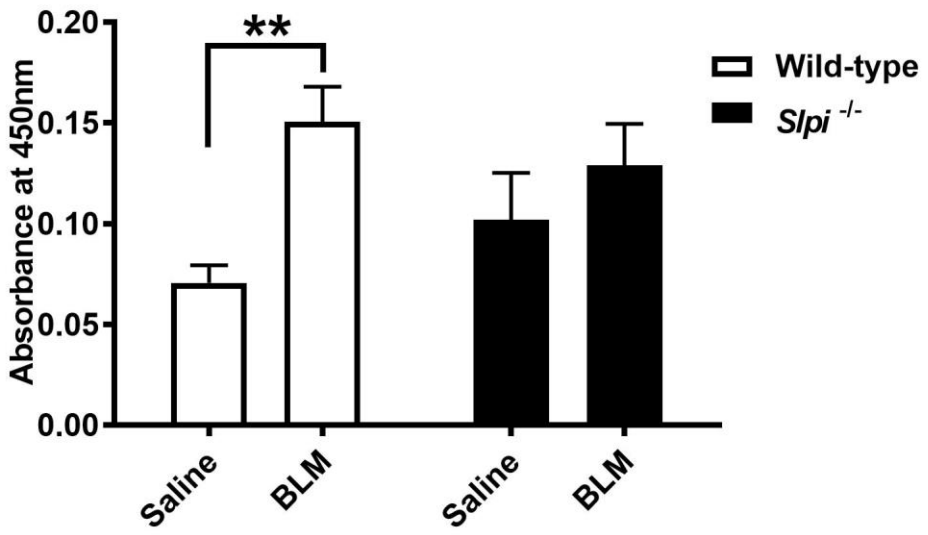


Figure 5.10 The effect of *Slpi* deletion on alveolar macrophage TGF-β activation and pulmonary fibrosis. pSmad2 levels in nuclear extracts from BAL cells from *Slpi*$^{-/-}$ and wild-type mice 28 days post-bleomycin (BLM) were determined by ELISA. Data expressed as mean absorbance at 450 nm ± SEM; $n \geq 5$; $^{**}P<0.005$ BLM vs. saline.

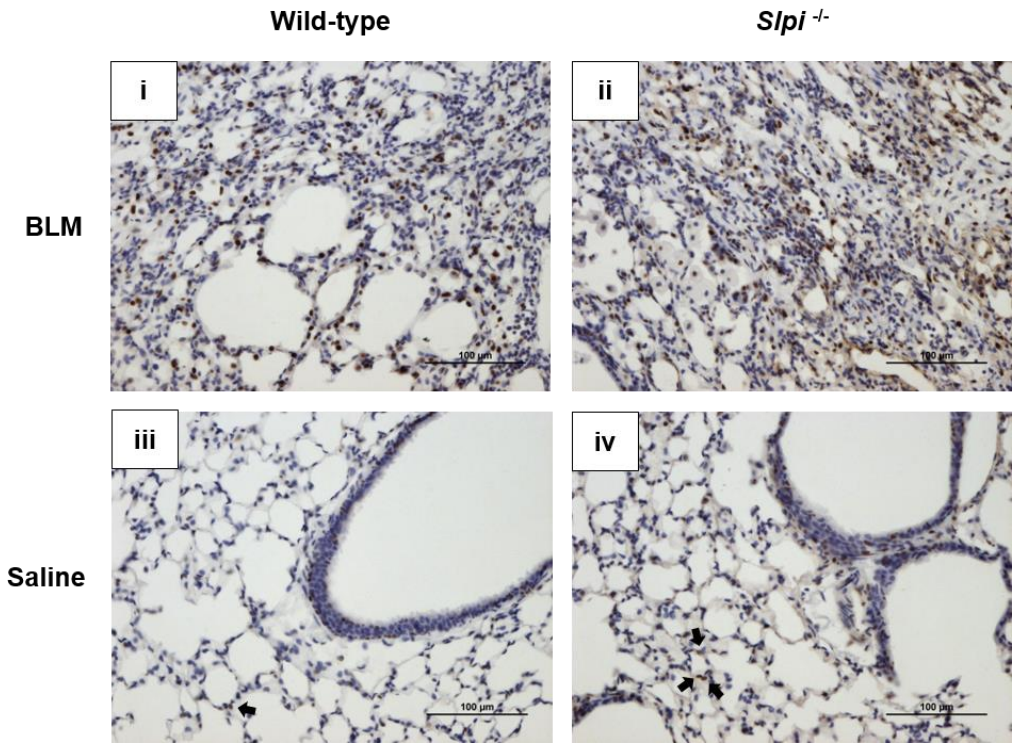


Figure 5.11 Global tissue TGF-β activation assessed by pSmad2 immunohistochemistry. TGF-β activation was assessed in lung tissue sections of wild-type and *Slpi*$^{-/-}$ mice treated with bleomycin via pSmad2 immunostaining. Arrows identify positively stained cells within a single, representative, alveolus in saline treated mice only; there is just one arrow in the wild-type mouse and three in the *Slpi*$^{-/-}$ mouse. Representative images captured using original magnification x20, scale bars 100 µm.

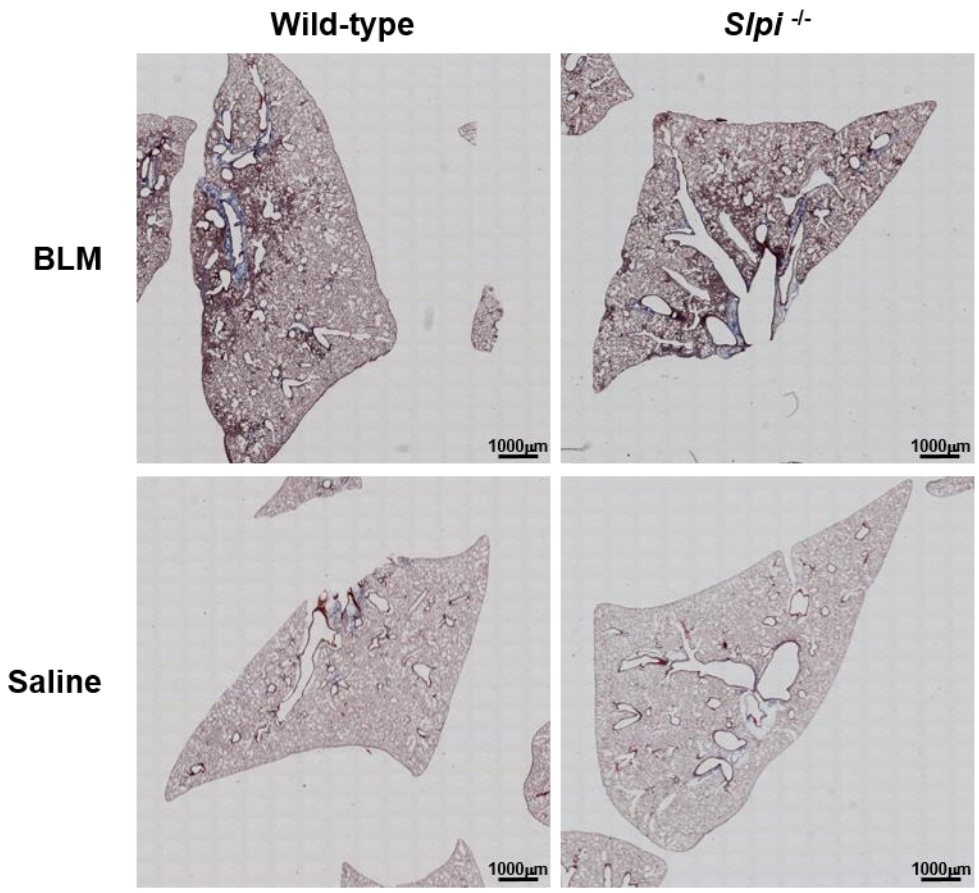


Figure 5.12 Masson's trichrome staining 28 days post-bleomycin treatment.

Examination of both wild-type and *Slpi*$^{-/-}$ mice demonstrated areas of severe fibrosis following bleomycin (BLM) exposure compared with saline controls.

Representative, whole lung lobe, cross sections, scale bars 1000µm.

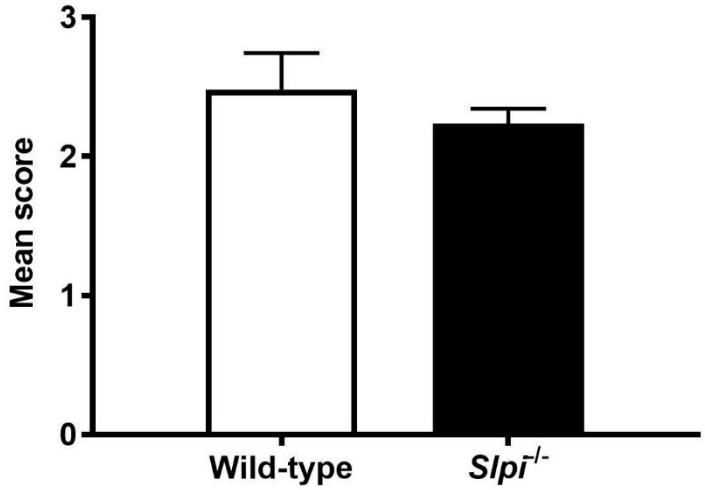


Figure 5.13 Quantitative assessment of trichrome staining. The Ashcroft scoring system was used to assess the severity of fibrosis in bleomycin treated wild-type and *Slpi*$^{-/-}$ mice. Data expressed as mean Ashcroft score ± SEM; $n \geq 3$.

5.4.4. *Slpi* gene deletion exacerbates bleomycin-induced weight loss but does not alter hydroxyproline deposition

These data show that *Slpi*$^{-/-}$ mice lost more weight in the acute lung injury phase of bleomycin-induced lung injury compared with wild-types (figure **5.14**). Weight loss was significantly greater in *Slpi*$^{-/-}$ mice 4 days post bleomycin treatment (P=0.002) and animals reached a maximum weight loss at 5 days.

Due to the early differences in weight loss, lung collagen deposition was assessed, through measurement of lung hydroxyproline concentration, during the inflammatory, early and late fibrotic phases of fibrogenesis following bleomycin exposure (7, 14, and 28 days post bleomycin, respectively). Figure **5.15** shows there

was a progressive increase in hydroxyproline deposition during all phases of fibrogenesis in wild-type mice that reached statistical significance during the late fibrotic phase, 28 days following bleomycin exposure (P<0.0001). *Slpi*$^{-/-}$ mice shared this same progressive increase in collagen across the time course although the concentration of hydroxyproline was somewhat but non-significantly lower at each time point (figure **5.15**).

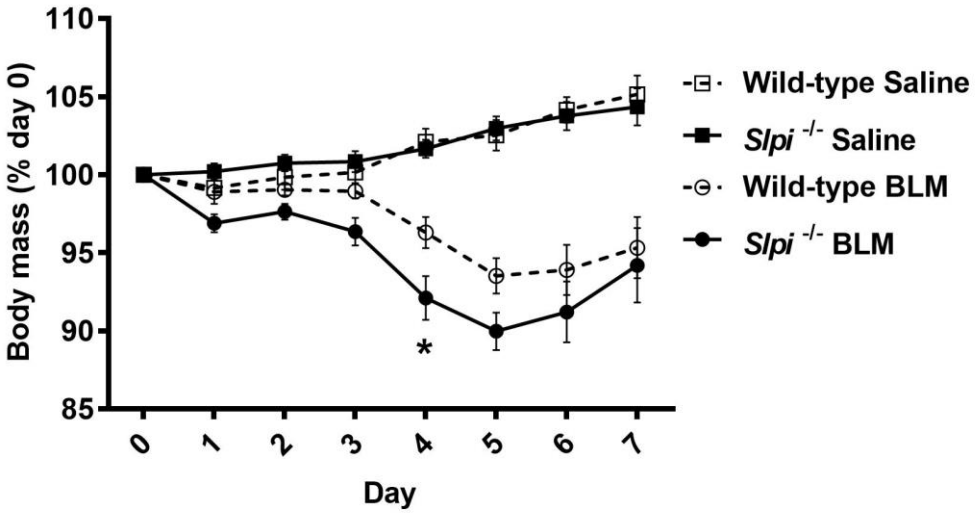


Figure 5.14 Body weight during the acute lung injury phase of bleomycin-induced fibrosis. Body weight was recorded for 7 days' post bleomycin (BLM) instillation, the acute lung injury phase, to compare the response of *Slpi*$^{-/-}$ mice with wild-type litter mate controls. Data expressed as mean percentage of initial (day 0) body mass (%) ± SEM; $n \geq 9$; Significant difference determined at day 4 *P<0.05 *Slpi*$^{-/-}$ vs. wild-type post-bleomycin, Two-way ANOVA. Mean average starting body mass; wild-type saline 21.6 g, BLM 20.9 g and *Slpi*$^{-/-}$ saline 20.5 g and BLM 19.8 g. No statistical difference between genotype starting weight (t-test p = 0.10).

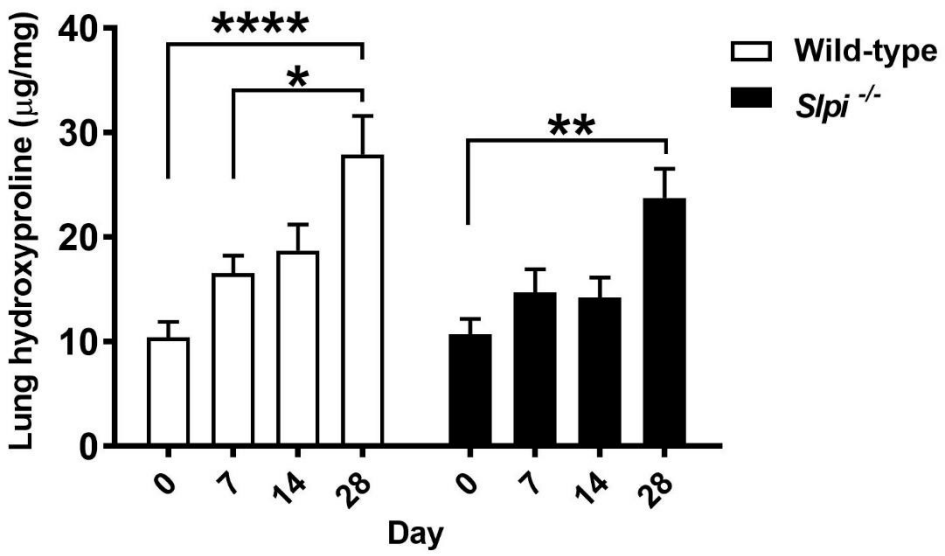


Figure 5.15 Lung hydroxyproline concentration during the early fibrotic and the late fibrotic stages of bleomycin induced pulmonary fibrosis in *Slpi*$^{-/-}$ and wild-type mice.

Lung hydroxyproline levels were assessed at 0, 7, 14 and 28 days; the acute lung injury, the early fibrotic and the late fibrotic stages of the bleomycin-induced fibrosis model, following bleomycin instillation in *Slpi*$^{-/-}$ vs. wild-type mice. Data expressed as the amount of hydroxyproline per mg of lung tissue (μg/mg) ± SEM; $n \geq 8$. **P*<0.05, ***P*<0.01 and *****P*<0.0001, Two-way ANOVA.

5.4.5. *Slpi* gene deletion impairs *Col1α1*, *Col3α1*, *Col4α1* gene expression during fibrogenesis but promotes an early transient increase in *Col6α1* gene expression

To determine whether there were collagen subtype specific differences in response to enhanced proteolysis in bleomycin exposed mice, collagen subtype specific gene expression was investigated. There was sustained expression of both *Col1α1* and

Col4α1 post bleomycin treatment. Expression of *Col1α1* and *Col4α1* did not increase until the late fibrotic phase in *Slpi*$^{-/-}$ mice and *Col1α1* expression was significantly higher at 28 days in wild-type mice compared with *Slpi*$^{-/-}$ animals (*P*=0.0124 figure **5.16**). In wild-type animals, the expression of *Col3α1* mRNA was significantly increased 28 days post bleomycin and, again, there was no increase in *Slpi*$^{-/-}$ animals. Analysis of *Col6a1* showed an early and transient increase at 7 days, during acute lung injury, in *Slpi*$^{-/-}$ mice only (*P*=0.011).

To see how this gene expression related to protein expression, lung tissue sections, 28 days post bleomycin instillation, were stained for collagen type I, III, IV and VI (figure **5.17**). In fibrotic lesions greater than 7 500 μm^2, collagen type I and VI positively stained tissue was assessed as a percentage of the total tissue area. Despite differences in gene expression between wild-type and *Slpi*$^{-/-}$ mice there are no difference in collagen type I and VI composition of bleomycin-induced fibrotic lesions (figure **5.18**).

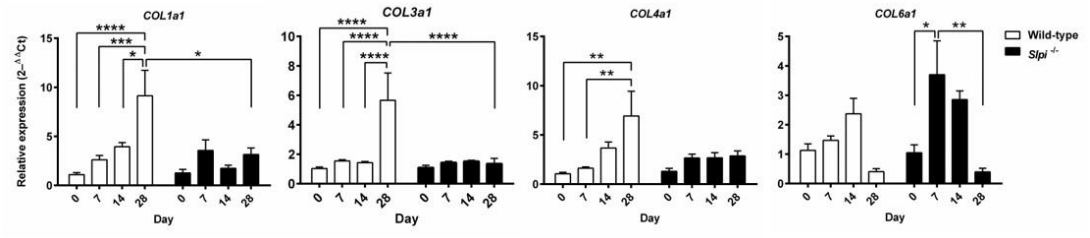


Figure 5.16 The effect of *Slpi* deletion on subtype specific collagen synthesis and deposition. *Col1α1*, *Col3α1*, *Col4α1* and *Col6α1* gene expression 0, 7, 14 and 28 days post-bleomycin. Data expressed as mean relative expression ($2^{-\Delta\Delta}C_t$) ± SEM; $n \geq 8$, **P*<0.05, ***P*<0.01, ****P*<0.001 and *****P*<0.0001, Two-way ANOVA.

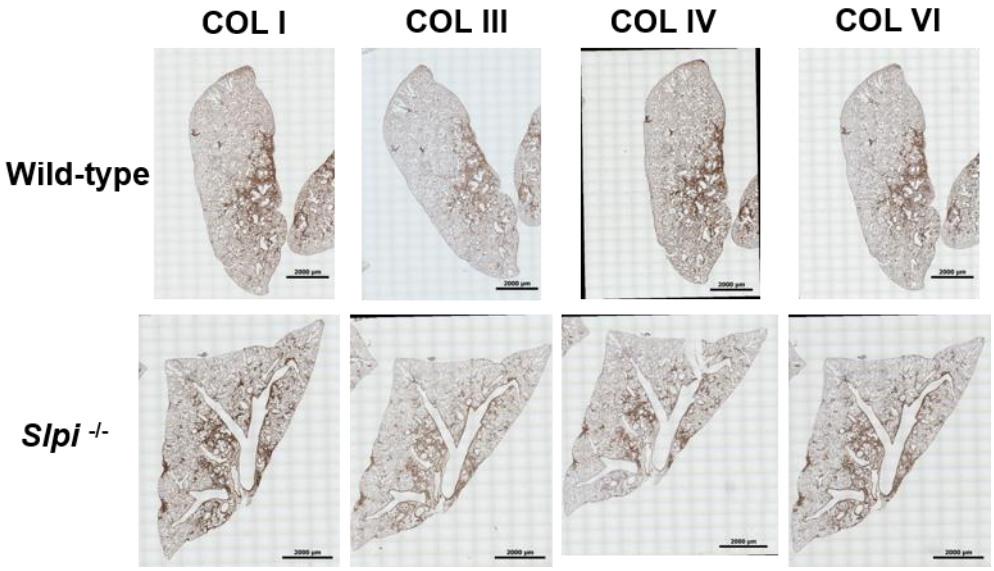


Figure 5.17 Collagen subtype specific immunohistochemistry of bleomycin treated *Slpi*$^{-/-}$ and wild-type mice. 5 µm thick tissue sections from bleomycin treated wild-type and *Slpi*$^{-/-}$ mice were stained with anti-collagen I, anti-collagen III, anti-collagen IV and anti-collagen VI. Low magnification (x10) images were stitched together to visualise whole lung lobes, scale bars 2000 µm. Images are representative of $n \geq 3$ animals.

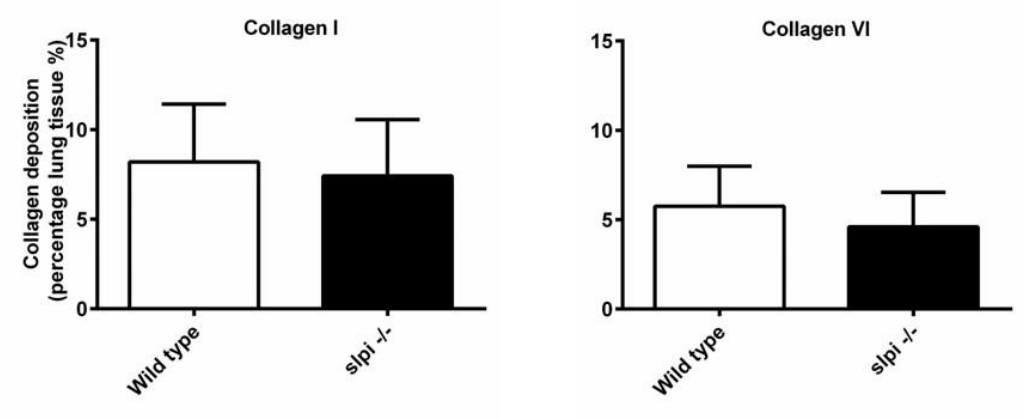


Figure 5.18 Collagen I and VI deposition quantification in lung tissue sections. The amount of stained collagen I or collagen VI in fibrotic lesions greater than 7 500 μm^2 was measured and difference between wild-type and *Slpi*$^{-/-}$ mice was assessed. Data expressed as mean percentage of total lung tissue comprised of fibrotic lesions greater than 7 500 μm^2 containing collagen I or collagen VI (%) ± SEM; $n \geq 3$

5.5. Discussion

When utilising genetically modified animals it is important to consider both the gene of interest and the genetic background on which the mutation is maintained. Initial experiments were conducted on *Slpi*$^{-/-}$ and *Slpi*$^{-/+}$ mice on a mixed B6D2F1 genetic background. Due to their mixed background it was unclear how susceptible these mice would be to bleomycin-induced lung fibrosis, however initial studies were conducted on these animals whilst the lengthy process of backcrossing the animals for 10 generations onto a C57BL/6 background, a bleomycin-induced pulmonary fibrosis susceptible strain was undertaken. Backcrossing also minimises genetic variation in these mice. as mentioned previously C57Bl/6 mice have been demonstrated to be the most susceptible strain to bleomycin-induced fibrosis,

however, C57Bl/6 mice are resistant to hepatic fibrosis which is the reverse for BALB/c mice that are resistant to bleomycin-induced lung injury put get hepatic fibrosis in response to carbon tetrachloride (Shi et al., 1997).

Initial studies determined that both *slpi*$^{-/-}$ and $^{-/+}$ mice on a B6D2F1 background were more susceptible to bleomycin induced lung injury compared with C57Bl/6 mice administered the 75 IU dose of bleomycin determined in the bleomycin dose ranging studies in chapter 3. As the effect of loss of SLPI was not known, pilot studies using 30 IU bleomycin were conducted and a large percentage of both *slpi*$^{-/-}$ and $^{-/+}$ animals lost more than 20 % of body weight during the acute lung injury phase and therefore had to be euthanized due to Home Office severity limits, which at the time, was a loss of 20 % of initial body weight. For this reason, the bleomycin dose was reduced further to 15 IU. This difference in response to bleomycin could be strain related as it is well documented that different strains have different susceptibilities to fibrosis (Walkin et al., 2013). Metabolism of bleomycin is also different between strains, with C57Bl/6 mice having particularly low lung bleomycin metabolism which correlates to this strains high sensitivity to bleomycin induced fibrosis compared to other stains such as BALB/c that have higher metabolism and lower sensitivity (Filderman and Lazo, 1991). As there is no true wild-type control in this experiment, it is difficult to determine if there is a strain dependent increase in susceptibility, but the *slpi*$^{-/+}$ animals that are used as the control for this experiment had greatly reduced SLPI mRNA expression (figure **5.4**) which could be the reason for the increased susceptibility to bleomycin-induced ALI. The initial studies showed that mice on a B6D2F1 background were susceptible to bleomycin-induced lung injury and fibrosis as they lose a significant amount of weight in response to bleomycin instillation, with weight loss peaking 6 days post bleomycin instillation, (figure **5.1**). In keeping with

previous reports that demonstrate mice on a B6D2F1 background have increases in collagen in response to bleomycin, the mice have increased collagen levels in their lungs 28 days post instillation, compared with saline treated control, as determined by both hydroxyproline assay and histological assessment (figure **5.2** and **5.3**) (Coker et al., 1997).

Although *Slpi*$^{-/+}$ mice express the SLPI allele, SLPI mRNA is only expressed at very low levels in these mice suggesting a single allele is insufficient to compensate for the loss of the gene in these mice which may offer one explanation for the lack of large phenotypical difference between *Slpi*$^{-/-}$ and *Slpi*$^{-/+}$ mice. Backcrossing mice can be costly and is also time consuming to backcross animals 5 to 10 generations, however, these data show the importance of backcrossing mice and using wild-type control animals.

Once backcrossed, congenic mice can be used to investigate the gene of interest. As previously described, SLPI deletion has been associated with increased elastase activity, enhanced TGF-β activity, prolonged wound healing and increased inflammatory cell influx into wounds (Ashcroft et al., 2000, Angelov et al., 2004). Loss of SLPI gene expression in the lungs of bleomycin treated animals leads to increased elastase activity as demonstrated by a significant increase in MMP-9 activity. *Slpi*$^{-/-}$ mice also have more severe acute lung injury and *Col6a1* gene expression, a collagen subtype associated with wound repair. At early time points, there was in fact no worsening in fibrosis when compared with wild-type controls.

TGF-β activity was determined through assessment of pSmad2 levels via two separate techniques; first by measuring nuclear Smad2 phosphorylation, in alveolar macrophages and also by immunohistochemistry (John et al., 2017). αvβ6 integrin is

the primary mediator of alveolar activation of TGF-β in normal lungs (Goodwin and Jenkins, 2009, Munger et al., 1999). Wild-type mice had a significant increase in phosphorylation of macrophage Smad2 following bleomycin which supports previously published data and highlights the important role of αvβ6 integrin-mediated TGF-β activation in this model (Munger et al., 1999). Although there is a trend towards an increased basal alveolar TGF-β activity in *Slpi*$^{-/-}$ mice, upon bleomycin instillation there was no significant further increase in activity. As mentioned in the introduction (10.1.4) tethering of the latent TGF-β complex to a stiff extracellular matrix is crucial for the force generation required for αvβ6 integrin-mediated TGF-β activation (Hori et al., 1998, Shi et al., 2011). It is therefore possible that increased matrix degradation associated with SLPI depletion may result in inadequate force generation for this mechanism of TGF-β activation to function. Increased pSmad2 levels were observed in alveolar macrophages at baseline in *Slpi*$^{-/-}$ mice; this is consistent with previously published reports (Ashcroft et al., 2000). pSmad2 levels were increased in fibroproliferative lesions in both wild-type and *Slpi*$^{-/-}$ mice using and levels of pSmad2 were not different using either assessment of TGF-β activation, which may explain why there are similar levels of fibrosis.

Neutrophil elastase activity was measured in lung homogenate (figure **5.6**) but no difference was detected between either genotype. It is possible that this may reflect the timing of the assay after the resolution of inflammation, at the peak of the fibroproliferative phase of the bleomycin model. It may also reflect the importance of other proteinases, such as the lysosomal cysteine proteinase cathepsin K. Cathepsin K has potent collagenolytic activity and transgenic mice over-expressing it have reduced lung fibrosis (Srivastava et al., 2008). Adding to this, mice that do not express cathepsin K (*Ctsk*$^{-/-}$) have increased bleomycin-induced pulmonary fibrosis

and cathepsin K inhibits TGF-β generation (Bühling et al., 2004, Zhang et al., 2011). A small number of osteoporosis patients treated with the cathepsin K inhibitor, Balicatib, in a clinical study, developed skin fibrosis consistent with the pro-fibrotic effect of cysteine proteinases (Rünger et al., 2012).

It has been previously reported that SLPI can inhibit MMP-9 expression, however this study did not demonstrate any difference in total lung Mmp-9 levels at the transcriptional level between wild-type and *Slpi*$^{-/-}$ mice suggesting that SLPI is required predominately to regulate post-translational modification of MMP-9 *in vivo*, consistent with previous studies assessing oral wounds (Ashcroft et al., 2000, Angelov et al., 2004) and the observation that NE can activate MMP-9 *in vivo*.(Ferry et al., 1997) Increased MMP-9 has been associated with both IPF (Selman et al., 2000) and experimental models of lung fibrosis (Ruiz et al., 2003, Selman and Pardo, 2006, Patterson et al., 2001). Increased MMP-9 activity stimulates fibrosis through proteolysis of the alveolar epithelial basement membrane, particularly collagen IV, resulting in impaired re-epithelialization, loss of a stable epithelial basement membrane allows for increased fibroblast migration into the alveolar space, (Ruiz et al., 2003, Selman and Pardo, 2006, Patterson et al., 2001) and this could in part explain the development of pulmonary fibrosis in *Slpi*$^{-/-}$ mice.

For further understanding of collagen gene expression during the various stages of the bleomycin-induced pulmonary fibrosis model, the expression of four different collagen subtypes was determined; *Col1α1*, *Col3α1*, *Col4α1* and *Col6α1*. Immunohistochemistry was then used to investigate the deposition of these collagen subtypes 28 days post bleomycin. These data show that there are sustained increases in *Col1α1* and *Col4α1* in wild-type animals in the first 4 weeks following bleomycin-induced fibrosis. This sustained increase was not replicated in *Slpi*$^{-/-}$ animals,

however, there were similar levels of collagen I, III, IV, and VI deposition in the lung, assessed by immunohistochemistry at 28 days post bleomycin instillation suggests that SLPI is somehow associated with their expression in the lung. Collagen I, III, IV, and VI deposition appeared to be co-localised in fibrotic lesions (figure **5.17**). As all collagens are characterised by an uninterrupted Glycine-x-y triplet repeat that is an essential part of the triple helical structure, generation of antibodies with specificity to individual collagen subtypes is difficult (Shoulders and Raines, 2009). If the subtype specific collagen staining in (figure **5.17**) lacked specificity, this might be one explanation for the disconnect between the deposition of subtype specific collagen without increases in subtype specific gene expression in *Slpi*$^{-/-}$ mice. Alternatively, it is possible that these mice are capable of depositing collagen without increases in gene expression, and that that post-translational modifications in this protease rich environment could be responsible. Interestingly, there is a significant transient increase in *Col6α1*. This is consistent with published data that suggests that collagen type VI is deposited during wound healing and precedes collagen I expression (Oono et al., 1993, Specks et al., 1995).

5.6. Conclusion

The data show the importance of backcrossing genetically modified animals onto the C57BL/6 background when using the bleomycin-induced pulmonary fibrosis model. Initial studies on *Slpi*$^{-/-}$ vs $^{-/+}$ mice on a mixed B6D2F1 background showed that although the mice were susceptible to bleomycin-induced fibrosis, there were few phenotypical differences as *Slpi*$^{-/+}$ mice only lowly expressed the SLPI gene. Studies on the backcrossed animals demonstrate that *Slpi*$^{-/-}$ mice have enhanced

metalloprotease activity and lung injury following bleomycin but they lack an exaggerated pulmonary fibrotic response in the first month following bleomycin-induced lung injury. Furthermore, SLPI null mice have impaired *Col1α1*, *Col3α1*, and *Col4α1* gene expression following injury despite collagen deposition. It is therefore hypothesised that a metalloprotease-rich environment promotes post-translational processing and collagen deposition resulting in lung fibrosis.

6 Comparison of the Efficacy of a Tranilast:salt to Inhibit Fibrosis Following Both Oropharyngeal and Oral Administration to a Rat Using a Bleomycin Model

6.1. Introduction

Tranilast is a drug registered in Japan and South Korea since 1982 for the treatment of asthma. Its main therapeutic effect is through the inhibition of mast cell degranulation via the inhibition of Ca^{++} uptake (Koda et al., 1985). In the late 1980s it was determined that Tranilast also had anti-fibroproliferative properties and in 1993 was registered for use in keloid and hypertrophic scar treatment. Its mechanisms of actions are still not fully understood but Tranilast inhibits fibroblast proliferation and also inhibits TGF-β (Yamada et al., 1994). Tranilast has been shown to have anti fibrotic effects in various renal fibrosis models that are linked with anti TGF-β activity (Wan and Flavell, 2008). Tranilast has been previously shown to supress bleomycin-induced fibrosis in mice, when administered orally, with

its effect being related to inhibition of alveolar macrophages (Mori et al., 1995). Stabilization of mast cells degranulation by Tranilast may have antifibrotic effects. Histamine has been demonstrated to stimulate fibroblast proliferation *in vitro* (Jordana et al., 1988). Furthermore, mice deficient of mast cells are protected against bleomycin-induced pulmonary fibrosis. Both histamine, via the histamine H_1 receptor, and renin, a protease that initiates the renin-angiotensin cascade that convert angiotensinogen to angiotensin II (ANGII) which can bind to the ANG II AT_1 receptor on fibroblast, cause activation of fibroblast, leading to proliferation, TGF-β production and collagen synthesis (Veerappan et al., 2013). Mast cell granules also contain a number of mast cell specific proteases including; tryptase, chymase and carboxypeptidase A, these can be released in their active form in high concentrations upon degranulation (Pejler et al., 2007). The proteolytic activity of these enzymes, particularly chymase, results in increased ANG II. Tryptase is also increased in the lungs of IPF patients, located in close proximity to fibroblast foci and is thought to stimulate fibroblast proliferation through a protease activated receptor-2 (PAR-2) mediated pathway (Akers et al., 2000, Wygrecka et al., 2013)

Nuformix Ltd have developed a Tranilast:lysine salt, due to Tranilast links with TGF-β inhibition and suppression of various fibrotic disorders, they have the aim of delivering it as a dry powder to patients with IPF to prevent / reverse collagen deposition in the lung.

6.2. Aims

The aim of this chapter is to evaluate the efficacy of Tranilast in inhibiting fibrosis in a therapeutic bleomycin model in rats, comparing the delivery of a Tranilast:lysine salt when given to rats via repeat daily oropharyngeal administration versus repeat daily administration of an oral gavage.

6.3. Methods

To determine if Tranilast could inhibit the development of bleomycin induced pulmonary fibrosis the 21-day rat pulmonary fibrosis model, established in chapter (2.3.2), was used. Rats were chosen over the better characterised mouse model as Nuformix Ltd had conducted all of their pharmacokinetic studies in rats as dry power delivery is more suitable in this animal. However, Nuformix Ltd opted to deliver Tranilast via oropharyngeal (*o.p.*) administration and not dry powder prior to the study commencing due to issues using Tranilast in PennCentury™ insufflator devices and not being able to get sufficient drug dispersion in the lung.

6.4. Administration of Test Items

36 Rats (Lewis, 7 weeks old, male) were split into 6 treatment groups as set out in table (5). Rats were dosed daily with compound from day 11 to day 21 post-bleomycin administration via the oropharyngeal or oral route as detailed in Table (5). All rats were euthanized on day 21 via an appropriate schedule 1 technique (anaesthetic overdose) and tissue collected for analysis.

- A single repeat oropharyngeal administration of 2.50 mg of Tranilast (equivalent to 3.615 mg of the Tranilast:Lysine salt), delivered as 250 μL of Tranilast formulation in 9.5% w/v lactose solution.

- A single repeat oral gavage administration using a syringe containing 300 mg/kg of Tranilast (equivalent to 433.80 mg/kg of the Tranilast:Lysine salt) dissolved in distilled water (2ml).

Table 5: Treatment groups for the bleomycin-induced pulmonary fibrosis Tranilast treated rats.

Group	Day 0 (*o.p.*)	Day 11	Route	Dose	Terminal time	Primary endpoint	Group size
1	Saline	*o.p.* cpd	*o.p.*	250µL	d21	Lung hyp / histo	4
2	Saline	Gavage Cpd	oral	2ml	d21	Lung hyp / histo	4
3	Saline	*o.p.* veh	*o.p.*	250µL	d21	Lung hyp / histo	4
4	BLM	*o.p.* cpd	*o.p.*	250µL	d21	Lung hyp / histo	8
5	BLM	Gavage Cpd	oral	2ml	d21	Lung hyp / histo	8
6	BLM	*o.p.* Veh	*o.p.*	250µL	d21	Lung hyp / histo	8

BLM=Bleomycin, Cpd=Tranilast, Veh= Vehicle control and Hyp= hydroxyproline.

6.4.1. Analysis of lung collagen content

The right lung was removed, frozen and stored at -80 °C. Lung tissue was weighed and then ground to a fine powder under liquid nitrogen. Approximately 100 mg of ground lung tissue (the exact amount used for each animal was recorded) was mixed in 1 ml distilled water and the hydroxyproline assay was conducted as previously stated in the methods (chapter 2.9). Using the weight of lung tissue added to the

assay and the total right lung weight the total amount of Hydroxyproline (mg) per right lung was calculated.

6.4.2. Masson's Trichrome

Eight random sections (x 20 magnification) across the section were scored using the Ashcroft scoring method and a mean score was determined for each section.

6.5. Results

6.5.1. The effect of Tranilast therapeutic treatment on body weight.

Bleomycin causes a significant decrease in body weight, with the average amount of weight lost in all three treatment groups being roughly equal at day 4, when they reach their lowest weights (see figure **6.1**). At day 4 bleomycin treated animals began to gain weight at a similar rate as the saline treated controls and there were no differences in body weight between the two Tranilast treatment groups and the lactose control group. There was a reduction in body weight in the saline / oral Tranilast treated group at day 11, when oral dosing started, but only for two days before animals began to regain weight. This loss in weight was not seen in the bleomycin/ oral Tranilast treated group.

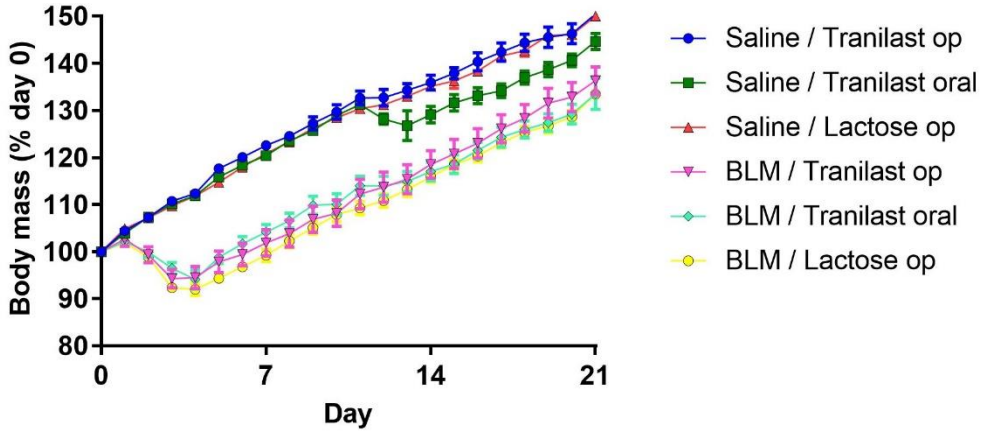


Figure 6.1 The effect of Tranilast therapeutic treatment on mean body mass. Data expressed as mean percentage of initial (day 0) body mass (%) ± SEM; Saline / Tranilast *o.p.* *n* = 4, Saline / Tranilast oral *n* = 3, Saline / Lactose *o.p.* *n* = 3, BLM / Tranilast *o.p.* *n* = 8, BLM / Tranilast oral *n* = 7 and BLM / Lactose *o.p.* *n* = 8. Mean average starting body mass; Saline / Tranilast *o.p.* 199.3 g, Saline / Tranilast oral 199.7 g, Saline /Lactose *o.p.* 206 g, BLM / Tranilast *o.p.* 197.9 g, BLM / Tranilast oral 205.9 g and BLM / Lactose *o.p.* 206.3 g.

6.5.2. The effect of Tranilast treatment on lung weight in bleomycin treated animals

Right lungs were removed and their wet weights recorded. There was a significant increase in wet lung weight in bleomycin treated animals compared with their saline treated controls (****P<0.0001) (figure **6.2**). This increase in lung weight was comparable between *o.p.* and oral dosed animals. However, there was no difference in the lung weight between drug treatment or control groups.

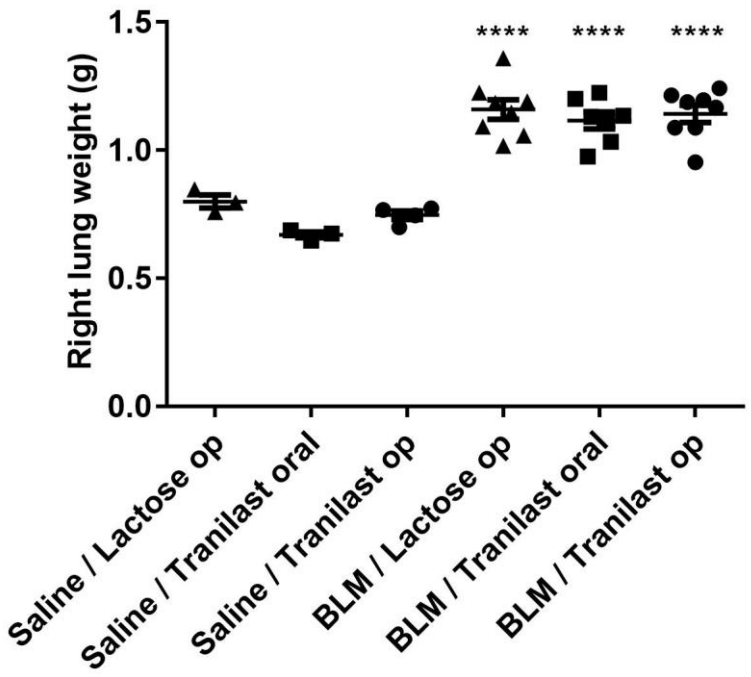


Figure 6.2 Right lung weights from animals treated with Tranilast administered by oral gavage or *o.p.* instillation. Mean ± SEM; Saline / Lactose *o.p.* $n = 3$, Saline / Tranilast oral $n = 3$, Saline / Tranilast *o.p.* $n = 4$, BLM / Lactose *o.p.* $n = 8$, BLM / Tranilast oral $n = 7$ and BLM / Tranilast *o.p.* $n = 8$. ****$P<0.0001$, ANOVA.

6.5.3. The effect of Tranilast treatment on right lung hydroxyproline concentration (µg/ml)

The right lung was weighed then homogenised in liquid nitrogen. A small sample approximately consistent in size was then weighed and removed for assessment of hydroxyproline concentration. There was only a very small trend towards increased hydroxyproline in the homogenised lung tissue samples post bleomycin administration in all three groups compared with their saline controls (figure **6.3**).

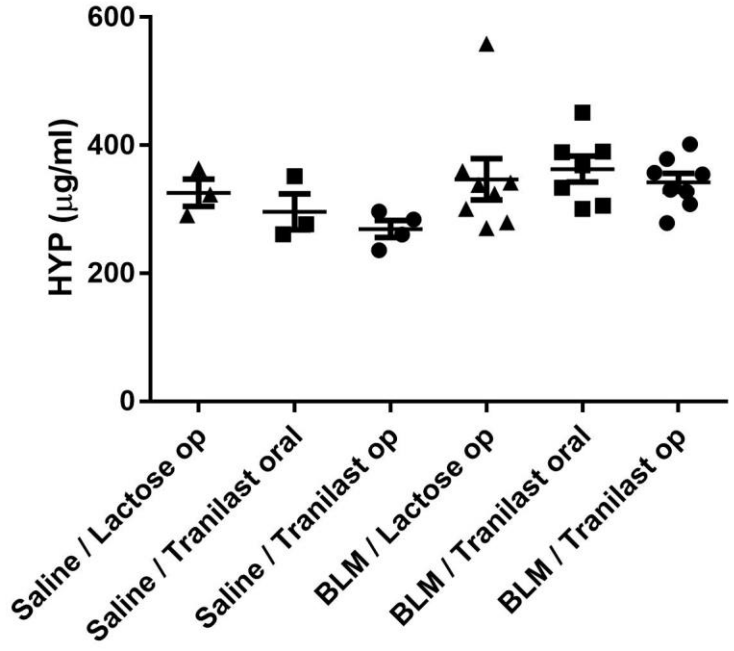


Figure 6.3 Hydroxyproline concentration (µg/ml) of the lung tissue samples tested taken from animals treated with Tranilast administered by oral gavage or *o.p.* instillation. Mean ± SEM; Saline / Lactose o.p. $n = 3$, Saline / Tranilast oral $n = 3$, Saline / Tranilast *o.p.* $n = 4$, BLM / Lactose *o.p.* $n = 8$, BLM / Tranilast oral $n = 7$ and BLM / Tranilast *o.p.* $n = 8$.

6.5.4. The effect of Tranilast treatment on right lung hydroxyproline concentration (µg/mg)

The amount of lung tissue (mg) per sample in the assay was used to calculate the effect Tranilast had on hydroxyproline concentration (µg of hydroxyproline / mg of lung tissue). The saline / Tranilast *o.p.* treated group 3.24 µg/mg had a significantly lower concentration of hydroxyproline compared with the saline / lactose *o.p.* control group 5.67 µg/mg (*P<0.05) (figure **6.4**). There was also a significant difference in the hydroxyproline concentration between bleomycin / Tranilast *o.p.* treatment group

6.12 µg/mg and the saline / Tranilast *o.p.* group 3.24 µg/mg (***P*<0.01). However, the saline / Tranilasst *o.p.* group appears to have reduced collagen compared to the other control groups which might account for this large difference as the bleomycin / Tranilast *o.p.* concentration, 6.12 µg/mg, was similar to the saline / lactose *o.p.* control group 5.67 µg/mg.

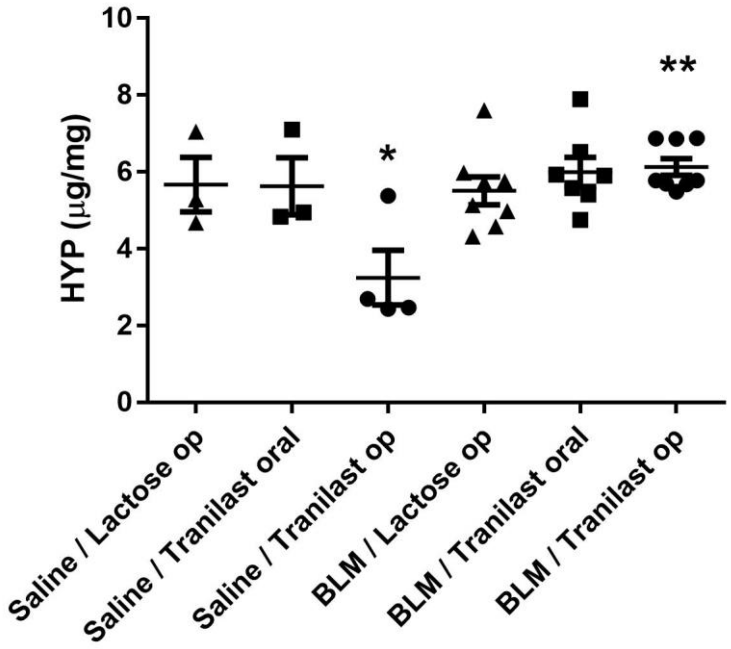


Figure 6.4 Hydroxyproline concentration per mg of lung tissue assayed (µg/mg).

Mean ± SEM; Saline / Lactose *o.p.* *n* = 3, Saline / Tranilast oral *n* = 3, Saline / Tranilast *o.p.* *n* = 4, BLM / Lactose *o.p.* *n* = 8, BLM / Tranilast oral *n* = 7 and BLM / Tranilast *o.p.* *n* = 8. ***P*<0.01 Saline / Tranilast *o.p.* Vs BLM / Tranilast *o.p.*, **P*<0.05 Saline / Lactose *o.p.* Vs Saline / Tranilast *o.p.*, ANOVA.

6.5.5. The effect of Tranilast treatment on right lung hydroxyproline concentration (mg/right lung)

Finally, the amount of hydroxyproline was adjusted to the total right lung weight to calculate how much hydroxyproline would have been in the whole right lung (figure **6.5**). Bleomycin induced increases in hydroxyproline levels in saline / Tranilast oral 3.77 mg Vs bleomycin / Tranilast oral 6.73 mg ***P*<0.01, saline / Tranilast *o.p.* 2.39 mg Vs bleomycin / Tranilast *o.p.* 6.97 mg *****P*<0.0001 but only a trend towards an increase in the lactose *o.p.* control group saline / lactose *o.p.* bleomycin / lactose *o.p.*

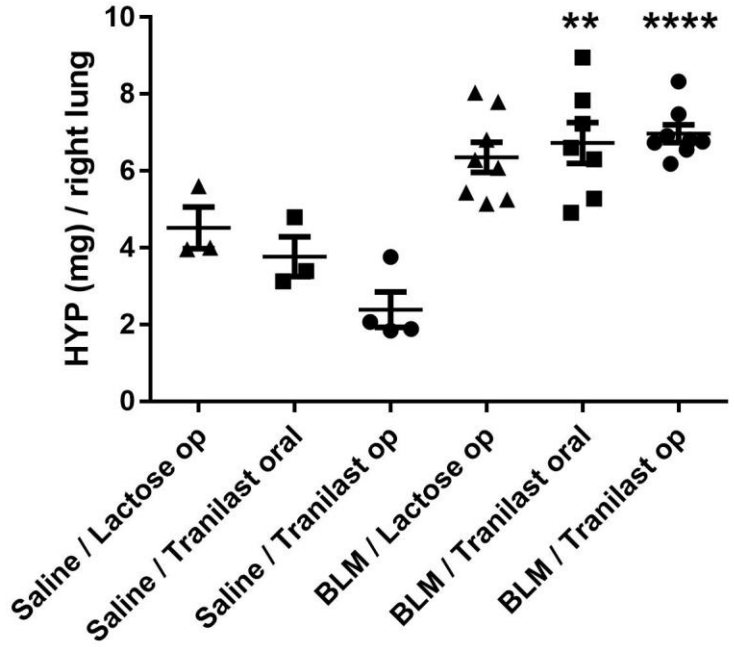


Figure 6.5 Lung hydroxyproline levels in animals treated with Tranilast administered by oral gavage or *o.p.* instillation. Mean ± SEM; Saline / Lactose *o.p.* *n* = 3, Saline / Tranilast oral *n* = 3, Saline / Tranilast *o.p.* *n* = 4, BLM / Lactose *o.p.* *n* = 8, BLM / Tranilast oral *n* = 7 and BLM / Tranilast *o.p.* *n* = 8. ***P*<0.01 Saline / Tranilast *o.p.* Vs BLM / Tranilast *o.p.*, *****P*<0.0001 Saline / Tranilast *o.p.* Vs BLM / Tranilast *o.p.*, ANOVA.

6.5.6. Histological analysis on the effect of Tranilast treatment on bleomycin-induced pulmonary fibrosis

Histological analysis shows that bleomycin treated animals developed severe fibrosis following bleomycin exposure (figure **6.6**) the severity of which was assessed by Ashcroft scoring (figure **6.7**). The scorer was blinded as to which treatment group the lung sections were from to eliminate bias. Mean Ashcroft scores demonstrated that Tranilast treatment, regardless of administration route, 2.03 *o.p.* and 1.94 oral (mean Ashcroft score), had no effect on severity of pulmonary fibrosis (2.03 lactose *o.p.* control).

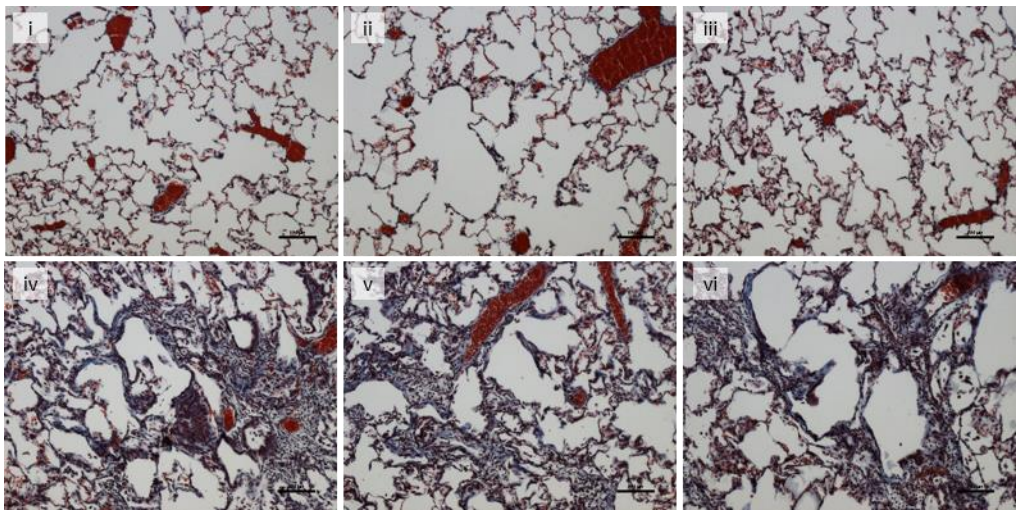


Figure 6.6 Masson's trichrome staining 21 days post-bleomycin treatment.

Representative images of I) Saline / Lactose *o.p.*, ii) Saline / Tranilast *o.p.*, iii) Saline / Tranilast oral, iv) BLM / Lactose *o.p.*, v) BLM / Tranilast *o.p.* and vi) BLM / Tranilast oral treatment. Images captured using x10 magnification, scale bars 100 µm.

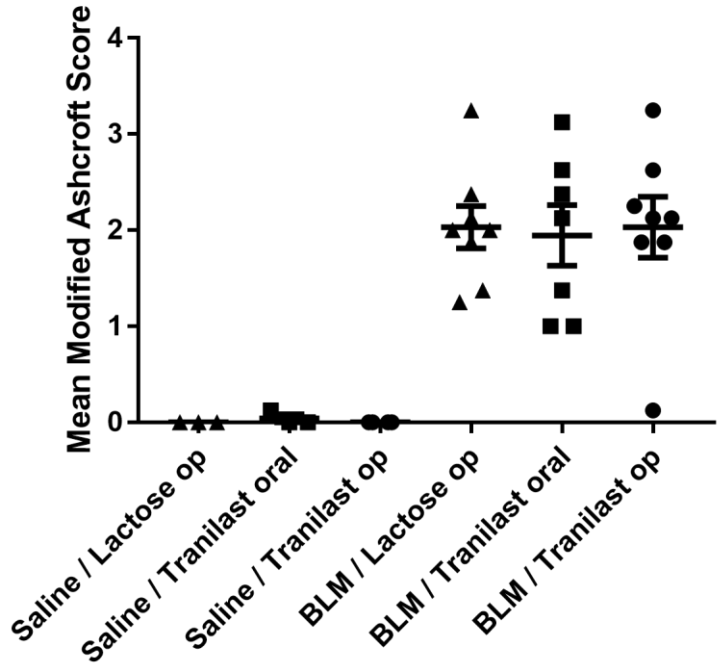


Figure 6.7 Histologic scoring of Masson's Trichrome stained tissue. Eight random sections (x 20 magnification) across the section were scored using the Ashcroft scoring method and a mean score was determined for each section. Data expressed as mean modified Ashcroft Score ± SEM; Saline / Lactose *o.p.* $n = 3$, Saline / Tranilast oral $n = 3$, Saline / Tranilast *o.p.* $n = 4$, BLM / Lactose *o.p.* $n = 8$, BLM / Tranilast oral $n = 7$ and BLM / Tranilast *o.p.* $n = 8$.

6.6. Discussion

The data analysed suggests that rats in this experiment had a mild to moderate fibrotic response to *o.p.* bleomycin. Animals demonstrated significant weight loss following bleomycin instillation, in comparison with controls (figure **6.1**), and there was a significant increase in lung weight in bleomycin treated animals (figure **6.2**).

This increase in lung weight in both *o.p.* and oral dosed animals was comparable. There was no difference in the lung weight between drug treatment or control groups. As hydroxyproline levels were measured in equal amount of lung tissue (~100 mg) the amount of hydroxyproline per ml of sample could be compared (figure **6.3**). This demonstrated that there was only a very slight, non-significant, trend towards an increase in hydroxyproline in rats treated with bleomycin compared with their saline controls. When corrected to amount of hydroxyproline per mg of lung tissue this slight difference is lost except for in the saline / Tranilast *o.p.* group which has a significant reduction in hydroxyproline when compared to both the saline / lactose control and the bleomycin / tranilast *o.p.* group (figure **6.4**). When hydroxyproline levels are corrected to total right lung weight, hydroxyproline levels showed only a trend towards an increase above the saline / lactose *o.p.* treated group. However, there was a trend towards reduced collagen levels in the saline / Tranilast oral and saline / Tranilast *o.p.* control groups compared with the saline /lactose *o.p*, therefore small increases in hydroxyproline, above the saline /lactose *o.p.* levels, meant that they were significantly increased above their respective controls. However, as histological data shows that there were no abnormalities found in the saline treated groups and there was mild to moderate fibrous thickening of alveolar walls across whole sections from all bleomycin treated groups. Taking both the hydroxyproline data and histology data into consideration it was concluded that there was a mild to moderate increase in fibrosis in the bleomycin treated rats. Tranilast treatment had no effect on the bleomycin induced increase in hydroxyproline levels either by *o.p.* or by oral administration (figure **6.5**). Published research has shown Tranilast to supress bleomycin induced fibrosis when administered orally, however, there was no suppression in our experiment (Mori et al., 1995). It was concluded by,

(Mori et al., 1995), that the suppressive effects of Tranilast were likely to be due to alveolar macrophage inhibition during the acute lung injury phase of the model, day 6 in the study. Furthermore, as discussed in the introduction to this chapter (6.1), Tranilast's therapeutic effects on asthma are through inhibition of mast cell degranulation, therefore, it is probable that peak mast cell degranulation would co-inside with the initial bleomycin-induced inflammatory response and therefore treatment with Tranilast started too late to mediate this. As dosing with Tranilast did not occur until day 11, the dosing strategy was only intended to target collagen deposition pathways and not acute lung injury. If a future study was to be conducted investigating the effects of Tranilast:lysine salt *o.p.* during the ALI phase of the model to determine what effect Tranilast has on mast cell degranulation in the bleomycin model Tranilast's target engagement could be assessed with mast cell degranulation kits that measure the activity of enzymes released in degranulation such as tryptase. If Tranilast was causing stabilisation of mast cells, then tryptase activity would not increase with bleomycin treatment.

6.7. Conclusion

Data obtained from this study suggest that Tranilast had no effect on the development of bleomycin induced pulmonary fibrosis when delivered either orally or via oropharyngeal administration. This is the first instance that this formulation of Tranilast:lysine has been dosed therapeutically in a bleomycin induced fibrosis model therefore it is difficult to determine if Tranilast had no effect on the development on bleomycin induced fibrosis due to the formulation or the dosing strategy. Further investigation into the activation of TGF-β through the expression of

pSmad2 via immunohistochemistry would help to clarify if the dose was having any effect.

7 Developing a PCLS Model to Help Assess the Efficacy of Tranilast in Inhibiting Fibrosis

7.1. Introduction

Precision cut lung slice (PCLS) technology has been developed allowing lungs to be sliced into multiple 150 µm thick slices that historically have been used to investigate airway contractions (Dandurand et al., 1993, Bergner and Sanderson, 2002) as the slices maintain their structure and can be easily visualised. Slices are obtained, from animals with induced lung fibrosis or controls, by inflating the lungs *in situ* with low-melting point agarose and allowing it to cool, to solidify. The lungs are then removed, *en bloc*, before being sliced as individual lobes by a vibrating microtome. Slices can be cultured for up to seven days and treated with drugs, the effect of which can then be measured through assessment of collagen via HPLC. With over 30 slices attainable from a mouse lung, it offers the potential to test multiple drugs/doses using very few animals.

Nuformix Ltd have developed a Tranilast:lysine salt with the aim of delivering it as a dry powder to patients with IPF to prevent / reverse collagen deposition in the lung. Evaluating the efficacy of a compound *in vivo* can require the use of large numbers of animals, particularly if attempting to determine an inhibitory concentrotion$_{50}$

(IC_{50}) for collagen deposition. The PCLS model could therefore be ideal for testing this.

7.2. Aims

The objective of this chapter was to develop a PCLS model of fibrosis utilising fibrotic lung slices from mice treated with bleomycin. Tranilast was then used to establish if the mouse PCLS model can be used for assessing a drug's efficacy at inhibiting collagen deposition.

7.3. Methods

Male mice, 6-8 weeks old, were anaesthetised with isoflurane-anaesthetic (2.5 %, 2 L/min flow of oxygen) and exposed to 60 IU of bleomycin sulphate in 50 µl sterile 0.9 % saline, or 50 µl sterile 0.9 % saline control, via oropharyngeal administration (*o.p.*). Mice were sacrificed on day 28 by overdose of anaesthetic. The thoracic cavity was opened and the trachea cannulated. The lungs were inflated with 1.2 ml, 2 % low melting point agarose (in liquid state) and then 0.3 ml air injected to flush the agarose into the distal air spaces. The lungs were then rinsed with ice cold PBS before being removed *en bloc* and placed in ice cold Dulbecco's Modified Eagle Medium (DMEM) to gel the agarose. Once gelled, the lobes are separated and one lobe was sliced at a time. Each slice is cut 150 µm thick using a vibrating microtome (1 mm amplitude. 1mm/sec speed.). Slices were cut in ice cold HANKS buffer to insure tissue remains hydrated and the agarose remains solid.

Incubate all of the slices overnight to melt remaining agarose, whilst insuring slices have access to CO_2. 3 slices were added to 500 µl of pre-warmed DMEM to 24 well plates for 1 hour. The media was then aspirated and the slices stimulate as required with 500 µl Tranilast/control DMEM.

Tranilast preparation: A concentration of Tranilast in dimethyl sulfoxide (DMSO) is 2500 µM. 40.8 mg of Tranilast was dissolved in 0.5 ml of DMSO. Then added in a drop-wise manner to 49.5 ml of DMEM (just using a pipette) whilst stirring. There is some initial cloudiness but this rapidly dissolved with stirring to give a clear solution of a concentration of 2500 µM. The final DMSO concertation in the DMEM is 1 %. 2500 µM Tranilast was chosen as the top concentration to use in this assay by Nuformix as thought to be both soluble in 1% DMSO at this concentration and also non-toxic.

Compound was diluted 1 in 5 in DMSO and then added to DMEM to maintain a volume of 1 % DMSO in DMEM. Concentrations used were 2500, 500, 100, 20 and 4 µM. Media/compound was replaced daily and lung slice were processed 5 days post initial treatment with collagen being measured by HPLC and TGF-β activity determined via assessment of pSMAD2 levels as discussed below.

7.3.1.Hydroxyproline assay (tissue slices)

Slices were blotted with tissue to remove excess media prior to weighing and snap freezing. The samples were then sent to University College London where the collagen content of the slices was assessed (mg collagen / mg of tissue) using high performance liquid chromatography (HPLC).

7.3.2. pSmad2 ELISA

Media was aspirated and the slices were rinsed with PBS and placed into 250 µl RDL lysis buffer containing phosphatase inhibitor (Active-motif). Samples were frozen at -80 ºC. Prior to running the ELISA slices were homogenised, on ice, using a tissue tearer then centrifuged at 20 800 x g (4 °C) for 10 minutes prior to the supernatant being removed and aliquoted. pSmad2 levels were assessed using the PathScan® Phospho-Smad2 (465/467) Sandwich ELISA Kit #7348 (Cell Signaling Technology, Inc.). BCA assay was performed on each aliquoted sample and 10 µg of total protein was assayed from each sample.

7.4. Results

7.4.1. Determining if precision cut lung slices can be used to test the efficacy of Tranilast in inhibiting both TGF-β activation and collagen deposition

Firstly, the aim was to establish if an increase in TGF-β activation could be detected in precision cut lung slices (PCLS) that were extracted from the lungs of bleomycin treated mice, then cultured for 5 days *ex vivo*, compared to saline treated controls. TGF-β activation was assessed via measurements of phosphorylated Smad2 (pSmad2) via ELISA. The data shows there is no significant increase between bleomycin treated and saline treated controls (see figure **7.1**). Furthermore, Tranilast treatment, daily, for five days had no effect on pSmad2 levels in either bleomycin or

saline treated slices across a range of concentrations (0 μM, 4 μM, 20 μM, 100 μM, 500 μM and 2500 μM).

To test if Tranilast could inhibit collagen deposition, the same PCLS model was used and high-performance liquid chromatography (HPLC) was utilised to determine the concentration of collagen in the PCLS post Tranilast treatment (see figure **7.2**). Bleomycin caused a significant increase in collagen 5.87 compared with saline treated slices 2.60 μg/mg (***P*<0.01). Daily treatment with 4 μM, 20 μM, 100 μM, 500 μM and 2500 μM Tranilast for 5 days had no effect on collagen concentration.

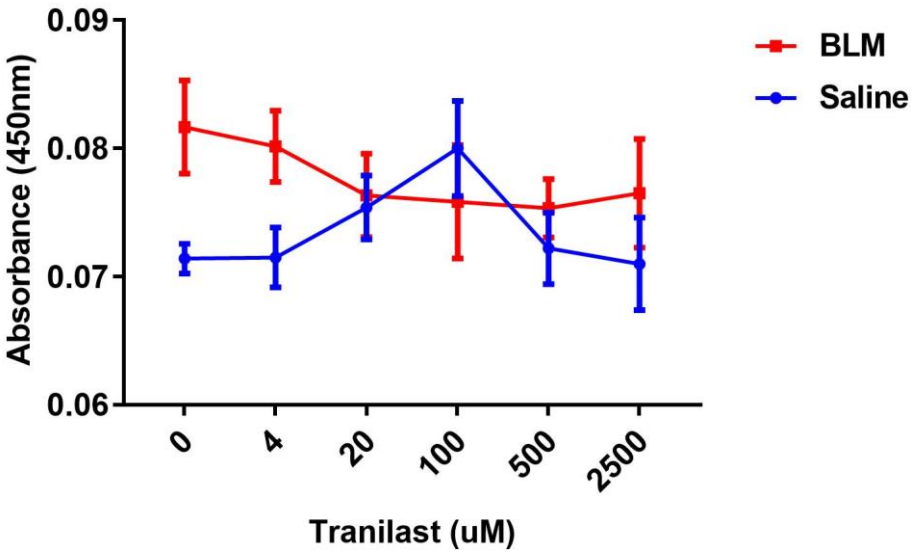


Figure 7.1 Concentration response of Tranilast on TGF-β activation. PCLS were extracted from the lungs of bleomycin-treated (BLM) or saline-treated mice and treated, *ex vivo*, for 5 days with 0 μM, 4 μM, 20 μM, 100 μM, 500 μM and 2500 μM Tranilast. TGF-β activation was then determined through assessment of levels of phosphorylated Smad2 (pSmad2) in lung slice homogenate by ELISA. Data are expressed as mean absorbance ± SEM; n = 4 - 6. A two-way ANOVA determined

NS between BLM and saline treated slices and also between Tranilast concentrations.

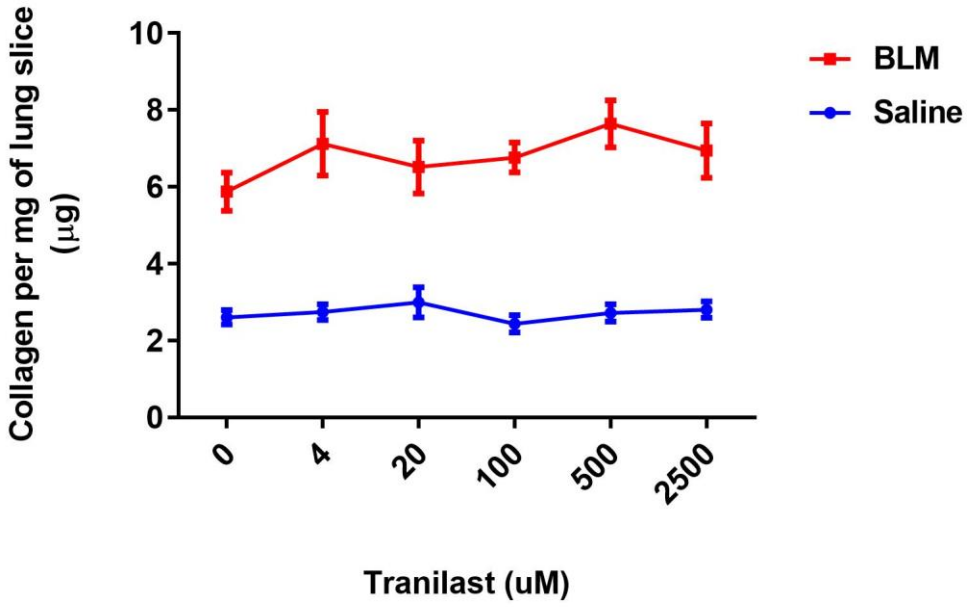


Figure 7.2 Concentration response of Tranilast on hydroxyproline concentration.

PCLS were extracted from the lungs of bleomycin-treated (BLM) or saline-treated mice and treated, *ex vivo*, for 5 days with 0 µM, 4 µM, 20 µM, 100 µM, 500 µM and 2500 µM Tranilast. Data expressed as mean collagen per mg of lung slice (µg) ± SEM; n = 6 - 10. A two-way ANOVA determined NS between Tranilast concentrations.

7.5. Discussion

The aim of this chapter was to determine if PCLS could be used to reduce the number of animals required to assess the efficacy of a compound in both the inhibition of bleomycin-induced TGF-β activation and collagen deposition. PCLS

were extracted from the lungs of bleomycin-treated or saline-treated mice and treated 28 days post administration. The PCLS were then cultured *ex vivo* for 5 days and treated daily with 0 μM, 4 μM, 20 μM, 100 μM, 500 μM and 2500 μM of Tranilast using pSmad2 as a direct measurement of TGF-β activation there was no increase in the bleomycin treated slices. As only low absorbance levels are detected, it is possible the increase is not large enough to be determined. Although an increase in TGF-β was not detected, an increase in collagen in slices treated with bleomycin was measured. Tranilast treatment at any concentration was unable to affect the amount of collagen in the PCLS. Since conducting these experiments, caffeine (100 μM) has been reported to reduce the amount of collagen in PCLS treated with bleomycin at 5 days (Tatler et al., 2016a). Furthermore, both of the current treatments for IPF, Nintedanib and pirfenidone, have been shown to inhibit the upregulation of fibrotic markers in both human and mouse 3D lung tissue lung slices (Mareike et al., 2016). This suggests that it is possible to both reduce collagen deposition and fibrotic markers in PCLS. After conducting these experiments, the stability of Tranilast in DMEM was questioned and it is now thought that it was possible that the half-life of Tranilast in DMEM is very short and daily dosing might not have been frequent enough. If the study were to be repeated the dosing strategy should be reviewed. This highlights the need for comprehensive study design.

7.6. Conclusion

Data obtained from this study suggest HPLC was sensitive enough, in this study, to determine increases in collagen in PCLS extracted from the lungs of bleomycin-treated animals compared with those of saline controls. Taking this data into

consideration along with that published by others, (Tatler et al., 2016a), this model is not only sensitive enough to detect differences between bleomycin treated and saline treated slices but also able to detect drug induced reductions in collagen in bleomycin treated slices. Therefore, this suggests that this model will be a useful tool at greatly reducing the number of mice used in compound efficacy testing.

8 Elk1 Gene Deletion Leads to Spontaneous Early Fibrotic Changes in the Ageing Lung

8.1. Introduction

The incidence and prevalence of IPF suggests it is a disease of ageing, with nearly two thirds of IPF patients being older than 60 years old upon diagnosis and survival times reducing significantly with age (Raghu et al., 2006, Navaratnam et al., 2011). The most commonly used animal model to study IPF is the bleomycin model and this routinely uses young adult mice; aged 6-10 weeks. Although there are age-related animal models of lung fibrosis available, as discussed in the introduction section 1.6.4, there is further need for models where by fibrosis develops spontaneously in aged animals, it is progressive and also the causes of the injury genetically linked to the disease state. *Elk1*$^{-/0}$ mice are a promising possible new model. It has already been demonstrated that *Elk1*$^{-/0}$ mice are more susceptible to bleomycin induced pulmonary fibrosis compared with wild-type mice. Bleomycin treated *Elk1*$^{-/0}$ mice have increased αvβ6 expression in the lung and pSmad2, demonstrating increased TGF-β activity. This results in increased collagen deposition in the lung as assessed by hydroxyproline concentration and Masson's trichrome staining (Tatler et al.,

2016b). If Elk1-mediated repression of αvβ6 is important when the expression of αvβ6 is exacerbated with bleomycin treatment, it is possible that loss of Elk1 repression on basal expression of αvβ6 over a prolonged period may also be important in the development of pulmonary fibrosis.

8.2. Aims

αvβ6 integrins are upregulated in lung fibrosis and are associated with increased activation of the profibrotic cytokine TGF-β. Gene expression of β6 is repressed by the transcription factor Elk1. I therefore hypothesise that animals lacking functional Elk1 (*Elk1*$^{-/0}$) will develop age related pulmonary fibrosis. The aim of this chapter is to determine not only if *Elk1*$^{-/0}$ mice develop age related pulmonary fibrosis but to also determine if they have the potential to be utilised as an age-induced model of pulmonary fibrosis.

8.3. Methods

Male *Elk1*$^{-/0}$ mice and wild-type ($^{+/0}$) litter mate controls were aged for 12 months and the development of pulmonary fibrosis was assessed by hydroxyproline measurement and immunohistochemistry. Collagen subtype specific gene expression was also determined in the lung. In a small number of mice (n = 3) *ACTA* gene expression, in the lung, was determined at 12 weeks of age, as it induces αSMA protein expression.

8.4. Results

8.4.1. Loss of *Elk1* results in age related pulmonary fibrosis.

To determine whether loss of *Elk1* results in age related pulmonary fibrosis $Elk1^{-/0}$ male mice and wild-type littermate controls ($Elk1^{+/0}$) were aged for 12 months prior to their lungs being removed *en bloc* for assessment of fibrosis. Firstly, the body weight of $Elk1^{-/0}$ and $Elk1^{+/0}$ was recorded from 30 weeks of age onwards. There appears to be no significant difference between the two genotypes in body mass, however, there is a trend towards reduced body mass in $Elk1^{-/0}$ evident as early as 42 weeks but the inclination becoming more obvious at 50 weeks; this is still nonsignificant (see figure **8.1**). Only body mass data from mice that survived to the end of the 12 months experimental period were included in the analysis. Three mice were lost from the wild-type control group, one of which was found dead but had shown no sign of distress or weight loss. A further two mice were sacrificed due to scratching of open wounds caused through fighting which did not heal even after treatment with a non-steroidal anti-inflammatory (NSAID), Metacam. The $Elk1^{-/0}$ animal that had to be euthanized was also due to fighting.

At 12 months old, mice were sacrificed, the lungs were excised and wet lung weights were recorded and revealed no difference between $Elk1^{-/0}$ and the $Elk1^{+/0}$ controls (175.7 mg, 161.8 mg respectively $n = 6 – 8$) (figure **8.2**). Lung fibrosis was quantified by measuring levels of hydroxyproline in lung tissue and by assessing histology using Masson trichrome stain. Assessment of total lung hydroxyproline established that there was significantly more hydroxyproline in $Elk1^{-/0}$ mice compared with $Elk1^{+/0}$ controls (852.3, 758.4 µg/lung set, respectively, $n = 5–8$,

P=0.0346) (figure **8.3**). To confirm that there was increased collagen being deposited in the lungs of aged *Elk1*$^{-/0}$ animals compared with control animals, histological sections of lung tissue were stained with Masson trichrome. Assessment of entire lung lobe cross sections demonstrated the very patchy nature of lung fibrosis in *Elk1*$^{-/0}$ aged animals. Figure **8.4** confirms normal lung architecture in *Elk1*$^{+/0}$ control mice (**i**) and a representative fibrotic lesion in a *Elk1*$^{-/0}$ animal is displayed in figure **8.4.** (**ii**). Furthermore, there was a trend towards increased alveolar wall median thickness in *Elk1*$^{-/0}$ mice compared with *Elk1*$^{+/0}$ animals (5.94 vs 5.56 μm respectively) (figure **8.5**).

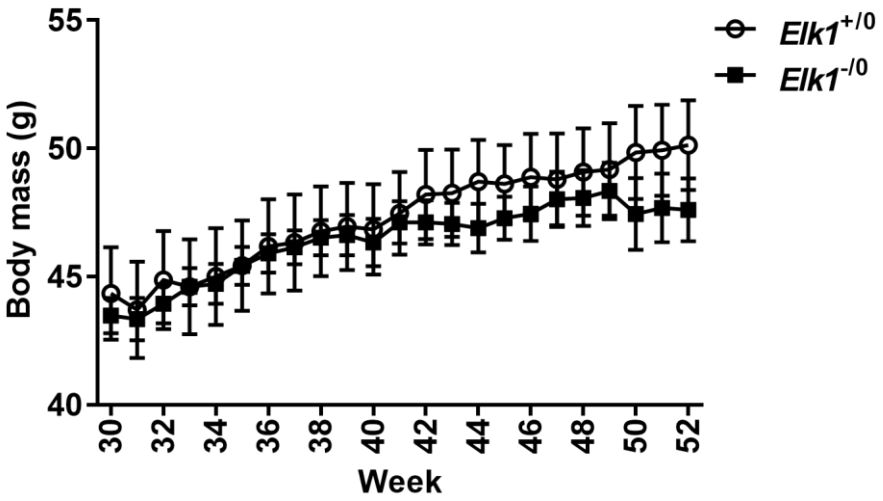


Figure 8.1 The effect of loss of *Elk1* on mean body mass. *Elk1*$^{-/0}$ and *Elk1*$^{+/0}$ control mice were weighed weekly from 30 weeks onwards to determine if loss of *Elk1* influenced body mass (an indication of general health). Data expressed as mean body mass (g) ± SEM; n = 7 – 13.

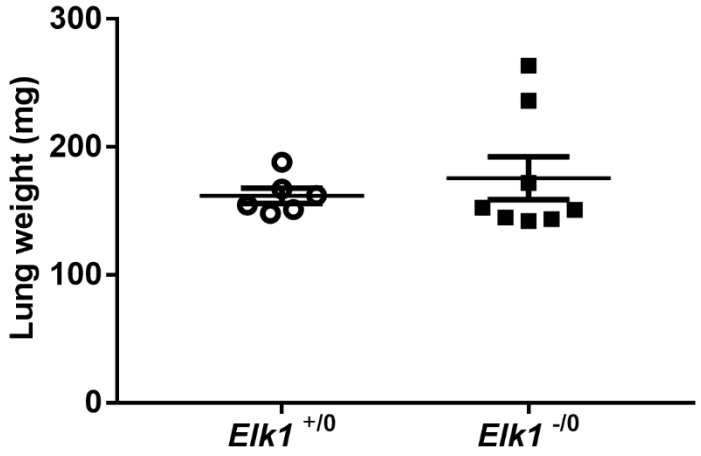


Figure 8.2 The effect of loss of *Elk1* on wet lung weight. Lungs were removed *en bloc* from *Elk1*$^{-/0}$ and *Elk1*$^{+/0}$ mice at 12 months and lung wet lung weights were recorded. Mean wet lung weight (mg) ± SEM; $n = 6 – 8$.

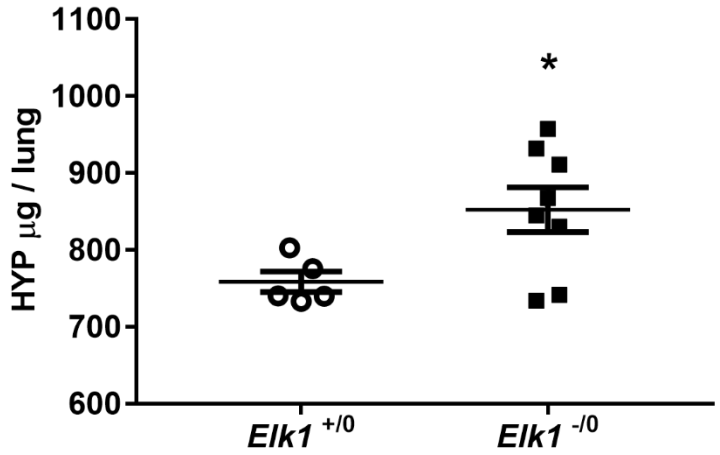


Figure 8.3 Loss of *Elk1* results in age related collagen deposition. To assess if loss of *Elk1* caused age related lung collagen deposition, hydroxyproline levels were measured in the lungs of *Elk1*$^{-/0}$ and *Elk1*$^{+/0}$ control mice at 12 months. Data expressed as the amount of hydroxyproline (µg) per lung ± SEM; $n = 5 – 8$. *$P<0.05$ *Elk1*$^{-/0}$ compared with *Elk1*$^{+/0}$, t-test.

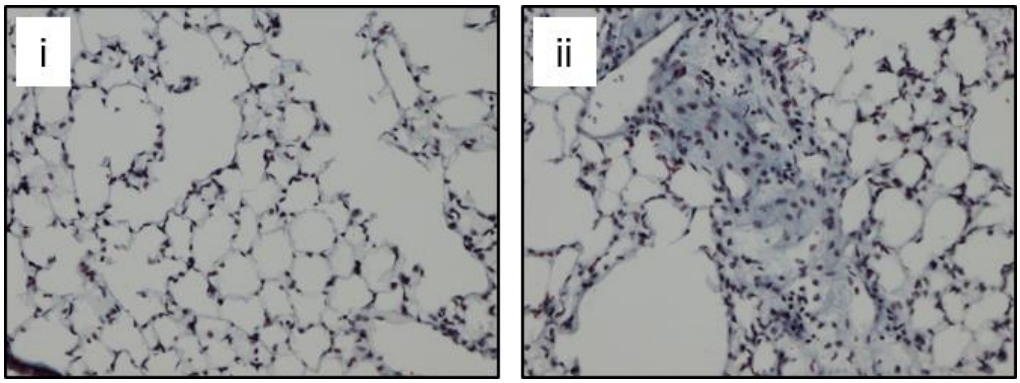


Figure 8.4 Loss of *Elk1* results in age related fibrosis. Lung collagen was stained using Masson's trichrome. Wild-type ($Elk1^{+/0}$) (i) and $Elk1^{-/0}$ lung tissue sections (ii) demonstrate small, infrequent, fibrotic foci were present in $Elk1^{-/0}$ mice. Representative images captured using x10 magnification.

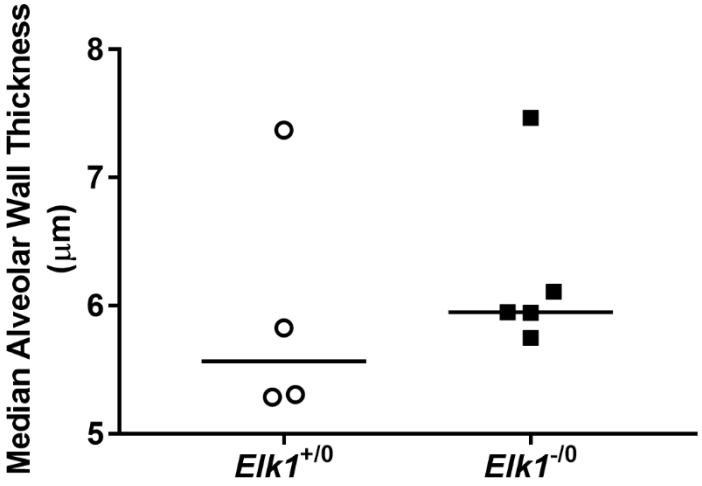


Figure 8.5 The effect of loss of *Elk1* on alveolar wall thickness. Alveolar wall thickness was measures in wild-type ($Elk1^{+/0}$) and $Elk1^{-/0}$ lung tissue sections to determine if there is age related thickening of the alveoli in the absence of *Elk1*, in 12 month old mice. Lines represent median alveolar wall thickness (μm); $n = 4 – 5$.

8.4.2. α-smooth muscle actin expression in mice lacking *Elk1*

Integrin mediated activation of TGF-β has been linked to increased expression of αSMA resulting in airway remodelling. To determine if loss of repression of transcription of the β6 gene by *Elk1* had an effect in aged animals the expression of *ACTA*, the gene that encodes the protein αSMA, and airway remodelling were analysed in wild-type ($Elk1^{+/0}$) and $Elk1^{-/0}$ mice. *ACTA* mRNA expression was determined at 12 weeks of age in a small number of mice (n = 3) to determine if there was any early indication into airway remodelling in $Elk1^{-/0}$ mice. A trend towards increased ACTA mRNA expression in the lungs of $Elk1^{-/0}$ mice compared with $Elk1^{+/0}$ controls (9.40, 2.24 median relative expression, respectively) can be seen in figure **8.6**. I therefore performed immunohistochemical staining for αSMA in the lungs of mice aged to 12 months and demonstrated visible increases in expression of αSMA in the alveolar epithelium of $Elk1^{-/0}$ mice (see figure **8.7 ii**) but none or very little in the alveolar epithelium of $Elk1^{+/0}$ controls (see figure **8.7 i**).

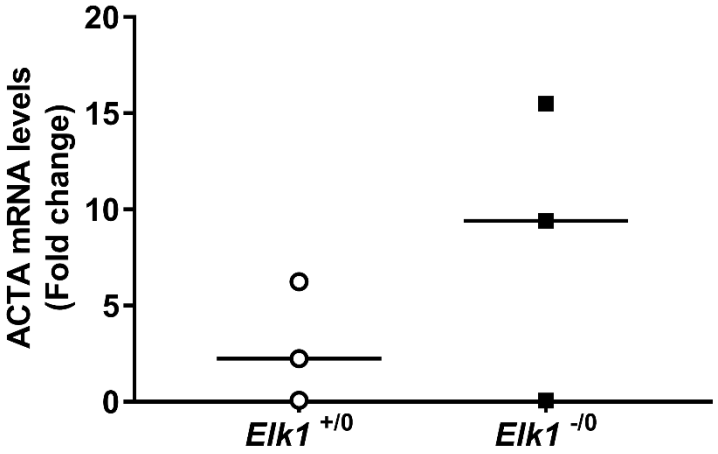


Figure 8.6 The effect of loss of *Elk1* on *ACTA* expression at 12 weeks of age. *ACTA* expression was measured in lung homogenate taken from *Elk1*$^{-/0}$ and *Elk1*$^{+/0}$ control mice at 12 weeks of age. Data points express fold change over mean control (*Elk1*$^{+/0}$) expression, line represents median expression; $n = 3$.

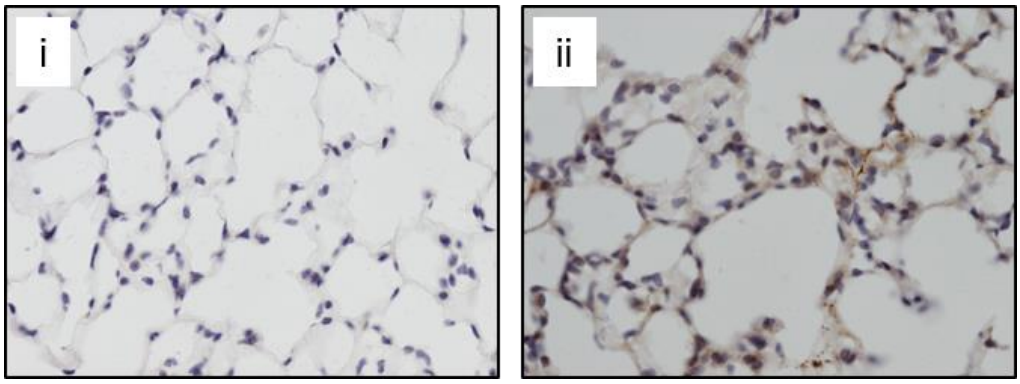


Figure 8.7 The effect of loss of *Elk1* on αSMA deposition in the lung at 12 months. Immunohistochemistry was used to determine differences in αSMA deposition in the lungs between *Elk1*$^{-/o}$ and *Elk1*$^{+/0}$ control animals. Representative images captured using original magnification x40. There is a significant increase in brown positively stained alveolar epithelial cells in *Elk1*$^{-/0}$ mice (ii) compared with control mice (*Elk1*$^{+/0}$) that have very little or no expression in alveolar epithelial cells (i).

8.5. Discussion

IPF is a disease with significantly worse prognosis and increased incidence in the ageing. Therefore, developing age-related animal models of IPF is of great importance. It was hypothesised that animals lacking functional Elk1 (*Elk1*$^{-/0}$) will develop age-related pulmonary fibrosis. Elk1 represses the transcription of integrin β6 that I proposed would result in higher basal levels of TGF-β activation, which in time may result in pulmonary fibrosis. These data demonstrate that *Elk1*$^{-/0}$ mice show a trend towards reduced body mass at 12 months in combination with significantly increased collagen deposition in the lungs. The collagen deposition was further confirmed by analysis of Masson trichome tissue sections that showed that 12 months old *Elk1*$^{-/0}$ mice had infrequent patchy fibrotic lesions and demonstrated a trend towards increased alveolar wall thickness. These data suggest that *Elk1*$^{-/0}$ mice develop pulmonary fibrosis which is consistent with reports that IPF patients have reduced levels of Elk1 (Tatler et al., 2016b). This link makes the use of *Elk1*$^{-/0}$ mice as a model of pulmonary fibrosis more disease relevant than the other age-related models of pulmonary fibrosis, the *RAGE*$^{-/-}$ and *Relaxin*$^{-/-}$ mice. As fibrotic lesions are still patchy in *Elk1*$^{-/0}$ mice, if these mice were aged for longer, these areas of fibrosis may increase in size and frequency. *RAGE*$^{-/-}$ mice developed fibrosis spontaneously at 19–24 months old; future experiments should determine if indeed the fibrosis is progressive in *Elk*$^{-/0}$ mice (Englert et al., 2008). Fibrosis was assessed in 12 month old animals; this has been calculated to be equivalent to the human age of 38-47 years (Geifman and Rubin, 2013). If measurements were made in mice aged 18-24 months, the equivalent of a more typical age of human patients at age of IPF

diagnosis 56-69 years, changes seen in these mice might have been amplified. Another advantage this model has is that it only uses male mice as the Elk1 gene is on the X chromosome which further adds to the disease relevance of this model as there are gender differences associated with IPF.

Although it is not clear what causes silencing of Elk1 in patients with reduced Elk1 expression, a number of epigenetic modification could be involved. Histone deacetylation and methylation are both involved in the repression of genes linked to IPF and these modifications could be involved in Elk1 silencing (Coward et al., 2010b, Conforti et al., 2017).

Elk1 binding motifs have also been identified in the promoter of the *ACTA2* gene that encodes the α-smooth muscle actin protein (Tatler et al., 2016b). *Elk1*$^{-/0}$ mice have a trend towards an increase in *ACTA* expression in lung tissue as early as 12 weeks old and also have an increase alveolar epithelial cell α-SMA expression at 12 months. Increased expression of α-SMA in the alveolar epithelium may suggest that epithelial-to-mesenchymal transition (EMT) is occurring and the presence of myofibroblast will form areas of active fibrosis, foci (Hinz, 2012).

Elk1 may have implications in other pathways of pulmonary fibrosis other than αvβ6 integrins and α-SMA. These include regulating the expression of elastin in lung fibroblasts and hyaluronan expression in dermal fibroblasts (Carreras et al., 2001, Röck et al., 2011).

8.6. Conclusion

These data suggest that Elk1 gene deletion resulted in age-related early fibrotic changes associated with the development of pulmonary fibrosis. In summary, *Elk1*$^{-/0}$ mice have a significant increase in collagen deposition in their lungs at 12 months old as assessed through measurements of lung hydroxyproline concentration and Masson's trichrome staining of tissues sections. *Elk1*$^{-/0}$ mice are a potentially attractive new model of pulmonary fibrosis as they have a clinically relevant gene 'knocked out' offering not only the potential to further study the effects of the loss of Elk1 and the subsequent increase in αvβ6 expression but also using *Elk1*$^{-/0}$ mice as a disease model.

9 Conclusions and future directions

9.1. Conclusions

Idiopathic pulmonary fibrosis is a chronic, progressive lung disease with a worse prognosis than most cancers with limited treatment options. Better treatments are urgently required and *in vivo* models remain vital in the development of new treatments for pulmonary fibrosis. Therefore, there continues to be a need for robust, and reproducible, animal models of pulmonary fibrosis and at the same time there an ever increasing responsibility to apply the principles of the 3Rs (Replacement, Reduction and Refinement of the use of animals) to all scientific research.

Initial work performed in this thesis established optimal bleomycin doses for both ALI and fibrosis models in mice and rats.

The optimum dose for stimulating bleomycin-induced fibrosis in mice was determined to be between 75 and 50 IU. 75 IU bleomycin caused significant collagen deposition around areas of inflammation in the interstitial space, however, this dose also caused mice to lose substantial weight. The 50 IU dose induced only a small amount of fibrosis. Therefore, taking the animals welfare into consideration, the optimum dose should be between 50 and 75 IU bleomycin. Bleomycin has also shown to have some batch to batch variation, as demonstrated in research conducted by myself and others at the University of Nottingham. Therefore, dose ranging studies with new batches of bleomycin like the ones set out in chapter 3 of this thesis are advisable, prior to undertaking large bleomycin-induced lung fibrosis studies. The conditions determined for the bleomycin-induced lung fibrosis model have been utilised across the research group on numerous publications, each using a dose of 60 IU bleomycin (John et al., 2013, Tatler et al., 2016b, Habgood et al., 2016, Philp et al., 2018). A dose-response to bleomycin was seen in rats administered with 300, 400, 500, 750 or 1000 IU bleomycin. 750 and 1000 IU bleomycin was too high a dose leading to considerable adverse events and rats had to be euthanized due to welfare reasons, however, there was a good fibrotic response with acceptable systemic affects in the other three doses and 500 IU produced the most severe fibrosis and was used as the optimum dose.

This thesis advances understanding of the bleomycin-induced fibrosis model further through mapping of cytokine expression across a time course during the lung injury and early fibrotic stages of the model. IL-6, IL-1β and KC were all demonstrated to be increased in lung tissue homogenate during the first 1-2 days post bleomycin instillation, which is in keeping with the literature that suggest these cytokines are all involved in the development of ALI (Saito et al., 2008, Hybertson et al., 1997).

These data show that levels also return to, or close to, baseline at day 4; the day used for investigating ALI via histology.

Having established the bleomycin model of fibrosis, I used it to assess various mechanisms of fibrogenesis. Bleomycin enhanced proteolysis in *Slpi*$^{-/-}$ mice but did not further enhance TGF-β activation as measured by pSmad2 ELISA and histological staining even though they had increased acute lung injury. Furthermore, *Slpi*$^{-/-}$ mice with enhanced proteolysis lost the sustained increase in *Col1α1*, *Col3α1* and *Col4α1* gene expression following bleomycin seen in wild-type animals yet still deposit similar levels of collagen at 28 days. This is most likely due to a metalloprotease-rich environment promotes post-translational processing and collagen deposition resulting in lung fibrosis.

Once established, the rat bleomycin model was used to determine the efficacy of a Tranilast:lysine salt in inhibiting fibrosis. Tranilast:lysine salt when given therapeutically (at day 11) to rats via repeat daily oropharyngeal administration versus repeat daily administration of an oral gavage and the development of fibrosis was assessed via hydroxyproline assay and histology. In parallel with this study I setup a PCLS model of fibrosis, that cultured lung slices taken from mice treated with bleomycin to test the efficacy of Tranilast at inhibiting / reversing fibrosis *ex vivo*. Combining data from the two separate models provided greater confidence in the final results.

In the rat, 21 day, bleomycin model, Tranilast administered via either dose route had no effect on the development of fibrosis with both groups developing fibrosis to a similar extent as the control bleomycin / lactose *o.p.* group. It was concluded it was difficult to determine if Tranilast had no effect on the development on bleomycin

induced fibrosis due to the formulation or the dosing strategy, however, as Tranilast has been shown to inhibit bleomycin induced fibrosis in past studies (Mori et al., 1995) when treated from day 0, there is the potential it may have been interfering with the bleomycin induced inflammatory response and not the development of fibrosis showing the importance of using the correct dosing strategy. However, the data from the PCLS model also shows that Tranilast has no effect on the development of fibrosis as, the results demonstrate that slices taken from mice treated with bleomycin have significantly more hydroxyproline in them than saline treated control lungs. Tranilast treatment at all concentrations was unable to inhibit this increase in hydroxyproline although this may be due to the fact that the half-life of Tranilast in DMEM was later discovered to be very short and once daily dosing may not have been frequent enough. Therefore, the PCLS model has the potential for use to assess a compound's ability to inhibit collagen deposition, which would greatly reduce the number of animals required when determining an EC50.

A model of radiation-induced lung fibrosis was established. Utilising a unique setup, with an x ray source generated by a Gulmay RS225 orthovoltage cabinet 17.5 Gy was determined to be the optimum dose to administer to the thorax of female, C57BL/6, mice. Upon sacrifice or study end (26 weeks post irradiation) mice had developed substantial fibrosis. One of the reasons for establishing this model was to determine if SPECT/CT scanning could be used to non-invasively measure αvβ6 integrins and the development of fibrosis in a long term, progressive disease model. Levels of αvβ6 integrins were measured 8, 12 and 17 weeks post 17.5 Gy thoracic irradiation and determined a significant increase in αvβ6 integrin 17 weeks post irradiation and a slight trend towards an increase at 12 weeks. This is the first instance of this imaging technique used in the RILF model and offers the ability to

monitor treatments without the need for culling animals to assess disease progression.

Finally, this thesis investigated the effects of *Elk1* gene deletion in mice. Elk1 is a transcription factor that represses the transcription of integrin αvβ6, the increased expression of which is heavily linked with progressive and severe fibrosis. I therefore hypothesised that mice that do not express Elk1 may develop spontaneous pulmonary fibrosis in the ageing lung. *Elk1* $^{-/-}$ mice were aged for 12 months and showed signs of fibrotic deposition in the lung with increased hydroxyproline levels compared with wild-type control and patchy but frequent areas of fibrosis were seen via histology. These *Elk1* $^{-/-}$ mice could potentially be used as a model of age-induced fibrosis as it is a progressive model.

9.2. Future directions

Future work investigating the usefulness of SPECT/CT imaging at assessing the development of RILF and its treatment would require testing multiple irradiation doses at different time points. Firstly, it is important to determine if SPECT/CT imaging is sensitive enough to determine differences in αvβ6 levels across a range of irradiation doses 12.5, 15.0 and 17.5 Gy to determine if it is sensitive enough to be used as a tool for predicting disease severity. Secondly SPECT/CT scanning should be assessed at 12 and 17 weeks with potentially a third time point in between to determine the earliest time-point that a significant increase in αvβ6 levels can be determined at.

Future work assessing the effects of Tranilast should continue by assessing the activation of TGF-β through the expression of pSmad2 via immunohistochemistry would as this would help to clarify if the Tranilast was having any effect on a molecular level.

As early fibrotic changes in aged lungs were assessed in *Elk1* $^{-/-}$ mice, there is still the scope to determine what effect loss of Elk1 is having on late fibrotic changes (24 months old). This could be assessed further for a full understanding of the development of fibrosis in these animals.

9.3. Concluding remarks

Bleomycin, radiation and age-induced models of fibrosis are all established and discussed in this thesis. There are also new techniques such as SPECT/CT imaging of αvβ6 to monitor disease progression, non-invasively, that not only reduce the use of animals required in experiments but improves the quality and diversity of data obtained in these *in vivo* experiments. Older techniques such as the PCLS have also been adopted to generate PCLS model of fibrosis that can be utilised to use small number of animals to test the efficacy of large numbers of treatment groups.

10 References

Abe, M., Harpel, J. G., Metz, C. N., Nunes, I., Loskutoff, D. J. and Rifkin, D. B. (1994) 'An assay for transforming growth factor-beta using cells transfected with a plasminogen activator inhibitor-1 promoter-luciferase construct', *Anal Biochem,* 216(2), pp. 276-84.

Abe, T., Kobayashi, N., Yoshimura, K., Trapnell, B. C., Kim, H., Hubbard, R. C., Brewer, M. T., Thompson, R. C. and Crystal, R. G. (1991) 'Expression of the secretory leukoprotease inhibitor gene in epithelial cells', *J Clin Invest,* 87(6), pp. 2207-15.

Akers, I. A., Parsons, M., Hill, M. R., Hollenberg, M. D., Sanjar, S., Laurent, G. J. and McAnulty, R. J. (2000) 'Mast cell tryptase stimulates human lung fibroblast proliferation via protease-activated receptor-2', *Am J Physiol Lung Cell Mol Physiol,* 278(1), pp. L193-201.

Aljandali, A., Pollack, H., Yeldandi, A., Li, Y., Weitzman, S. A. and Kamp, D. W. (2001) 'Asbestos causes apoptosis in alveolar epithelial cells: role of iron-induced free radicals', *J Lab Clin Med,* 137(5), pp. 330-9.

Ando, M., Miyazaki, E., Ito, T., Hiroshige, S., Nureki, S. I., Ueno, T., Takenaka, R., Fukami, T. and Kumamoto, T. (2010) 'Significance of serum vascular endothelial growth factor level in patients with idiopathic pulmonary fibrosis', *Lung,* 188(3), pp. 247-52.

Andrae, J., Gallini, R. and Betsholtz, C. (2008) 'Role of platelet-derived growth factors in physiology and medicine', *Genes Dev,* 22(10), pp. 1276-312.

Angelov, N., Moutsopoulos, N., Jeong, M. J., Nares, S., Ashcroft, G. and Wahl, S. M. (2004) 'Aberrant mucosal wound repair in the absence of secretory leukocyte protease inhibitor', *Thromb Haemost,* 92(2), pp. 288-97.

Annes, J. P., Munger, J. S. and Rifkin, D. B. (2003) 'Making sense of latent TGFbeta activation', *J Cell Sci,* 116(Pt 2), pp. 217-24.

Antoniades, H. N., Bravo, M. A., Avila, R. E., Galanopoulos, T., Neville-Golden, J., Maxwell, M. and Selman, M. (1990) 'Platelet-derived growth factor in idiopathic pulmonary fibrosis', *J Clin Invest,* 86(4), pp. 1055-64.

Araya, J., Cambier, S., Markovics, J. A., Wolters, P., Jablons, D., Hill, A., Finkbeiner, W., Jones, K., Broaddus, V. C., Sheppard, D., Barzcak, A., Xiao, Y., Erle, D. J. and Nishimura, S. L. (2007) 'Squamous metaplasia amplifies pathologic epithelial-mesenchymal interactions in COPD patients', *J Clin Invest,* 117(11), pp. 3551-62.

Ashcroft, G. S., Lei, K., Jin, W., Longenecker, G., Kulkarni, A. B., Greenwell-Wild, T., Hale-Donze, H., McGrady, G., Song, X. Y. and Wahl, S. M. (2000) 'Secretory leukocyte protease inhibitor mediates non-redundant functions necessary for normal wound healing', *Nat Med,* 6(10), pp. 1147-53.

Ashcroft, T., Simpson, J. M. and Timbrell, V. (1988) 'Simple method of estimating severity of pulmonary fibrosis on a numerical scale', *J Clin Pathol,* 41(4), pp. 467-70.
Bartram, U. and Speer, C. P. (2004) 'The role of transforming growth factor beta in lung development and disease', *Chest,* 125(2), pp. 754-65.
Bergner, A. and Sanderson, M. J. (2002) 'Acetylcholine-induced calcium signaling and contraction of airway smooth muscle cells in lung slices', *J Gen Physiol,* 119(2), pp. 187-98.
Bernard, G. R., Artigas, A., Brigham, K. L., Carlet, J., Falke, K., Hudson, L., Lamy, M., LeGall, J. R., Morris, A. and Spragg, R. (1994) 'Report of the American-European Consensus conference on acute respiratory distress syndrome: definitions, mechanisms, relevant outcomes, and clinical trial coordination. Consensus Committee', *J Crit Care,* 9(1), pp. 72-81.
Bhargava, M. and Wendt, C. H. (2012) 'Biomarkers in acute lung injury', *Transl Res,* 159(4), pp. 205-17.
Bhatia, M., Zemans, R. L. and Jeyaseelan, S. (2012) 'Role of chemokines in the pathogenesis of acute lung injury', *Am J Respir Cell Mol Biol,* 46(5), pp. 566-72.
Bradham, D. M., Igarashi, A., Potter, R. L. and Grotendorst, G. R. (1991) 'Connective tissue growth factor: a cysteine-rich mitogen secreted by human vascular endothelial cells is related to the SRC-induced immediate early gene product CEF-10', *J Cell Biol,* 114(6), pp. 1285-94.
Brower, R. G., Matthay, M. A., Morris, A., Schoenfeld, D., Thompson, B. T., Wheeler, A. and Network, A. R. D. S. (2000) 'Ventilation with lower tidal volumes as compared with traditional tidal volumes for acute lung injury and the acute respiratory distress syndrome', *N Engl J Med,* 342(18), pp. 1301-8.
Brown, P. D., Wakefield, L. M., Levinson, A. D. and Sporn, M. B. (1990) 'Physicochemical activation of recombinant latent transforming growth factor-beta's 1, 2, and 3', *Growth Factors,* 3(1), pp. 35-43.
Byrne, A. J., Maher, T. M. and Lloyd, C. M. (2016) 'Pulmonary Macrophages: A New Therapeutic Pathway in Fibrosing Lung Disease?', *Trends Mol Med,* 22(4), pp. 303-316.
Bühling, F., Röcken, C., Brasch, F., Hartig, R., Yasuda, Y., Saftig, P., Brömme, D. and Welte, T. (2004) 'Pivotal role of cathepsin K in lung fibrosis', *Am J Pathol,* 164(6), pp. 2203-16.
Caravan, P., Yang, Y., Zachariah, R., Schmitt, A., Mino-Kenudson, M., Chen, H. H., Sosnovik, D. E., Dai, G., Fuchs, B. C. and Lanuti, M. (2013) 'Molecular magnetic resonance imaging of pulmonary fibrosis in mice', *Am J Respir Cell Mol Biol,* 49(6), pp. 1120-6.
Carreras, I., Rich, C. B., Jaworski, J. A., Dicamillo, S. J., Panchenko, M. P., Goldstein, R. and Foster, J. A. (2001) 'Functional components of basic fibroblast growth factor signaling that inhibit lung elastin gene expression', *Am J Physiol Lung Cell Mol Physiol,* 281(4), pp. L766-75.

Cavanaugh, D., Johnson, E., Price, R. E., Kurie, J., Travis, E. L. and Cody, D. D. (2004) 'In vivo respiratory-gated micro-CT imaging in small-animal oncology models', *Mol Imaging,* 3(1), pp. 55-62.
Cavarra, E., Carraro, F., Fineschi, S., Naldini, A., Bartalesi, B., Pucci, A. and Lungarella, G. (2004) 'Early response to bleomycin is characterized by different cytokine and cytokine receptor profiles in lungs', *Am J Physiol Lung Cell Mol Physiol,* 287(6), pp. L1186-92.
Cesari, F., Rennekampff, V., Vintersten, K., Vuong, L. G., Seibler, J., Bode, J., Wiebel, F. F. and Nordheim, A. (2004) 'Elk-1 knock-out mice engineered by Flp recombinase-mediated cassette exchange', *Genesis,* 38(2), pp. 87-92.
Chaudhary, N. I., Schnapp, A. and Park, J. E. (2006) 'Pharmacologic differentiation of inflammation and fibrosis in the rat bleomycin model', *Am J Respir Crit Care Med,* 173(7), pp. 769-76.
Christensen, P. J., Goodman, R. E., Pastoriza, L., Moore, B. and Toews, G. B. (1999) 'Induction of lung fibrosis in the mouse by intratracheal instillation of fluorescein isothiocyanate is not T-cell-dependent', *Am J Pathol,* 155(5), pp. 1773-9.
Chua, F., Dunsmore, S. E., Clingen, P. H., Mutsaers, S. E., Shapiro, S. D., Segal, A. W., Roes, J. and Laurent, G. J. (2007) 'Mice lacking neutrophil elastase are resistant to bleomycin-induced pulmonary fibrosis', *Am J Pathol,* 170(1), pp. 65-74.
Chua, F., Gauldie, J. and Laurent, G. J. (2005) 'Pulmonary fibrosis: searching for model answers', *Am J Respir Cell Mol Biol,* 33(1), pp. 9-13.
Chua, F. and Laurent, G. J. (2006) 'Neutrophil elastase: mediator of extracellular matrix destruction and accumulation', *Proc Am Thorac Soc,* 3(5), pp. 424-7.
Coggle, J. E., Lambert, B. E. and Moores, S. R. (1986) 'Radiation effects in the lung', *Environ Health Perspect,* 70, pp. 261-91.
Coker, R. K., Laurent, G. J., Shahzeidi, S., Lympany, P. A., du Bois, R. M., Jeffery, P. K. and McAnulty, R. J. (1997) 'Transforming growth factors-beta 1, -beta 2, and -beta 3 stimulate fibroblast procollagen production in vitro but are differentially expressed during bleomycin-induced lung fibrosis', *Am J Pathol,* 150(3), pp. 981-91.
Conforti, F., Davies, E. R., Calderwood, C. J., Thatcher, T. H., Jones, M. G., Smart, D. E., Mahajan, S., Alzetani, A., Havelock, T., Maher, T. M., Molyneaux, P. L., Thorley, A. J., Tetley, T. D., Warner, J. A., Packham, G., Ganesan, A., Skipp, P. J., Marshall, B. J., Richeldi, L., Sime, P. J., O'Reilly, K. M. A. and Davies, D. E. (2017) 'The histone deacetylase inhibitor, romidepsin, as a potential treatment for pulmonary fibrosis', *Oncotarget,* 8(30), pp. 48737-48754.
Coward, W. R., Saini, G. and Jenkins, G. (2010a) 'The pathogenesis of idiopathic pulmonary fibrosis', *Ther Adv Respir Dis,* 4(6), pp. 367-88.
Coward, W. R., Watts, K., Feghali-Bostwick, C. A., Jenkins, G. and Pang, L. (2010b) 'Repression of IP-10 by interactions between histone deacetylation and hypermethylation in idiopathic pulmonary fibrosis', *Mol Cell Biol,* 30(12), pp. 2874-86.

Cross, L. J. and Matthay, M. A. (2011) 'Biomarkers in acute lung injury: insights into the pathogenesis of acute lung injury', *Crit Care Clin,* 27(2), pp. 355-77.

Dandurand, R. J., Wang, C. G., Phillips, N. C. and Eidelman, D. H. (1993) 'Responsiveness of individual airways to methacholine in adult rat lung explants', *J Appl Physiol (1985),* 75(1), pp. 364-72.

Daopin, S., Piez, K. A., Ogawa, Y. and Davies, D. R. (1992) 'Crystal structure of transforming growth factor-beta 2: an unusual fold for the superfamily', *Science,* 257(5068), pp. 369-73.

Degryse, A. L. and Lawson, W. E. (2011) 'Progress toward improving animal models for idiopathic pulmonary fibrosis', *Am J Med Sci,* 341(6), pp. 444-9.

Degryse, A. L., Tanjore, H., Xu, X. C., Polosukhin, V. V., Jones, B. R., Boomershine, C. S., Ortiz, C., Sherrill, T. P., McMahon, F. B., Gleaves, L. A., Blackwell, T. S. and Lawson, W. E. (2011) 'TGFβ signaling in lung epithelium regulates bleomycin-induced alveolar injury and fibroblast recruitment', *Am J Physiol Lung Cell Mol Physiol,* 300(6), pp. L887-97.

Degryse, A. L., Tanjore, H., Xu, X. C., Polosukhin, V. V., Jones, B. R., McMahon, F. B., Gleaves, L. A., Blackwell, T. S. and Lawson, W. E. (2010) 'Repetitive intratracheal bleomycin models several features of idiopathic pulmonary fibrosis', *Am J Physiol Lung Cell Mol Physiol,* 299(4), pp. L442-52.

Demling, N., Ehrhardt, C., Kasper, M., Laue, M., Knels, L. and Rieber, E. P. (2006) 'Promotion of cell adherence and spreading: a novel function of RAGE, the highly selective differentiation marker of human alveolar epithelial type I cells', *Cell Tissue Res,* 323(3), pp. 475-88.

Derynck, R. and Zhang, Y. E. (2003) 'Smad-dependent and Smad-independent pathways in TGF-beta family signalling', *Nature,* 425(6958), pp. 577-84.

Dik, W. A., McAnulty, R. J., Versnel, M. A., Naber, B. A., Zimmermann, L. J., Laurent, G. J. and Mutsaers, S. E. (2003) 'Short course dexamethasone treatment following injury inhibits bleomycin induced fibrosis in rats', *Thorax,* 58(9), pp. 765-71.

Dushianthan, A., Grocott, M. P., Postle, A. D. and Cusack, R. (2011) 'Acute respiratory distress syndrome and acute lung injury', *Postgrad Med J,* 87(1031), pp. 612-22.

Englert, J. M., Hanford, L. E., Kaminski, N., Tobolewski, J. M., Tan, R. J., Fattman, C. L., Ramsgaard, L., Richards, T. J., Loutaev, I., Nawroth, P. P., Kasper, M., Bierhaus, A. and Oury, T. D. (2008) 'A role for the receptor for advanced glycation end products in idiopathic pulmonary fibrosis', *Am J Pathol,* 172(3), pp. 583-91.

Fan, X., Patera, A. C., Pong-Kennedy, A., Deno, G., Gonsiorek, W., Manfra, D. J., Vassileva, G., Zeng, M., Jackson, C., Sullivan, L., Sharif-Rodriguez, W., Opdenakker, G., Van Damme, J., Hedrick, J. A., Lundell, D., Lira, S. A. and Hipkin, R. W. (2007) 'Murine CXCR1 is a functional receptor for GCP-2/CXCL6 and interleukin-8/CXCL8', *J Biol Chem,* 282(16), pp. 11658-66.

Ferguson, N. D., Fan, E., Camporota, L., Antonelli, M., Anzueto, A., Beale, R., Brochard, L., Brower, R., Esteban, A., Gattinoni, L., Rhodes, A., Slutsky, A. S., Vincent, J. L., Rubenfeld, G. D., Thompson, B. T. and Ranieri, V. M. (2012) 'The Berlin definition of ARDS: an expanded rationale, justification, and supplementary material', *Intensive Care Med,* 38(10), pp. 1573-82.

Fernandez, I. E. and Eickelberg, O. (2012) 'The impact of TGF-β on lung fibrosis: from targeting to biomarkers', *Proc Am Thorac Soc,* 9(3), pp. 111-6.

Ferry, G., Lonchampt, M., Pennel, L., de Nanteuil, G., Canet, E. and Tucker, G. C. (1997) 'Activation of MMP-9 by neutrophil elastase in an in vivo model of acute lung injury', *FEBS Lett,* 402(2-3), pp. 111-5.

Filderman, A. E. and Lazo, J. S. (1991) 'Murine strain differences in pulmonary bleomycin metabolism', *Biochem Pharmacol,* 42(1), pp. 195-8.

Flechsig, P., Dadrich, M., Bickelhaupt, S., Jenne, J., Hauser, K., Timke, C., Peschke, P., Hahn, E. W., Grone, H. J., Yingling, J., Lahn, M., Wirkner, U. and Huber, P. E. (2012) 'LY2109761 attenuates radiation-induced pulmonary murine fibrosis via reversal of TGF-beta and BMP-associated proinflammatory and proangiogenic signals', *Clin Cancer Res,* 18(13), pp. 3616-27.

Fujita, M., Ye, Q., Ouchi, H., Harada, E., Inoshima, I., Kuwano, K. and Nakanishi, Y. (2006) 'Doxycycline attenuated pulmonary fibrosis induced by bleomycin in mice', *Antimicrob Agents Chemother,* 50(2), pp. 739-43.

Fukushima, T., Tanaka, K., Lim, H. and Moriyama, M. (2002) 'Mechanism of cytotoxicity of paraquat', *Environ Health Prev Med,* 7(3), pp. 89-94.

Geifman, N. and Rubin, E. (2013) 'The mouse age phenome knowledgebase and disease-specific inter-species age mapping', *PLoS One,* 8(12), pp. e81114.

Goodwin, A. and Jenkins, G. (2009) 'Role of integrin-mediated TGFbeta activation in the pathogenesis of pulmonary fibrosis', *Biochem Soc Trans,* 37(Pt 4), pp. 849-54.

Habgood, A. N., Tatler, A. L., Porte, J., Wahl, S. M., Laurent, G. J., John, A. E., Johnson, S. R. and Jenkins, G. (2016) 'Secretory leukocyte protease inhibitor gene deletion alters bleomycin-induced lung injury, but not development of pulmonary fibrosis', *Lab Invest,* 96(6), pp. 623-31.

Hahm, K., Lukashev, M. E., Luo, Y., Yang, W. J., Dolinski, B. M., Weinreb, P. H., Simon, K. J., Chun Wang, L., Leone, D. R., Lobb, R. R., McCrann, D. J., Allaire, N. E., Horan, G. S., Fogo, A., Kalluri, R., Shield, C. F., Sheppard, D., Gardner, H. A. and Violette, S. M. (2007) 'Alphav beta6 integrin regulates renal fibrosis and inflammation in Alport mouse', *Am J Pathol,* 170(1), pp. 110-25.

Hajjar, A. M., Ernst, R. K., Tsai, J. H., Wilson, C. B. and Miller, S. I. (2002) 'Human Toll-like receptor 4 recognizes host-specific LPS modifications', *Nat Immunol,* 3(4), pp. 354-9.

Harrison, J. H., Jr. and Lazo, J. S. (1987) 'High dose continuous infusion of bleomycin in mice: a new model for drug-induced pulmonary fibrosis', *J Pharmacol Exp Ther,* 243(3), pp. 1185-94.
Haston, C. K. and Travis, E. L. (1997) 'Murine susceptibility to radiation-induced pulmonary fibrosis is influenced by a genetic factor implicated in susceptibility to bleomycin-induced pulmonary fibrosis', *Cancer Res,* 57(23), pp. 5286-91.
Hecker, L., Vittal, R., Jones, T., Jagirdar, R., Luckhardt, T. R., Horowitz, J. C., Pennathur, S., Martinez, F. J. and Thannickal, V. J. (2009) 'NADPH oxidase-4 mediates myofibroblast activation and fibrogenic responses to lung injury', *Nat Med,* 15(9), pp. 1077-81.
Heldin, C. H., Miyazono, K. and ten Dijke, P. (1997) 'TGF-beta signalling from cell membrane to nucleus through SMAD proteins', *Nature,* 390(6659), pp. 465-71.
Heldin, C. H. and Westermark, B. (1999) 'Mechanism of action and in vivo role of platelet-derived growth factor', *Physiol Rev,* 79(4), pp. 1283-316.
Hinck, A. P. (2012) 'Structural studies of the TGF-βs and their receptors - insights into evolution of the TGF-β superfamily', *FEBS Lett,* 586(14), pp. 1860-70.
Hinz, B. (2012) 'Mechanical aspects of lung fibrosis: a spotlight on the myofibroblast', *Proc Am Thorac Soc,* 9(3), pp. 137-47.
Hojo, S., Fujita, J., Yoshinouchi, T., Yamanouchi, H., Kamei, T., Yamadori, I., Otsuki, Y., Ueda, N. and Takahara, J. (1997) 'Hepatocyte growth factor and neutrophil elastase in idiopathic pulmonary fibrosis', *Respir Med,* 91(9), pp. 511-6.
Horan, G. S., Wood, S., Ona, V., Li, D. J., Lukashev, M. E., Weinreb, P. H., Simon, K. J., Hahm, K., Allaire, N. E., Rinaldi, N. J., Goyal, J., Feghali-Bostwick, C. A., Matteson, E. L., O'Hara, C., Lafyatis, R., Davis, G. S., Huang, X., Sheppard, D. and Violette, S. M. (2008) 'Partial inhibition of integrin alpha(v)beta6 prevents pulmonary fibrosis without exacerbating inflammation', *Am J Respir Crit Care Med,* 177(1), pp. 56-65.
Hori, Y., Katoh, T., Hirakata, M., Joki, N., Kaname, S., Fukagawa, M., Okuda, T., Ohashi, H., Fujita, T., Miyazono, K. and Kurokawa, K. (1998) 'Anti-latent TGF-beta binding protein-1 antibody or synthetic oligopeptides inhibit extracellular matrix expression induced by stretch in cultured rat mesangial cells', *Kidney Int,* 53(6), pp. 1616-25.
Howell, D. C., Laurent, G. J. and Chambers, R. C. (2002) 'Role of thrombin and its major cellular receptor, protease-activated receptor-1, in pulmonary fibrosis', *Biochem Soc Trans,* 30(2), pp. 211-6.
Huang, X. Z., Wu, J. F., Cass, D., Erle, D. J., Corry, D., Young, S. G., Farese, R. V. and Sheppard, D. (1996) 'Inactivation of the integrin beta 6 subunit gene reveals a role of epithelial integrins in regulating inflammation in the lung and skin', *J Cell Biol,* 133(4), pp. 921-8.
Hurmuz, P., Kivanc, H., Canbolat, A., Yavas, G., Yuce, D., Onder, S. C., Sargon, M. F. and Yildiz, F. (2014) 'Evaluation of the Effect of Changes in Dose Rate on Rat Lung Cells', *Technol Cancer Res Treat*.

Hybertson, B. M., Lee, Y. M. and Repine, J. E. (1997) 'Phagocytes and acute lung injury: dual roles for interleukin-1', *Ann N Y Acad Sci,* 832, pp. 266-73.
Hynes, R. O. (2002) 'Integrins: bidirectional, allosteric signaling machines', *Cell,* 110(6), pp. 673-87.
Ihn, H. (2002) 'Pathogenesis of fibrosis: role of TGF-beta and CTGF', *Curr Opin Rheumatol,* 14(6), pp. 681-5.
Inomata, K., Aoto, T., Binh, N. T., Okamoto, N., Tanimura, S., Wakayama, T., Iseki, S., Hara, E., Masunaga, T., Shimizu, H. and Nishimura, E. K. (2009) 'Genotoxic stress abrogates renewal of melanocyte stem cells by triggering their differentiation', *Cell,* 137(6), pp. 1088-99.
Jackson, I. L., Vujaskovic, Z. and Down, J. D. (2010) 'Revisiting strain-related differences in radiation sensitivity of the mouse lung: recognizing and avoiding the confounding effects of pleural effusions', *Radiat Res,* 173(1), pp. 10-20.
Jenkins, R. G., Moore, B. B., Chambers, R. C., Eickelberg, O., Königshoff, M., Kolb, M., Laurent, G. J., Nanthakumar, C. B., Olman, M. A., Pardo, A., Selman, M., Sheppard, D., Sime, P. J., Tager, A. M., Tatler, A. L., Thannickal, V. J., White, E. S. and Biology, A. A. o. R. C. a. M. (2017) 'An Official American Thoracic Society Workshop Report: Use of Animal Models for the Preclinical Assessment of Potential Therapies for Pulmonary Fibrosis', *Am J Respir Cell Mol Biol,* 56(5), pp. 667-679.
Jenkins, R. G., Simpson, J. K., Saini, G., Bentley, J. H., Russell, A. M., Braybrooke, R., Molyneaux, P. L., McKeever, T. M., Wells, A. U., Flynn, A., Hubbard, R. B., Leeming, D. J., Marshall, R. P., Karsdal, M. A., Lukey, P. T. and Maher, T. M. (2015) 'Longitudinal change in collagen degradation biomarkers in idiopathic pulmonary fibrosis: an analysis from the prospective, multicentre PROFILE study', *Lancet Respir Med,* 3(6), pp. 462-72.
John, A. E., Luckett, J. C., Tatler, A. L., Awais, R. O., Desai, A., Habgood, A., Ludbrook, S., Blanchard, A. D., Perkins, A. C., Jenkins, R. G. and Marshall, J. F. (2013) 'Preclinical SPECT/CT imaging of alphavbeta6 integrins for molecular stratification of idiopathic pulmonary fibrosis', *J Nucl Med,* 54(12), pp. 2146-52.
John, A. E., Porte, J., Jenkins, G. and Tatler, A. L. (2017) 'Methods for the Assessment of Active Transforming Growth Factor-β in Cells and Tissues', *Methods Mol Biol,* 1627, pp. 351-365.
Jordana, M., Befus, A. D., Newhouse, M. T., Bienenstock, J. and Gauldie, J. (1988) 'Effect of histamine on proliferation of normal human adult lung fibroblasts', *Thorax,* 43(7), pp. 552-8.
Kakugawa, T., Sakamoto, N., Sato, S., Yura, H., Harada, T., Nakashima, S., Hara, A., Oda, K., Ishimoto, H., Yatera, K., Ishimatsu, Y., Obase, Y., Kohno, S. and Mukae, H. (2016) 'Risk factors for an acute exacerbation of idiopathic pulmonary fibrosis', *Respir Res,* 17(1), pp. 79.
Kenyon, N. J., Ward, R. W., McGrew, G. and Last, J. A. (2003) 'TGF-beta1 causes airway fibrosis and increased collagen I and III mRNA in mice', *Thorax,* 58(9), pp. 772-7.

Kilkenny, C., Browne, W. J., Cuthill, I. C., Emerson, M. and Altman, D. G. (2010) 'Improving bioscience research reporting: the ARRIVE guidelines for reporting animal research', *PLoS Biol,* 8(6), pp. e1000412.

Kim, K. K., Kugler, M. C., Wolters, P. J., Robillard, L., Galvez, M. G., Brumwell, A. N., Sheppard, D. and Chapman, H. A. (2006) 'Alveolar epithelial cell mesenchymal transition develops in vivo during pulmonary fibrosis and is regulated by the extracellular matrix', *Proc Natl Acad Sci U S A,* 103(35), pp. 13180-5.

King, T. E., Bradford, W. Z., Castro-Bernardini, S., Fagan, E. A., Glaspole, I., Glassberg, M. K., Gorina, E., Hopkins, P. M., Kardatzke, D., Lancaster, L., Lederer, D. J., Nathan, S. D., Pereira, C. A., Sahn, S. A., Sussman, R., Swigris, J. J., Noble, P. W. and Group, A. S. (2014) 'A phase 3 trial of pirfenidone in patients with idiopathic pulmonary fibrosis', *N Engl J Med,* 370(22), pp. 2083-92.

King, T. E., Jr., Tooze, J. A., Schwarz, M. I., Brown, K. R. and Cherniack, R. M. (2001) 'Predicting survival in idiopathic pulmonary fibrosis: scoring system and survival model', *Am J Respir Crit Care Med,* 164(7), pp. 1171-81.

Kling, M. A. (2011) 'A review of respiratory system anatomy, physiology, and disease in the mouse, rat, hamster, and gerbil', *Vet Clin North Am Exot Anim Pract,* 14(2), pp. 287-337, vi.

Koda, A., Kurashina, Y. and Nakazawa, M. (1985) 'The inhibition mechanism of histamine release by N-(3,4-dimethoxycinnamoyl) anthranilic acid', *Int Arch Allergy Appl Immunol,* 77(1-2), pp. 244-5.

Kolb, M., Margetts, P. J., Anthony, D. C., Pitossi, F. and Gauldie, J. (2001) 'Transient expression of IL-1beta induces acute lung injury and chronic repair leading to pulmonary fibrosis', *J Clin Invest,* 107(12), pp. 1529-36.

Lawson, W. E., Grant, S. W., Ambrosini, V., Womble, K. E., Dawson, E. P., Lane, K. B., Markin, C., Renzoni, E., Lympany, P., Thomas, A. Q., Roldan, J., Scott, T. A., Blackwell, T. S., Phillips, J. A., Loyd, J. E. and du Bois, R. M. (2004) 'Genetic mutations in surfactant protein C are a rare cause of sporadic cases of IPF', *Thorax,* 59(11), pp. 977-80.

Lawson, W. E. and Loyd, J. E. (2006) 'The genetic approach in pulmonary fibrosis: can it provide clues to this complex disease?', *Proc Am Thorac Soc,* 3(4), pp. 345-9.

Lawson, W. E., Polosukhin, V. V., Stathopoulos, G. T., Zoia, O., Han, W., Lane, K. B., Li, B., Donnelly, E. F., Holburn, G. E., Lewis, K. G., Collins, R. D., Hull, W. M., Glasser, S. W., Whitsett, J. A. and Blackwell, T. S. (2005) 'Increased and prolonged pulmonary fibrosis in surfactant protein C-deficient mice following intratracheal bleomycin', *Am J Pathol,* 167(5), pp. 1267-77.

Lee, C. G., Cho, S. J., Kang, M. J., Chapoval, S. P., Lee, P. J., Noble, P. W., Yehualaeshet, T., Lu, B., Flavell, R. A., Milbrandt, J., Homer, R. J. and Elias, J. A. (2004) 'Early growth response gene 1-mediated apoptosis is essential for transforming growth factor beta1-induced pulmonary fibrosis', *J Exp Med,* 200(3), pp. 377-89.

Lee, C. G., Kang, H. R., Homer, R. J., Chupp, G. and Elias, J. A. (2006) 'Transgenic modeling of transforming growth factor-beta(1): role of apoptosis in fibrosis and alveolar remodeling', *Proc Am Thorac Soc,* 3(5), pp. 418-23.

Li, H., Hao, Y., Zhang, H., Ying, W., Li, D., Ge, Y., Ying, B., Cheng, B., Lian, Q. and Jin, S. (2017) 'Posttreatment with Protectin DX ameliorates bleomycin-induced pulmonary fibrosis and lung dysfunction in mice', *Sci Rep,* 7, pp. 46754.

Li, M., Abdollahi, A., Grone, H. J., Lipson, K. E., Belka, C. and Huber, P. E. (2009) 'Late treatment with imatinib mesylate ameliorates radiation-induced lung fibrosis in a mouse model', *Radiat Oncol,* 4, pp. 66.

Lin, C. H., Yu, M. C., Tung, W. H., Chen, T. T., Yu, C. C., Weng, C. M., Tsai, Y. J., Bai, K. J., Hong, C. Y., Chien, M. H. and Chen, B. C. (2013) 'Connective tissue growth factor induces collagen I expression in human lung fibroblasts through the Rac1/MLK3/JNK/AP-1 pathway', *Biochim Biophys Acta,* 1833(12), pp. 2823-2833.

Maeda, A., Hiyama, K., Yamakido, H., Ishioka, S. and Yamakido, M. (1996) 'Increased expression of platelet-derived growth factor A and insulin-like growth factor-I in BAL cells during the development of bleomycin-induced pulmonary fibrosis in mice', *Chest,* 109(3), pp. 780-6.

Maher, T. M., Wells, A. U. and Laurent, G. J. (2007) 'Idiopathic pulmonary fibrosis: multiple causes and multiple mechanisms?', *Eur Respir J,* 30(5), pp. 835-9.

Mapel, D. W., Samet, J. M. and Coultas, D. B. (1996) 'Corticosteroids and the treatment of idiopathic pulmonary fibrosis. Past, present, and future', *Chest,* 110(4), pp. 1058-67.

Mareike, L., Lara, B., Darcy, W., Jürgen, B., Michael, L. and Melanie, K. 2016. LATE-BREAKING ABSTRACT: Anti-fibrotic effects of nintedanib and pirfenidone in 2D versus 3D lung cultures. European Respiratory Journal.

Massague, J. (1990) 'The Transforming Growth Factor-beta Family', *Annual Review of Cell Biology,* 6(1), pp. 597-641.

Matthay, M. A. and Zemans, R. L. (2011) 'The acute respiratory distress syndrome: pathogenesis and treatment', *Annu Rev Pathol,* 6, pp. 147-63.

Matthay, M. A. and Zimmerman, G. A. (2005) 'Acute lung injury and the acute respiratory distress syndrome: four decades of inquiry into pathogenesis and rational management', *Am J Respir Cell Mol Biol,* 33(4), pp. 319-27.

Matute-Bello, G., Frevert, C. W. and Martin, T. R. (2008) 'Animal models of acute lung injury', *Am J Physiol Lung Cell Mol Physiol,* 295(3), pp. L379-99.

Mauri, T., Masson, S., Pradella, A., Bellani, G., Coppadoro, A., Bombino, M., Valentino, S., Patroniti, N., Mantovani, A., Pesenti, A. and Latini, R. (2010) 'Elevated plasma and alveolar levels of soluble receptor for advanced glycation endproducts are associated with severity of lung dysfunction in ARDS patients', *Tohoku J Exp Med,* 222(2), pp. 105-12.

McElroy, M. C. and Kasper, M. (2004) 'The use of alveolar epithelial type I cell-selective markers to investigate lung injury and repair', *Eur Respir J,* 24(4), pp. 664-73.
Meduri, G. U., Headley, S., Kohler, G., Stentz, F., Tolley, E., Umberger, R. and Leeper, K. (1995) 'Persistent elevation of inflammatory cytokines predicts a poor outcome in ARDS. Plasma IL-1 beta and IL-6 levels are consistent and efficient predictors of outcome over time', *Chest,* 107(4), pp. 1062-73.
Mitsuhashi, H., Asano, S., Nonaka, T., Hamamura, I., Masuda, K. and Kiyoki, M. (1996) 'Administration of truncated secretory leukoprotease inhibitor ameliorates bleomycin-induced pulmonary fibrosis in hamsters', *Am J Respir Crit Care Med,* 153(1), pp. 369-74.
Miyazaki, Y., Araki, K., Vesin, C., Garcia, I., Kapanci, Y., Whitsett, J. A., Piguet, P. F. and Vassalli, P. (1995) 'Expression of a tumor necrosis factor-alpha transgene in murine lung causes lymphocytic and fibrosing alveolitis. A mouse model of progressive pulmonary fibrosis', *J Clin Invest,* 96(1), pp. 250-9.
Miyazono, K., Olofsson, A., Colosetti, P. and Heldin, C. H. (1991) 'A role of the latent TGF-beta 1-binding protein in the assembly and secretion of TGF-beta 1', *EMBO J,* 10(5), pp. 1091-101.
Modi, W. S. and Yoshimura, T. (1999) 'Isolation of novel GRO genes and a phylogenetic analysis of the CXC chemokine subfamily in mammals', *Mol Biol Evol,* 16(2), pp. 180-93.
Moeller, A., Ask, K., Warburton, D., Gauldie, J. and Kolb, M. (2008) 'The bleomycin animal model: a useful tool to investigate treatment options for idiopathic pulmonary fibrosis?', *Int J Biochem Cell Biol,* 40(3), pp. 362-82.
Moore, B. B. and Hogaboam, C. M. (2008) 'Murine models of pulmonary fibrosis', *Am J Physiol Lung Cell Mol Physiol,* 294(2), pp. L152-60.
Mori, H., Tanaka, H., Kawada, K., Nagai, H. and Koda, A. (1995) 'Suppressive effects of tranilast on pulmonary fibrosis and activation of alveolar macrophages in mice treated with bleomycin: role of alveolar macrophages in the fibrosis', *Jpn J Pharmacol,* 67(4), pp. 279-89.
Mu, D., Cambier, S., Fjellbirkeland, L., Baron, J. L., Munger, J. S., Kawakatsu, H., Sheppard, D., Broaddus, V. C. and Nishimura, S. L. (2002) 'The integrin alpha(v)beta8 mediates epithelial homeostasis through MT1-MMP-dependent activation of TGF-beta1', *J Cell Biol,* 157(3), pp. 493-507.
Munger, J. S., Huang, X., Kawakatsu, H., Griffiths, M. J., Dalton, S. L., Wu, J., Pittet, J. F., Kaminski, N., Garat, C., Matthay, M. A., Rifkin, D. B. and Sheppard, D. (1999) 'The integrin alpha v beta 6 binds and activates latent TGF beta 1: a mechanism for regulating pulmonary inflammation and fibrosis', *Cell,* 96(3), pp. 319-28.
Murphy-Ullrich, J. E. and Poczatek, M. (2000) 'Activation of latent TGF-beta by thrombospondin-1: mechanisms and physiology', *Cytokine Growth Factor Rev,* 11(1-2), pp. 59-69.
Nakagome, K., Dohi, M., Okunishi, K., Tanaka, R., Miyazaki, J. and Yamamoto, K. (2006) 'In vivo IL-10 gene delivery attenuates

bleomycin induced pulmonary fibrosis by inhibiting the production and activation of TGF-beta in the lung', *Thorax,* 61(10), pp. 886-94.
Navaratnam, V., Fleming, K. M., West, J., Smith, C. J., Jenkins, R. G., Fogarty, A. and Hubbard, R. B. (2011) 'The rising incidence of idiopathic pulmonary fibrosis in the U.K', *Thorax,* 66(6), pp. 462-7.
NC3Rs, BBSRC, Defra, MRC, NERC and Wellcome-Trust 2017. Responsibility in the use of animals in bioscience research: expectations of the major research councils and charitable funding bodies. London: NC3Rs
Neff, T. A., Stocker, R., Frey, H. R., Stein, S. and Russi, E. W. (2003) 'Long-term assessment of lung function in survivors of severe ARDS', *Chest,* 123(3), pp. 845-53.
Noble, P. W. and Homer, R. J. (2005) 'Back to the future: historical perspective on the pathogenesis of idiopathic pulmonary fibrosis', *Am J Respir Cell Mol Biol,* 33(2), pp. 113-20.
Nomura, M. and Li, E. (1998) 'Smad2 role in mesoderm formation, left-right patterning and craniofacial development', *Nature,* 393(6687), pp. 786-90.
Obayashi, Y., Yamadori, I., Fujita, J., Yoshinouchi, T., Ueda, N. and Takahara, J. (1997) 'The role of neutrophils in the pathogenesis of idiopathic pulmonary fibrosis', *Chest,* 112(5), pp. 1338-43.
Oono, T., Specks, U., Eckes, B., Majewski, S., Hunzelmann, N., Timpl, R. and Krieg, T. (1993) 'Expression of type VI collagen mRNA during wound healing', *J Invest Dermatol,* 100(3), pp. 329-34.
Opitz, B., van Laak, V., Eitel, J. and Suttorp, N. (2010) 'Innate immune recognition in infectious and noninfectious diseases of the lung', *Am J Respir Crit Care Med,* 181(12), pp. 1294-309.
Ou, X. M., Li, W. C., Liu, D. S., Li, Y. P., Wen, F. Q., Feng, Y. L., Zhang, S. F., Huang, X. Y., Wang, T., Wang, K., Wang, X. and Chen, L. (2009) 'VEGFR-2 antagonist SU5416 attenuates bleomycin-induced pulmonary fibrosis in mice', *Int Immunopharmacol,* 9(1), pp. 70-9.
Overall, C. M., Wrana, J. L. and Sodek, J. (1989) 'Independent regulation of collagenase, 72-kDa progelatinase, and metalloendoproteinase inhibitor expression in human fibroblasts by transforming growth factor-beta', *J Biol Chem,* 264(3), pp. 1860-9.
Owen, C. A., Campbell, M. A., Sannes, P. L., Boukedes, S. S. and Campbell, E. J. (1995) 'Cell surface-bound elastase and cathepsin G on human neutrophils: a novel, non-oxidative mechanism by which neutrophils focus and preserve catalytic activity of serine proteinases', *J Cell Biol,* 131(3), pp. 775-89.
Parekh, D., Dancer, R. C. and Thickett, D. R. (2011) 'Acute lung injury', *Clin Med,* 11(6), pp. 615-8.
Park, B. S., Song, D. H., Kim, H. M., Choi, B. S., Lee, H. and Lee, J. O. (2009) 'The structural basis of lipopolysaccharide recognition by the TLR4-MD-2 complex', *Nature,* 458(7242), pp. 1191-5.
Park, D. S., Cohen, A. W., Frank, P. G., Razani, B., Lee, H., Williams, T. M., Chandra, M., Shirani, J., De Souza, A. P., Tang, B., Jelicks, L. A., Factor, S. M., Weiss, L. M., Tanowitz, H. B. and Lisanti, M. P. (2003)

'Caveolin-1 null (-/-) mice show dramatic reductions in life span', *Biochemistry,* 42(51), pp. 15124-31.
Parsons, P. E., Eisner, M. D., Thompson, B. T., Matthay, M. A., Ancukiewicz, M., Bernard, G. R., Wheeler, A. P. and Network, N. A. R. D. S. C. T. (2005) 'Lower tidal volume ventilation and plasma cytokine markers of inflammation in patients with acute lung injury', *Crit Care Med,* 33(1), pp. 1-6; discussion 230-2.
Patterson, M. L., Atkinson, S. J., Knäuper, V. and Murphy, G. (2001) 'Specific collagenolysis by gelatinase A, MMP-2, is determined by the hemopexin domain and not the fibronectin-like domain', *FEBS Lett,* 503(2-3), pp. 158-62.
Pejler, G., Abrink, M., Ringvall, M. and Wernersson, S. (2007) 'Mast cell proteases', *Adv Immunol,* 95, pp. 167-255.
Philp, C. J., Siebeke, I., Clements, D., Miller, S., Habgood, A., John, A. E., Navaratnam, V., Hubbard, R. B., Jenkins, G. and Johnson, S. R. (2018) 'Extracellular Matrix Cross-Linking Enhances Fibroblast Growth and Protects against Matrix Proteolysis in Lung Fibrosis', *Am J Respir Cell Mol Biol,* 58(5), pp. 594-603.
Pierrakos, C., Karanikolas, M., Scolletta, S., Karamouzos, V. and Velissaris, D. (2012) 'Acute respiratory distress syndrome: pathophysiology and therapeutic options', *J Clin Med Res,* 4(1), pp. 7-16.
Pini, A., Shemesh, R., Samuel, C. S., Bathgate, R. A., Zauberman, A., Hermesh, C., Wool, A., Bani, D. and Rotman, G. (2010) 'Prevention of bleomycin-induced pulmonary fibrosis by a novel antifibrotic peptide with relaxin-like activity', *J Pharmacol Exp Ther,* 335(3), pp. 589-99.
Pittet, J. F., Griffiths, M. J., Geiser, T., Kaminski, N., Dalton, S. L., Huang, X., Brown, L. A., Gotwals, P. J., Koteliansky, V. E., Matthay, M. A. and Sheppard, D. (2001) 'TGF-beta is a critical mediator of acute lung injury', *J Clin Invest,* 107(12), pp. 1537-44.
Pociask, D. A., Sime, P. J. and Brody, A. R. (2004) 'Asbestos-derived reactive oxygen species activate TGF-beta1', *Lab Invest,* 84(8), pp. 1013-23.
Porte, J. and Jenkins, G. (2014) 'Assessment of the effect of potential antifibrotic compounds on total and αVβ6 integrin-mediated TGF-β activation', *Pharmacol Res Perspect,* 2(4), pp. e00030.
Povirk, L. F. and Houlgrave, C. W. (1988) 'Effect of apurinic/apyrimidinic endonucleases and polyamines on DNA treated with bleomycin and neocarzinostatin: specific formation and cleavage of closely opposed lesions in complementary strands', *Biochemistry,* 27(10), pp. 3850-7.
Puthawala, K., Hadjiangelis, N., Jacoby, S. C., Bayongan, E., Zhao, Z., Yang, Z., Devitt, M. L., Horan, G. S., Weinreb, P. H., Lukashev, M. E., Violette, S. M., Grant, K. S., Colarossi, C., Formenti, S. C. and Munger, J. S. (2008) 'Inhibition of integrin alpha(v)beta6, an activator of latent transforming growth factor-beta, prevents radiation-induced lung fibrosis', *Am J Respir Crit Care Med,* 177(1), pp. 82-90.
Rackley, C. R. and Stripp, B. R. (2012) 'Building and maintaining the epithelium of the lung', *J Clin Invest,* 122(8), pp. 2724-30.

Raghu, G., Weycker, D., Edelsberg, J., Bradford, W. Z. and Oster, G. (2006) 'Incidence and prevalence of idiopathic pulmonary fibrosis', *Am J Respir Crit Care Med,* 174(7), pp. 810-6.

Rasooli, R., Rajaian, H., Pardakhty, A. and Mandegary, A. (2018) 'Preference of Aerosolized Pirfenidone to Oral Intake: An Experimental Model of Pulmonary Fibrosis by Paraquat', *J Aerosol Med Pulm Drug Deliv,* 31(1), pp. 25-32.

Rawlins, E. L. and Perl, A. K. (2012) 'The a"MAZE"ing world of lung-specific transgenic mice', *Am J Respir Cell Mol Biol,* 46(3), pp. 269-82.

Richeldi, L., du Bois, R. M., Raghu, G., Azuma, A., Brown, K. K., Costabel, U., Cottin, V., Flaherty, K. R., Hansell, D. M., Inoue, Y., Kim, D. S., Kolb, M., Nicholson, A. G., Noble, P. W., Selman, M., Taniguchi, H., Brun, M., Le Maulf, F., Girard, M., Stowasser, S., Schlenker-Herceg, R., Disse, B., Collard, H. R. and Investigators, I. T. (2014) 'Efficacy and safety of nintedanib in idiopathic pulmonary fibrosis', *N Engl J Med,* 370(22), pp. 2071-82.

Rifkin, D. B. (2005) 'Latent transforming growth factor-beta (TGF-beta) binding proteins: orchestrators of TGF-beta availability', *J Biol Chem,* 280(9), pp. 7409-12.

Rodt, T., von Falck, C., Dettmer, S., Halter, R., Maus, R., Ask, K., Kolb, M., Gauldie, J., Länger, F., Hoy, L., Welte, T., Galanski, M., Maus, U. A. and Borlak, J. (2010) 'Micro-computed tomography of pulmonary fibrosis in mice induced by adenoviral gene transfer of biologically active transforming growth factor-β1', *Respir Res,* 11, pp. 181.

Roggli, V. L., Gibbs, A. R., Attanoos, R., Churg, A., Popper, H., Cagle, P., Corrin, B., Franks, T. J., Galateau-Salle, F., Galvin, J., Hasleton, P. S., Henderson, D. W. and Honma, K. (2010) 'Pathology of asbestosis- An update of the diagnostic criteria: Report of the asbestosis committee of the college of american pathologists and pulmonary pathology society', *Arch Pathol Lab Med,* 134(3), pp. 462-80.

Rube, C. E., Uthe, D., Schmid, K. W., Richter, K. D., Wessel, J., Schuck, A., Willich, N. and Rube, C. (2000) 'Dose-dependent induction of transforming growth factor beta (TGF-beta) in the lung tissue of fibrosis-prone mice after thoracic irradiation', *Int J Radiat Oncol Biol Phys,* 47(4), pp. 1033-42.

Rubenfeld, G. D., Caldwell, E., Peabody, E., Weaver, J., Martin, D. P., Neff, M., Stern, E. J. and Hudson, L. D. (2005) 'Incidence and outcomes of acute lung injury', *N Engl J Med,* 353(16), pp. 1685-93.

Rubenfeld, G. D. and Herridge, M. S. (2007) 'Epidemiology and outcomes of acute lung injury', *Chest,* 131(2), pp. 554-62.

Ruiz, V., Ordóñez, R. M., Berumen, J., Ramírez, R., Uhal, B., Becerril, C., Pardo, A. and Selman, M. (2003) 'Unbalanced collagenases/TIMP-1 expression and epithelial apoptosis in experimental lung fibrosis', *Am J Physiol Lung Cell Mol Physiol,* 285(5), pp. L1026-36.

Ryerson, C. J., Cottin, V., Brown, K. K. and Collard, H. R. (2015) 'Acute exacerbation of idiopathic pulmonary fibrosis: shifting the paradigm', *Eur Respir J,* 46(2), pp. 512-20.

Röck, K., Grandoch, M., Majora, M., Krutmann, J. and Fischer, J. W. (2011) 'Collagen fragments inhibit hyaluronan synthesis in skin fibroblasts in response to ultraviolet B (UVB): new insights into mechanisms of matrix remodeling', *J Biol Chem,* 286(20), pp. 18268-76.

Rünger, T. M., Adami, S., Benhamou, C. L., Czerwiński, E., Farrerons, J., Kendler, D. L., Mindeholm, L., Realdi, G., Roux, C. and Smith, V. (2012) 'Morphea-like skin reactions in patients treated with the cathepsin K inhibitor balicatib', *J Am Acad Dermatol,* 66(3), pp. e89-96.

Saha, A., Ellison, D., Thomas, G. J., Vallath, S., Mather, S. J., Hart, I. R. and Marshall, J. F. (2010) 'High-resolution in vivo imaging of breast cancer by targeting the pro-invasive integrin alphavbeta6', *J Pathol,* 222(1), pp. 52-63.

Saharinen, J. and Keski-Oja, J. (2000) 'Specific sequence motif of 8-Cys repeats of TGF-beta binding proteins, LTBPs, creates a hydrophobic interaction surface for binding of small latent TGF-beta', *Mol Biol Cell,* 11(8), pp. 2691-704.

Saini, G., Porte, J., Weinreb, P. H., Violette, S. M., Wallace, W. A., McKeever, T. M. and Jenkins, G. (2015) 'αvβ6 integrin may be a potential prognostic biomarker in interstitial lung disease', *Eur Respir J,* 46(2), pp. 486-94.

Saito, F., Tasaka, S., Inoue, K., Miyamoto, K., Nakano, Y., Ogawa, Y., Yamada, W., Shiraishi, Y., Hasegawa, N., Fujishima, S., Takano, H. and Ishizaka, A. (2008) 'Role of interleukin-6 in bleomycin-induced lung inflammatory changes in mice', *Am J Respir Cell Mol Biol,* 38(5), pp. 566-71.

Sakashita, A., Nishimura, Y., Nishiuma, T., Takenaka, K., Kobayashi, K., Kotani, Y. and Yokoyama, M. (2007) 'Neutrophil elastase inhibitor (sivelestat) attenuates subsequent ventilator-induced lung injury in mice', *Eur J Pharmacol,* 571(1), pp. 62-71.

Samuel, C. S. (2005) 'Relaxin: antifibrotic properties and effects in models of disease', *Clin Med Res,* 3(4), pp. 241-9.

Samuel, C. S., Zhao, C., Bathgate, R. A., Bond, C. P., Burton, M. D., Parry, L. J., Summers, R. J., Tang, M. L., Amento, E. P. and Tregear, G. W. (2003) 'Relaxin deficiency in mice is associated with an age-related progression of pulmonary fibrosis', *FASEB J,* 17(1), pp. 121-3.

Schrier, D. J., Kunkel, R. G. and Phan, S. H. (1983) 'The role of strain variation in murine bleomycin-induced pulmonary fibrosis', *Am Rev Respir Dis,* 127(1), pp. 63-6.

Scotton, C. J. and Chambers, R. C. (2007) 'Molecular targets in pulmonary fibrosis: the myofibroblast in focus', *Chest,* 132(4), pp. 1311-21.

Scotton, C. J., Hayes, B., Alexander, R., Datta, A., Forty, E. J., Mercer, P. F., Blanchard, A. and Chambers, R. C. (2013) 'Ex vivo micro-computed tomography analysis of bleomycin-induced lung fibrosis for preclinical drug evaluation', *Eur Respir J,* 42(6), pp. 1633-45.

Seifirad, S., Keshavarz, A., Taslimi, S., Aran, S., Abbasi, H. and Ghaffari, A. (2012) 'Effect of pirfenidone on pulmonary fibrosis due to paraquat poisoning in rats', *Clin Toxicol (Phila),* 50(8), pp. 754-8.

Selman, M., King, T. E., Pardo, A., Society, A. T., Society, E. R. and Physicians, A. C. o. C. (2001) 'Idiopathic pulmonary fibrosis: prevailing and evolving hypotheses about its pathogenesis and implications for therapy', *Ann Intern Med,* 134(2), pp. 136-51.

Selman, M. and Pardo, A. (2006) 'Role of epithelial cells in idiopathic pulmonary fibrosis: from innocent targets to serial killers', *Proc Am Thorac Soc,* 3(4), pp. 364-72.

Selman, M., Ruiz, V., Cabrera, S., Segura, L., Ramírez, R., Barrios, R. and Pardo, A. (2000) 'TIMP-1, -2, -3, and -4 in idiopathic pulmonary fibrosis. A prevailing nondegradative lung microenvironment?', *Am J Physiol Lung Cell Mol Physiol,* 279(3), pp. L562-74.

Shao, X., Li, M., Luo, C., Wang, Y. Y., Lu, Y. Y., Feng, S., Li, H., Lang, X. B., Wang, Y. C., Lin, C., Shen, X. J., Zhou, Q., Jiang, H. and Chen, J. H. (2015) 'Effects of rapamycin against paraquat-induced pulmonary fibrosis in mice', *J Zhejiang Univ Sci B,* 16(1), pp. 52-61.

Sheppard, D. (2006) 'Transforming growth factor beta: a central modulator of pulmonary and airway inflammation and fibrosis', *Proc Am Thorac Soc,* 3(5), pp. 413-7.

Shi, M., Zhu, J., Wang, R., Chen, X., Mi, L., Walz, T. and Springer, T. A. (2011) 'Latent TGF-β structure and activation', *Nature,* 474(7351), pp. 343-9.

Shi, Z., Wakil, A. E. and Rockey, D. C. (1997) 'Strain-specific differences in mouse hepatic wound healing are mediated by divergent T helper cytokine responses', *Proc Natl Acad Sci U S A,* 94(20), pp. 10663-8.

Shimizu, S., Gabazza, E. C., Taguchi, O., Yasui, H., Taguchi, Y., Hayashi, T., Ido, M., Shimizu, T., Nakagaki, T., Kobayashi, H., Fukudome, K., Tsuneyoshi, N., D'Alessandro-Gabazza, C. N., Izumizaki, M., Iwase, M., Homma, I., Adachi, Y. and Suzuki, K. (2003) 'Activated protein C inhibits the expression of platelet-derived growth factor in the lung', *Am J Respir Crit Care Med,* 167(10), pp. 1416-26.

Shoulders, M. D. and Raines, R. T. (2009) 'Collagen structure and stability', *Annu Rev Biochem,* 78, pp. 929-58.

Sime, P. J., Xing, Z., Graham, F. L., Csaky, K. G. and Gauldie, J. (1997) 'Adenovector-mediated gene transfer of active transforming growth factor-beta1 induces prolonged severe fibrosis in rat lung', *J Clin Invest,* 100(4), pp. 768-76.

Smedly, L. A., Tonnesen, M. G., Sandhaus, R. A., Haslett, C., Guthrie, L. A., Johnston, R. B., Jr., Henson, P. M. and Worthen, G. S. (1986) 'Neutrophil-mediated injury to endothelial cells. Enhancement by endotoxin and essential role of neutrophil elastase', *J Clin Invest,* 77(4), pp. 1233-43.

Specks, U., Nerlich, A., Colby, T. V., Wiest, I. and Timpl, R. (1995) 'Increased expression of type VI collagen in lung fibrosis', *Am J Respir Crit Care Med,* 151(6), pp. 1956-64.

Srivastava, M., Steinwede, K., Kiviranta, R., Morko, J., Hoymann, H. G., Länger, F., Buhling, F., Welte, T. and Maus, U. A. (2008) 'Overexpression of cathepsin K in mice decreases collagen deposition

and lung resistance in response to bleomycin-induced pulmonary fibrosis', *Respir Res,* 9, pp. 54.
Stockley, R. A. (1999) 'Neutrophils and protease/antiprotease imbalance', *Am J Respir Crit Care Med,* 160(5 Pt 2), pp. S49-52.
Sueblinvong, V., Neujahr, D. C., Mills, S. T., Roser-Page, S., Ritzenthaler, J. D., Guidot, D., Rojas, M. and Roman, J. (2012) 'Predisposition for disrepair in the aged lung', *Am J Med Sci,* 344(1), pp. 41-51.
Summers, C., Singh, N. R., Worpole, L., Simmonds, R., Babar, J., Condliffe, A. M., Gunning, K. E., Johnston, A. J. and Chilvers, E. R. (2016) 'Incidence and recognition of acute respiratory distress syndrome in a UK intensive care unit', *Thorax,* 71(11), pp. 1050-1051.
Tager, A. M., LaCamera, P., Shea, B. S., Campanella, G. S., Selman, M., Zhao, Z., Polosukhin, V., Wain, J., Karimi-Shah, B. A., Kim, N. D., Hart, W. K., Pardo, A., Blackwell, T. S., Xu, Y., Chun, J. and Luster, A. D. (2008) 'The lysophosphatidic acid receptor LPA1 links pulmonary fibrosis to lung injury by mediating fibroblast recruitment and vascular leak', *Nat Med,* 14(1), pp. 45-54.
Taipale, J., Miyazono, K., Heldin, C. H. and Keski-Oja, J. (1994) 'Latent transforming growth factor-beta 1 associates to fibroblast extracellular matrix via latent TGF-beta binding protein', *J Cell Biol,* 124(1-2), pp. 171-81.
Tanaka, K., Honda, M., Kuramochi, T. and Morioka, S. (1994) 'Prominent inhibitory effects of tranilast on migration and proliferation of and collagen synthesis by vascular smooth muscle cells', *Atherosclerosis,* 107(2), pp. 179-85.
Tang, B. M. P., Craig, J. C., Eslick, G. D., Seppelt, I. and McLean, A. S. (2009) 'Use of corticosteroids in acute lung injury and acute respiratory distress syndrome: A systematic review and meta-analysis', *Critical Care Medicine,* 37(5), pp. 1594-1603.
Taooka, Y., Maeda, A., Hiyama, K., Ishioka, S. and Yamakido, M. (1997) 'Effects of neutrophil elastase inhibitor on bleomycin-induced pulmonary fibrosis in mice', *Am J Respir Crit Care Med,* 156(1), pp. 260-5.
Tashiro, J., Rubio, G. A., Limper, A. H., Williams, K., Elliot, S. J., Ninou, I., Aidinis, V., Tzouvelekis, A. and Glassberg, M. K. (2017) 'Exploring Animal Models That Resemble Idiopathic Pulmonary Fibrosis', *Front Med (Lausanne),* 4, pp. 118.
Tatler, A. L., Barnes, J., Habgood, A., Goodwin, A., McAnulty, R. J. and Jenkins, G. (2016a) 'Caffeine inhibits TGFβ activation in epithelial cells, interrupts fibroblast responses to TGFβ, and reduces established fibrosis in ex vivo precision-cut lung slices', *Thorax,* 71(6), pp. 565-7.
Tatler, A. L., Habgood, A., Porte, J., John, A. E., Stavrou, A., Hodge, E., Kerama-Likoko, C., Violette, S. M., Weinreb, P. H., Knox, A. J., Laurent, G., Parfrey, H., Wolters, P. J., Wallace, W., Alberti, S., Nordheim, A. and Jenkins, G. (2016b) 'Reduced Ets Domain-containing Protein Elk1 Promotes Pulmonary Fibrosis via Increased Integrin αvβ6 Expression', *J Biol Chem,* 291(18), pp. 9540-53.

Tkalcevic, J., Novelli, M., Phylactides, M., Iredale, J. P., Segal, A. W. and Roes, J. (2000) 'Impaired immunity and enhanced resistance to endotoxin in the absence of neutrophil elastase and cathepsin G', *Immunity,* 12(2), pp. 201-10.

Togbe, D., Schnyder-Candrian, S., Schnyder, B., Doz, E., Noulin, N., Janot, L., Secher, T., Gasse, P., Lima, C., Coelho, F. R., Vasseur, V., Erard, F., Ryffel, B., Couillin, I. and Moser, R. (2007) 'Toll-like receptor and tumour necrosis factor dependent endotoxin-induced acute lung injury', *Int J Exp Pathol,* 88(6), pp. 387-91.

Travis, E. L., Peters, L. J., McNeill, J., Thames, H. D., Jr. and Karolis, C. (1985) 'Effect of dose-rate on total body irradiation: lethality and pathologic findings', *Radiother Oncol,* 4(4), pp. 341-51.

Tsushima, K., King, L. S., Aggarwal, N. R., De Gorordo, A., D'Alessio, F. R. and Kubo, K. (2009) 'Acute lung injury review', *Intern Med,* 48(9), pp. 621-30.

Vanderbilt, J. N., Mager, E. M., Allen, L., Sawa, T., Wiener-Kronish, J., Gonzalez, R. and Dobbs, L. G. (2003) 'CXC chemokines and their receptors are expressed in type II cells and upregulated following lung injury', *Am J Respir Cell Mol Biol,* 29(6), pp. 661-8.

Veerappan, A., O'Connor, N. J., Brazin, J., Reid, A. C., Jung, A., McGee, D., Summers, B., Branch-Elliman, D., Stiles, B., Worgall, S., Kaner, R. J. and Silver, R. B. (2013) 'Mast cells: a pivotal role in pulmonary fibrosis', *DNA Cell Biol,* 32(4), pp. 206-18.

Wahl, S. M., Hunt, D. A., Wakefield, L. M., McCartney-Francis, N., Wahl, L. M., Roberts, A. B. and Sporn, M. B. (1987) 'Transforming growth factor type beta induces monocyte chemotaxis and growth factor production', *Proc Natl Acad Sci U S A,* 84(16), pp. 5788-92.

Walkin, L., Herrick, S. E., Summers, A., Brenchley, P. E., Hoff, C. M., Korstanje, R. and Margetts, P. J. (2013) 'The role of mouse strain differences in the susceptibility to fibrosis: a systematic review', *Fibrogenesis Tissue Repair,* 6(1), pp. 18.

Wan, Y. Y. and Flavell, R. A. (2008) 'TGF-beta and regulatory T cell in immunity and autoimmunity', *J Clin Immunol,* 28(6), pp. 647-59.

Wang, Q., Usinger, W., Nichols, B., Gray, J., Xu, L., Seeley, T. W., Brenner, M., Guo, G., Zhang, W., Oliver, N., Lin, A. and Yeowell, D. (2011) 'Cooperative interaction of CTGF and TGF-β in animal models of fibrotic disease', *Fibrogenesis Tissue Repair,* 4(1), pp. 4.

Wang, X. M., Zhang, Y., Kim, H. P., Zhou, Z., Feghali-Bostwick, C. A., Liu, F., Ifedigbo, E., Xu, X., Oury, T. D., Kaminski, N. and Choi, A. M. (2006) 'Caveolin-1: a critical regulator of lung fibrosis in idiopathic pulmonary fibrosis', *J Exp Med,* 203(13), pp. 2895-906.

Wang, Z. L. (2009) 'Advances in understanding of idiopathic pulmonary fibrosis', *Chinese Medical Journal,* 122(7), pp. 844-857.

Wells, A. U. (2013) 'The revised ATS/ERS/JRS/ALAT diagnostic criteria for idiopathic pulmonary fibrosis (IPF)--practical implications', *Respir Res,* 14 Suppl 1, pp. S2.

Whyte, M., Hubbard, R., Meliconi, R., Whidborne, M., Eaton, V., Bingle, C., Timms, J., Duff, G., Facchini, A., Pacilli, A., Fabbri, M., Hall, I., Britton,

J., Johnston, I. and Di Giovine, F. (2000) 'Increased risk of fibrosing alveolitis associated with interleukin-1 receptor antagonist and tumor necrosis factor-alpha gene polymorphisms', *Am J Respir Crit Care Med,* 162(2 Pt 1), pp. 755-8.

Wipff, P. J., Rifkin, D. B., Meister, J. J. and Hinz, B. (2007) 'Myofibroblast contraction activates latent TGF-beta1 from the extracellular matrix', *J Cell Biol,* 179(6), pp. 1311-23.

Wygrecka, M., Dahal, B. K., Kosanovic, D., Petersen, F., Taborski, B., von Gerlach, S., Didiasova, M., Zakrzewicz, D., Preissner, K. T., Schermuly, R. T. and Markart, P. (2013) 'Mast cells and fibroblasts work in concert to aggravate pulmonary fibrosis: role of transmembrane SCF and the PAR-2/PKC-α/Raf-1/p44/42 signaling pathway', *Am J Pathol,* 182(6), pp. 2094-108.

Xaubet, A., Marin-Arguedas, A., Lario, S., Ancochea, J., Morell, F., Ruiz-Manzano, J., Rodriguez-Becerra, E., Rodriguez-Arias, J. M., Inigo, P., Sanz, S., Campistol, J. M., Mullol, J. and Picado, C. (2003) 'Transforming growth factor-beta1 gene polymorphisms are associated with disease progression in idiopathic pulmonary fibrosis', *Am J Respir Crit Care Med,* 168(4), pp. 431-5.

Xu, M. Y., Porte, J., Knox, A. J., Weinreb, P. H., Maher, T. M., Violette, S. M., McAnulty, R. J., Sheppard, D. and Jenkins, G. (2009) 'Lysophosphatidic acid induces alphavbeta6 integrin-mediated TGF-beta activation via the LPA2 receptor and the small G protein G alpha(q)', *Am J Pathol,* 174(4), pp. 1264-79.

Yamada, H., Tajima, S., Nishikawa, T., Murad, S. and Pinnell, S. R. (1994) 'Tranilast, a selective inhibitor of collagen synthesis in human skin fibroblasts', *J Biochem,* 116(4), pp. 892-7.

Yang, S. H., Bumpass, D. C., Perkins, N. D. and Sharrocks, A. D. (2002) 'The ETS domain transcription factor Elk-1 contains a novel class of repression domain', *Mol Cell Biol,* 22(14), pp. 5036-46.

Yang, Z., Mu, Z., Dabovic, B., Jurukovski, V., Yu, D., Sung, J., Xiong, X. and Munger, J. S. (2007) 'Absence of integrin-mediated TGFbeta1 activation in vivo recapitulates the phenotype of TGFbeta1-null mice', *J Cell Biol,* 176(6), pp. 787-93.

Yaroshenko, A., Hellbach, K., Yildirim, A., Conlon, T. M., Fernandez, I. E., Bech, M., Velroyen, A., Meinel, F. G., Auweter, S., Reiser, M., Eickelberg, O. and Pfeiffer, F. (2015) 'Improved In vivo Assessment of Pulmonary Fibrosis in Mice using X-Ray Dark-Field Radiography', *Sci Rep,* 5, pp. 17492.

Zambon, M. and Vincent, J. L. (2008) 'Mortality rates for patients with acute lung injury/ARDS have decreased over time', *Chest,* 133(5), pp. 1120-7.

Zani, M. L., Tanga, A., Saidi, A., Serrano, H., Dallet-Choisy, S., Baranger, K. and Moreau, T. (2011) 'SLPI and trappin-2 as therapeutic agents to target airway serine proteases in inflammatory lung diseases: current and future directions', *Biochem Soc Trans,* 39(5), pp. 1441-6.

Zhang, D., Huang, C., Yang, C., Liu, R. J., Wang, J., Niu, J. and Brömme, D. (2011) 'Antifibrotic effects of curcumin are associated with

overexpression of cathepsins K and L in bleomycin treated mice and human fibroblasts', *Respir Res,* 12, pp. 154.
Zhao, J., Shi, W., Wang, Y. L., Chen, H., Bringas, P., Datto, M. B., Frederick, J. P., Wang, X. F. and Warburton, D. (2002) 'Smad3 deficiency attenuates bleomycin-induced pulmonary fibrosis in mice', *Am J Physiol Lung Cell Mol Physiol,* 282(3), pp. L585-93.